Opioid receptors as therapeutic targets for nociceptor specific regional analgesia

Opioidrezeptoren als therapeutisches Target einer nozizeptionsspezifischen Regionalanalgesie

Doctoral thesis for a doctoral degree
at the Graduate School of Life Sciences,
Julius-Maximilians-Universität Würzburg,
Section Neuroscience

submitted by

Egle Maria Mambretti

from

Monza, Italy

Würzburg, 16th December 2015

Reverse page

Submitted on: ……..……..

Office stamp

Members of the *Promotionskomitee*:

Chairperson: **Prof. Dr. Ulrike Holzgrabe**

Primary Supervisor: **Prof. Dr. Heike L. Rittner**

Supervisor (Second): **Prof. Dr. Esther Asan**

Supervisor (Third): **Prof. Dr. Erhard Wischmeyer**

Supervisor (Fourth): …….

(If applicable)

Date of Public Defence: ……..……

Date of Receipt of Certificates: ……..

AFFIDAVIT

I hereby confirm that my thesis entitled *"Opioid receptors in the sciatic nerve as a target for peripheral analgesia"* is the results of my own work. I did not receive any help or support from commercial consultant. All sources and/or material applied are listed and specified in the thesis.
Furthermore, I confirm that this thesis is not yet been submitted as a part of another examination process neither in identical nor in similar form.

Würzburg, 16.12.2015

EIDESSTATTLICHE ERKLÄRUNG

Hiermit erkläre ich an Eides statt, die Dissertation *"Opioid receptors in the sciatic nerve as a target for peripheral analgesia"* eigenständig, d.h., insbesondere selbständig und ohne Hilfe eines kommerziellen Promotionsberaters, angefertigt und keine anderen als die von mir angegebenen Quelle und Hilfsmittel verwendet zu haben.
Ich erkläre außerdem, dass die Dissertation weder in gleicher noch in ähnlicher Form bereits in einem anderen Prüfungsverfahren vorgelegen hat.

Würzburg, 16.12.2015

“Nobody said it was easy,
no one ever said it would be this hard”
The scientist - Coldplay

ACKNOWLEDGMENTS

I would like to thank my thesis committee members, Prof. Dr. Heike L. Rittner, Prof. Dr. Esther Asan and Prof. Dr. Erhard Wischmeyer, for being my mentors during the past three years.
In particular, I would like to express my gratitude to Prof. Rittner and Prof. Asan, really good examples of successful women in science. Their scientific and technical advices, based on a broad knowledge and experience, were precious to pursue the difficult tasks of the project. Their moral support and encouragement were also precious. Last but not least, I would like to thank them for their enormous efforts during the "final rush" needed to allow me to submit the thesis in time.
I would also like to thank Prof. Dr. Alexander Brack: while following the project he originally co-authored with Prof. Rittner and Prof. Asan more "from the outside", he steadily contributed to my progress with valuable comments and suggestions.

I am also grateful to Karin and Kirsten for their competence in experimental procedures and for helping me in the development of experiments. Thanks also to all other members of the lab and to the people of the Anesthesiology and Anatomy departments, who kindly answered my questions, gave me useful suggestions or simply encouraged me with smiles: Solange, Beatice, Ann-Kristin, Shaobing, Milad, Fin, Judith, Johanna, Rafaela, Sabrina, Judith, Gosha, Anja, Elisabeth, Katy, Siglinde and Nicole.

A particular acknowledgment to the members of the Graduate School of Life Sciences – Dr. Gabriele Blum-Oehler, Dr. Franz-Xaver Kober, Bianca Putz, Jennifer Heilig and George Leigh – for their kind support with bureaucratic issues as well as for their extremely valid offer of symposia, seminars and workshops that helped me growing as a scientist and as a person. A special thanks to the IZKF who financially supported my PhD project.

Finally, an heartfelt thanks goes to my loved ones, my family and my friends, for all the moral support during those years. A special hug goes to my husband Giacomo, for his role of "private" scientific advisor and the more valuable role of my strongest supporter.

TABLE of CONTENTS

ABBREVIATIONS

Ab	antibody
AC	adenylate cyclase
ANOVA	analysis of variance
BCA	bicinchoninic acid
bd	bidistilled
bp	base pair
BSA	bovine albumin serum
cAMP	cyclic-adenosine monophosphate
CGRP	calcitonin gene related peptide
CNS	central nervous system
Cy	cyanine
d	distilled
DAB	3,3'-Diaminobenzidine
DAG	diacylglycerol
DAMGO	[D-Ala^2, N-MePhe^4, Gly-ol]-enkephalin
DAPI	4',6-diamidino-2-phenylindole
DOP	δ-opioid receptor
DRG	dorsal root ganglion
EM	electron microscopy
GABA	γ-amino butyric acid
GIRK	inward rectifying K^+ channel
HTS	hypertonic saline
Ic	intercalated nuclei of amygdala
IFL	immunofluorescence
IGS	immunogold-silver dots
IP_3	inositol-triphosphate
ir	immunoreactive
KOP	k-opioid receptor
MOP	μ-opioid receptor
NGS	normal goat serum
NLX	naloxone
PGP9.5	protein gene product 9.5
PKA	protein kinase A
PLC	phospholipase C

PNS	peripheral nervous system
PPT	paw pressure threshold
RNase	ribonuclease
RT	room temperature
RT-PCR	reverse transcription-polymerase chain reaction
SC	spinal cord
SDS-PAGE	sodium dodecyl sulfate-polyacrylamide gel
SN	sciatic nerve
WB	western blot
WT	wild type

SUMMARY

Opioids have been, since centuries, the gold standard for pain treatment and relief. They exert their effects after binding to opioid receptors (OP) that are expressed and functional in the central (CNS) and peripheral nervous system (PNS). As their systemic application has many side effects, including sedation and respiratory depression, a peripheral application of opioids and selective targeting of μ-OP (MOP) in nociceptive axons would be extremely beneficial. MOP presence and function has been conclusively demonstrated at nerve terminals; however it is still controversial whether functional MOPs are available on the membrane of peripheral nociceptive axons to mediate opioid-induced antinociception. While under pathologic conditions (i.e. nerve injury) exogenous as well as endogenous MOP agonists applied at the damaged nerve can elicit potent antinociception or anti-allodynia, under physiological conditions no antinociception was seen in rats. This could be caused by either a lack of functional opioid receptors in the axonal membranes or by the inability of injected opioids to cross the intact perineurial barrier and to reach nociceptors. Previous behavioral test results showed an antinociceptive effect (up to 5h) following perisciatic application of the hydrophilic DAMGO (MOP agonist) if coinjected with hypertonic saline solution (HTS; 10% NaCl), a treatment suited to open the perineural barrier. The effect was inhibited by naloxone, a MOP antagonist, documenting its specific action via MOP. Fentanyl, a lipophilic opioid, elicited an effect, which was enhanced by HTS treatment, indicating that HTS may act not only on the barrier but also directly on axonal MOP presence and/or functionality. To provide a basis for testing this hypothesis, the present work was designed to study the axonal localization of MOP in experimental animals under different conditions using molecular and morphological methods.

Initially four different commercial antibodies were tested for MOP detection. Immunoreactions with these antibodies specifically detected MOP in the hippocampus and in amygdala, while in the peripheral nervous system the reactions showed varying labeling patterns pointing towards less specificity with low signal-to-noise ratio. Double labelling with calcitonin gene related peptide (CGRP), a neuropeptide expressed in sensory fibers, with the non-compacted myelin marker S100 or with the neuronal marker PGP9.5 documented significant immunoreaction signals outside sensory nerve fibers. Therefore, none of these antibodies appeared suitable. Taking advantage of a new commercial monoclonal rabbit antibody (RabMAb) and of genetically modified mice in which the fluorescent protein mcherry was inserted in the C-tail of MOP (MOP-mcherry knock-in mice), MOP fusion protein expression in rat and mouse $CGRP^+$ sciatic nerve fibers and fiber bundles was confirmed by immunofluorescence labeling. Immunoelectron microscopic analysis indicated MOP/MOP-mcherry-localization in the cytoplasm and the membranes of unmyelinated axons organized in Remak bundles. Both antibodies detected bands of appropriate size in Western Blot in the CNS and additional larger bands in the PNS. Quantitative analyses 60 min after HTS-treatment

revealed no change in MOP mRNA in the sciatic nerve and DRG as well as no change in MOP immunoreactivity in the sciatic nerve. Thus, the opioid-induced long lasting antinociception enhanced by perisciatic injection of HTS were not due to a sustained increased MOP expression or content in sensory, putative nociceptive axons.

In summary, the current study succeeded to unequivocally document the presence of MOP protein in intact sensory axons of rat and mouse sciatic nerve. Thus, axonal MOPs may indeed mediate antinociceptive opioid effects observed in behavioral studies in naive animals possibly via activation of potassium or calcium channels. As HTS treatment does not lead to a sustained increase in axonal MOP protein or MOP mRNA expression, other mechanisms might enhance MOP function, including inhibition of MOP recycling or changes in functional coupling. Future studies should further explore the axonal mechanisms of antinociception by opioids and enhancing treatments.

ZUSAMMENFASSUNG

Opioide sind seit Jahrhunderten der Goldstandard für die Schmerzbehandlung. Sie entfalten ihre Wirkung nach der Bindung mit Opioidrezeptoren (OP), die im zentralen (ZNS) und peripheren (PNS) Nervensystem exprimiert und funktionell sind. Da die systemische Anwendung viele Nebenwirkungen hat, wie die Beruhigung und Atemdepression, wäre eine Anwendung von Opioiden und die gezielte Targeting von μ-OP (MOP) in nozizeptiven Axone in Rahmen einer Regionalanalgesie besser. Die Anwesenheit und die Funktionalität der MOP wurden zwar schon in Nervenendungen gezeigt, aber es ist noch strittig, ob funktionelle MOP in der Membran von peripheren nozizeptiven Axonen sind, um opioid-induzierte Antinozizeption zu vermitteln. Während bei Erkrankungen der Nerven (z.B. traumatische Nervenbeschädigung) exogene und endogene MOP-Agonisten Antinozizeption und Antiallodynie bewirken, konnte in gesunden Ratten kein Effekt bei perineuraler Injektion am Nerven beobachtet werden. Dies könnte entweder durch einen Mangel an funktionellen OP in axonalen Membranen verursacht sein. Alternativ könnte die mangelde Penetration der injizierten Opioide durch die Barriere des Perineuriums verantwortlich sein, die es verhindert, dass die Opioide die Nozizeptoren erreichen. Vorherige Ergebnisse aus Schmerzverhaltenstests zeigten eine Anhebung von mechanischen nozizeptiven Schwellen (bis 5 h) nach perineuraler Anwendung des hydrophilen MOP-Agonisten DAMGO, wenn dieser mit einer hypertonen Lösung (HTS; 10% NaCl) ko-injiziert war. Denn dies ist eine geeignete Behandlung, die die Barriere des Perineuriums öffnet. Der Effekt wurde von Naloxon, einem MOP-Antagonist, gehemmt, was eine spezifische Wirkung via MOP unterstützt. Die Wirkung von Fentanyl, einem lipophilen Opioid, wurde ebenfalls durch die HTS-Behandlung verbessert. Das führt zu unserer Hypothese, dass HTS nicht nur die Schranke öffnet, sondern auch direkt Expression und/oder Funktionalität von axonalen MOP verbessert. Um eine

Grundlage für die Untersuchung dieser Hypothese zu schaffen, war das Ziel dieser Arbeit, die axonale MOP bei Versuchstieren unter verschiedenen Bedingungen mit molekularen und morphologischen Methoden zu charaktiersieren.

Am Anfang wurden vier verschiedene kommerzielle Antikörper für die Erkennung der MOP getestet. Immunreaktionen mit diesen Antikörpern wiesen spezifisch MOP in dem Hippocampus und in der Amygdala nach, während im peripheren Nervensystem die Immunreaktion veränderliche Markierungsmuster und weniger Spezifität mit einem ungünstigeren Signal-zu-Hintergund Verhältnis zeigte. Die Doppelmarkierung mit calcitonin gene-related peptide (CGRP), einem Neuropeptid, das in sensorischen Fasern exprimiert ist, mit dem Marker für non-compacted Myelin S100 oder mit dem neuronalen Marker PGP9.5, bestätigte ein reproduzierbares Färbemuster außerhalb sensorischer Nervenfasern. Deshalb war keiner dieser Antikörper geeignet.

Mit der Anwendung eines neuen kommerziell erhältlichen monoklonalen Kaninchen Antikörpers (RabMAb) gegen MOP sowie gentechnisch veränderten Mäusen, bei denen das fluoreszierende Protein mCherry in das C-terminale Ende von MOP eingefügt wurde (MOP-mcherry knock-in Mäusen), wurden MOP und das MOP-Fusionprotein im CGRP+ im Ischiasnerv und Fasernbündeln durch Immunfluoreszenzmarkierung von Ratten und Mäuse bestätigt. Die immunelectron-mikroscopische Analyse zeigte MOP/MOP-mcherry im Zytoplasma und der Membran unmyelinizierter Axone, die in Remak Bündlen organisiert sind. Beide Antikörper erkannten Banden in richtige Größe in Western Blot in ZNS und mehrere größere Banden in PNS. Quantitative Analysen 60 min nach HTS-Behandlung zeigten keine Veränderung in MOP mRNA in dem Ischiasnerv und Hinterwurzelganglion sowie keine Veränderung in der MOP-Immunreaktivität in dem Ischiasnerv. Daher müssen noch weitere Ursachen für die verbesserte Wirkung von Opioiden am Nerven nach HTS in Betracht gezogen werden.

Zusammenfassend konnte diese Studie die MOP-Proteins in intakten sensorischen Axonen des N. ischiadicus der Ratte und Maus eindeutig nachweisen. Axonale MOPs könnten über Kaliumkanäle oder Calciumkanäle in den Verhaltenstests bei naiven Tiere antinozizeptiv wirken. Da die HTS Behandlung zu keiner deutlichen Steigerung von axonalem MOP-Protein führen kann, sollten anderen Mechanismen wie MOP-Recycling oder Veränderung der intrazellulären Singaltransduktion untersucht werden, die die Funktionalität von MOP erhöhen. Zukünftige Studien ferner den genauen Mechanismus klären, wie axonal Opioide antinozizeptiv wirken, um so die Behandlung von Schmerzen mit Regionalanalgesie weiter zu verbessert.

1. INTRODUCTION

1.1 Opioids and opioid receptors

In their very long history across centuries and cultures, opioids have always played – and still are playing – an important role in human life and society. Evidence of opioid use and cultivation date back to Sumerians (4000 b.C.), that employed "*Hul gill*" – the "*joy plant*" – for its euphoria-inducing effect. From Mesopotamia the use of opium spread throughout the ancient world and the major European and Asian civilizations that knew it with the name opium, from the Greek word "*opos*" that means "*juice*"[1, 2].

The first records of the use of opioids as an analgesic are ascribed to Paracelsus in the XVI century. He prescribed laudanum, a mixture of opium and other drugs, as pain relief after surgery [3]. From that moment on physicians started to overestimate the opium potency and started to prescribe it, at time indiscriminately, to cure any disease [3], leading to an increased number of addicted people [2]. However, Sertürner isolated the active ingredient in opium only at the beginning of the 19th century and named it morphine. This discovery led to the commercial production of morphine both in England and in Germany and an increased use of morphine in clinical practice. The invention of the hypodermic syringe by Wood in 1855 promoted the use of morphine also for small surgery, post-operative and chronic pain [2]. Due to a lack of regulation on opioid use until the first decades of the 20th century, the use of natural morphine-like opioids, such as the newly discovered codeine and the synthetized heroin, increased exponentially. To combat this development, certain states introduced laws to regulate the production and distribution of opioids [3]. In the middle of the ´50, the heightened awareness of surgeons to opioid addictive effects led to the introduction of several morphine derivatives and encouraged researchers to the discovery of opioid antagonists (i.e., substances able to inhibit opioid effects). In parallel, in the early 1950s the observation of opioid side effects, such as nausea, respiratory depression, constipation, dependence and tolerance, led to hypothesized presence of different opioid receptors [2, 3].

1.1.1 Opioid receptors

The existence of receptors for opioids (OPs) and opiate compounds – substances derived from *Papaver somniferum* - were first postulated in 1973 from three independent teams in an attempt to explain the binding of opioid to the brain membrane. Only a few years later the opioid binding sites were identified and named by Martin, Kosterlitz and Lord as mu, delta and kappa, depending on their pharmacological properties [4-6]. The first receptor gene, corresponding to the delta receptor, was isolated, characterized and cloned only in 1992 by Evans and colleagues [7]. Within ten years, the

other two receptors - mu and kappa - and the endogenous opioid system were completely characterized on a molecular level [4].

1.1.1.1 Opioid receptor structure

Thanks to the cloning and the subsequent molecular studies, opioid receptors are now clearly classified as 7-transmembrane domain receptors (Fig. 1A) belonging to the rhodopsin-G-protein coupled receptor (GPCR) family (Fig. 1B).

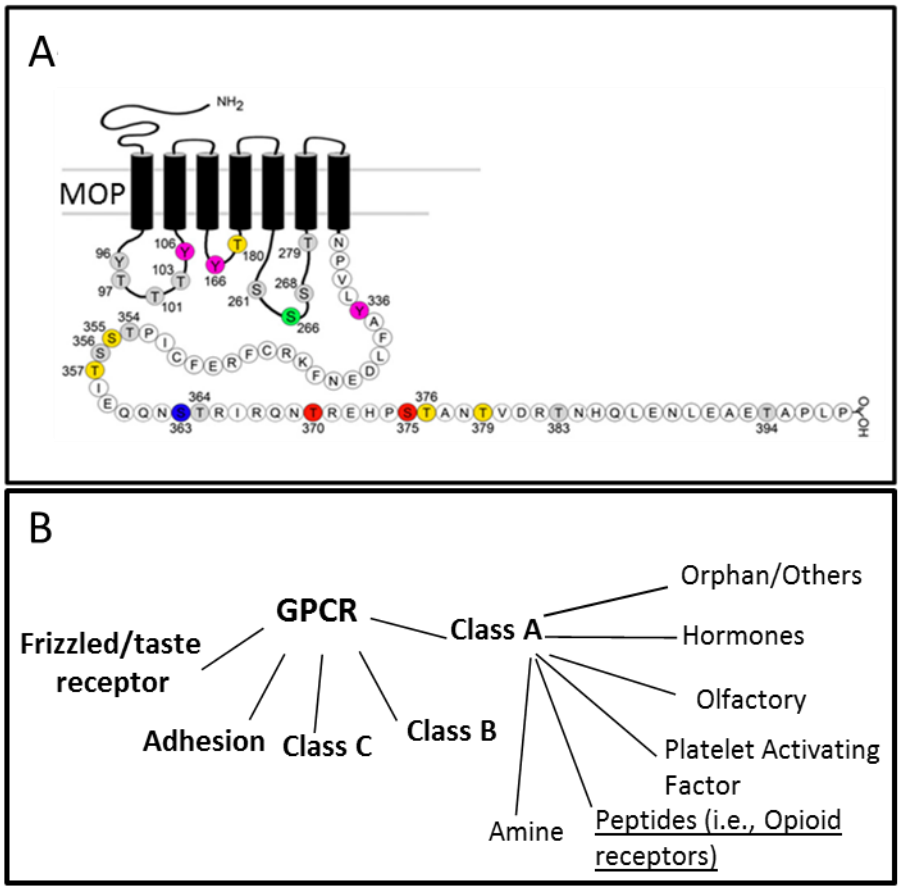

Fig. 1: Structure of MOP and scheme of the GPCR family. (A)Seven-transmembrane structure of MOP. The extracellular N-terminal tail is responsible for receptor selectivity while the intracellular C-terminal tail determines the interaction between the receptor and the GPCR. Colours indicate putative and established agonist-induced phosphorylation site and relative kinases. Image from Williams et al, 2013. (B) Opioid receptors belong to the rhodopsin-like receptor family (Class A) and represent only a small part of the large GPCR family. Modified basing on Tadevosyan et al, 2010 and www.gpcr.org

Mu, delta and kappa opioid receptors, recently named by IUPHAR (International Union of Basic and Clinical Pharmacology) as MOP, DOP and KOP [8], are encoded by three different genes: *Oprm1*, *Oprd1* and *Oprk1*, respectively. They share a high grade of homology, with up to 60% of identity in the amino acid sequences: the highest similarities can be found in the opioid binding pocket, localized in the transmembrane domains TM3, TM6 and TM7 [9].

In contrast, extracellular domains are highly divergent among different OPs: the three extracellular loops and the N-tail are responsible for receptor selectivity, while the intracellular C-tail is important for determining the interaction between the receptor and a specific GPCR [4, 10]. The three receptors demonstrate different affinity to the three endogenous opioid peptides – endorphins, enkephalins and dynorphin – synthetized *via* cleavage of the precursor proteins. MOP exhibits a high affinity for endorphin and a moderate affinity to enkephalin. DOP is characterized by the highest affinity to enkephalin and a high affinity for endorphin. Dynorphin presents preferable binding to KOP but possesses also a moderate MOP and DOP specificity [11].

Other structural and affinity differences between MOP, DOP and KOP and within the same OP-type are due to alternative splicing, dimerization and post-translational modification, as phosphorylation, glycosylation and methylation. Gene polymorphisms are also frequently occurring [11-13].

1.1.1.2 Opioid receptor expression

During the last decades, several studies using immunofluorescence staining, electron microscopy, *in situ* hybridization and behavioral tests revealed localization of OPs and expression in the central and peripheral nervous system as well as in non-neural tissues (e.g., vascular endothelium, cardiac muscle, immune cells) of mice and rats (Table 1). While the localization of opioid receptors in the central and sensory peripheral nervous system has been widely studied and confirmed in experimental animals, the functional role of opioid receptor in sympathetic fibers and immune cells still needs clarification [11, 14, 15]. A similar localization pattern was also seen by autoradiography, immunohistochemistry and electron microscopy on human tissues as well as by clinical research activities [16-18]. However, it is worthwhile to remember that OP expression and distribution varies significantly among different organs and species [19].

	Central nervous system (CNS)	**Peripheral nervous system (PNS)**	**Non-neural tissue**
MOP	neocortex, caudate-putamen, nucleus accumbens, thalamus, hippocampus, amygdala, brain stem, spinal cord	peripheral sensory neuron, dorsal root ganglia (DRG), peripheral nerve	vascular endothelium, cardiac epithelium, keratinocytes, vas deferens, Sertoli cells, spiral ganglia, oocyte, immune cells, kidney, lung, spleen, stomach, duodenum, jejunum, proximal and distal colon
DOP	olfactory-related areas, neocortex, caudate – putamen, nucleus accumbens, amygdala	peripheral sensory neuron, DRG	Stomach
KOP	caudate – putamen, nucleus accumbens, amygdala, neural lobe of the pituitary gland	peripheral sensory neuron, DRG	stomach, duodenum, jejunum, proximal and distal colon

Table 1: Area with significant localization and expression of OPs. Expression of MOP, DOP and KOP is comparable both in different areas of the brain and in peripheral nervous system. In non-neuronal tissue the localization of MOP has widely been studied, little is known about DOP and KOP [14-16].

OPs have a preferential subcellular localization. MOPs are mostly localized on the plasma membrane of neurons (dendrites, soma, axon terminals) while DOPs have a prevalent intracellular distribution both in dendrites and soma. KOPs are mainly localized in the cytoplasm but can also be present at the plasma membrane or in vesicles [10]. The differential subcellular localization suggests that the regulation of their trafficking is likely to be different [10].

A different intracellular localization – i.e. in the soma, dendrites or terminals – of OP also has a different functional action. For example, the activation of MOP when localized in the somatodendritic compartment decreases neuron excitability, whereas the engagement of MOP when localized in the axon terminal inhibits the release of neurotransmitters [20]. Moreover, MOP-mediated effects can be very different depending on the neuraxis compartment involved. Supraspinally, several structures play a role in morphine analgesia, including the locus coeruleus, nucleus raphe magnus, periaqueductal gray, medial thalamus, and limbic structures. At the spinal level, opioid action involves the dorsal horn where the receptors are both pre- and postsynaptic. The presynaptic ones are associated with the axons entering the dorsal horn from the DRG and from descending pathways. The DRG neurons also extend into the periphery where the presynaptic receptors on the axon terminals modulate peripheral opioid analgesia [21].

This widespread localization indicates the pivotal role played by opioids and OPs in pain management and modulation. Among the three opioid receptors, MOP is the most important for pain treatment and analgesia since it binds to morphine and all other clinically used opioids. Several selective drugs

have also been generated and extensively tested for DOP and KOP, but none of them have entered clinical practice so far [21].

1.1.1.3 Opioid receptor activation and mechanism of action

Opioid receptors mediate many of their cellular and physiological effects by coupling to G-proteins both in the soma, on the plasma membrane and at the terminals of nociceptive neurons.
G-Proteins are heterotrimeric complexes consisting of α, β and γ- subunits; after activation the G-protein dissociates in α monomer and βγ dimer. Based on the characteristics of their α-subunits, G-proteins have been classified into four families: G_i (also known as $G_{i/o}$), G_q, G_s and G_{12} [22, 23]. Each of them shows differences in its patterns of expression [23].

OPs bind to different inhibitory-type Gα (G_i) subunits [24]. Binding to a specific $G\alpha_i$ subunit and the downstream pathway highly depends on the specific MOP agonist. Thereby different agonists can selectively activate one or more of these pathways giving rise to multiple agonist-selective signaling pathways through a single receptor subtype. This phenomenon is known as “biased agonism” or “functional selectivity” and refers to the ability of different agonist to either differentially activate signaling cascade or regulatory events, including differences in receptor trafficking [20, 24]. Furthermore, the cellular environment, the different proteins expressed in close proximity to the GPCRs, the variable combination of G-proteins subtypes across cell types as well as the capacity of OPs to form homo or heterodimers greatly increases the number of possible G protein-associated signaling pathways [4, 20, 24, 25].
OP activation results 1. in a short-term inhibition of neuronal activity that are G-protein-dependent and 2. In a long-term alteration of gene expression, which are G-protein- independent [4]. The majority of players involved in MOP-dependent signaling are summarized in Fig. 2 [20].

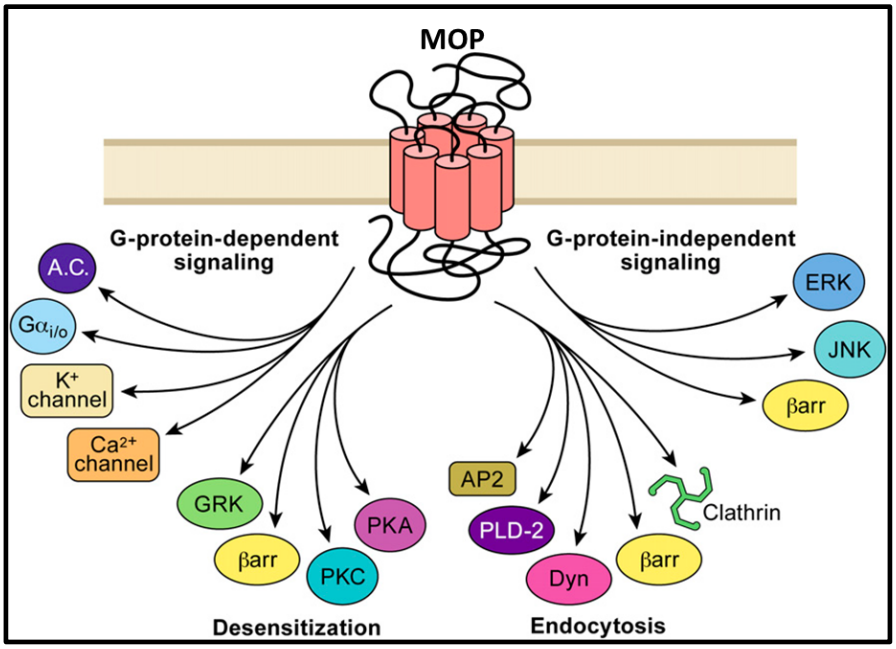

Fig. 2: Pathways activated by agonist binding to OP. G-protein dependent and independent signaling lead to the activation of different mechanisms involved in the inhibition of pain propagation, receptor endocytosis or transcriptional mechanisms [20].

G protein-dependent processes are characterized, after ligand engagement, by a GDP/GTP exchange inducing the dissociation of the trimeric GPCR in two subunits – Gα and Gβγ. The receptor turns back to the inactive state when the intrinsic GTPase activity of α subunit hydrolyses GTP to GDP and drives the trimeric structure reconstitution. This activation mechanism is shared by all G-protein and it is independent of the α-subtype family. However, most agonists with antinociceptive effects – i.e. opioids, cannabinoids, baclofen and acetylcholine – acting on class A or C of GPCRs, are coupled to inhibitory $G_{i/o}$ proteins [20, 23].

After agonist binding to GPCR, the Gα subunit inhibits the enzyme adenylate cyclase (AC), leading to a reduction of intracellular cyclic-adenosine monophosphate (cAMP). cAMP levels regulate the activity of ion channels, mainly potassium and calcium channels, and of protein kinase A (PKA). Ion channels and AC are also regulated by the Gβγ subunit; moreover, the Gβγ subunit determines the activation of phospholipase C (PLC), with the subsequent production of inositol-triphosphate (IP_3) and diacylglycerol (DAG) [20]. G protein-independent processes include signalling through many proteins, such as mitogen activated protein kinase (MAPK, e.g. ERK and JNK), that drive gene regulation and transcription [20].

Overall, OPs engagement by opioids leads to a GPCR- mediated increase of K^+ and a decrease of Ca^{2+} channel flux, with a decrease of nociceptive propagation. Activation of inward rectifying K^+ channels (GIRK channels) plays a critical role in maintaining resting neuronal membrane potential and reduces hyper-excitability, while the inhibition of voltage-dependent Ca^{2+} results in a decrease in presynaptic Ca^{2+} entry and inhibition of neurotransmitter release [25, 26].

After agonist activation, the receptor is phosphorylated by GPCR kinases (GRKs); the sites and the grade of phosphorylation depend on the agonists and their ability to promote interactions between the receptor and different intracellular kinases [24]. Phosphorylation induces the uncoupling of the receptor from the G protein, leading to the association between the receptor and β-arrestin. β-arrestin, in turn, interacts with clathrin to drive receptor endocytosis. After internalization into endosome, the receptor could be recycled or degraded, but both mechanisms lead to desensitization of receptor signaling [26, 27].

1.1.1.4 Opioid receptor visualization

In order to visualize OP localization and expression, different approaches can be used. Autoradiography, largely employed in the 1980s and 1990s [10], demonstrated the presence of MOP in CNS: Moyse and colleague showed MOP in the locus coeruleus [28] and recent ultrastructural immunolabeling studies supported MOP localization in spinal cord [29] and amygdala [30, 31]. MOP expression in nociceptors was also confirmed: using electron microscopy Coggeshall and colleagues [32] demonstrated the localization of MOP in unmyelinated cutaneous sensory axons, while Sanderson [33] indirectly provided evidence for the presence of MOP in DRG and primary afferent nociceptors showing co-localization of substance P and endomorphine, a tetrapeptide with high affinity for MOP. Immunohistochemistry studies using immunoenzyme reaction [34] and immunofluorescence also demonstrated MOPs localization in the brain, spinal cord [35], DRG [36] and in injured sciatic nerve [37].

In all immunohistochemical techniques, the validity of the results largely depends on the specificity and affinity of the antibodies [10]. A recent paper by Michel [38] highlighted the lack of sensitivity for many antibodies against GPCRs. One possible explanation for this lack is the high degree of homology of the conserved region of GPCRs, which allows the antibodies to recognize different subtypes within the same or between different GPCR families. However, the antibody directed against a less conserved region (i.e. N- or C-tail), could also lack specificity. Therefore, he pointed out the necessity to define new criteria to test antibody specificity and selectivity, such as using knock-out mice.

Several commercial specific antibodies recognizing each type of opioid receptor are available and have been characterized by different groups [10]. Some of them, however, demonstrated a tissue-dependent specificity [39], showing reliable labeling in the spinal cord but not in DRG. Fluorescent epitope-tagged receptors artificially introduced into animals using the knock-in technique or viral vector represent an advantageous approach to study opioid localization and avoid problems related to antibodies. Scherrer and colleagues [40] created a knock-in DOP-EGFP mouse to study the localization of DOP in the brain, spinal cord and DRG. A similar approach was recently developed to study MOP localization and MOP-DOP co-localization in central and peripheral nervous system in a

single or double knock-in mouse, respectively [41]. MOP was fused to the mcherry protein and visualized as a red fluorescence.

1.2 Opioids and pain

Pain is defined by the International Association for the Study of Pain (IASP) as an *unpleasant sensory and emotional experience associated with actual or potential tissue damage, or described in terms of such damage*.

It is therefore clear that the process of pain is not a simple naturally-occurring protective mechanism, but rather a more complex phenomenon, characterized by multidimensional aspects linked to the presence of real damage as well as to an individual and personal perception.

1.2.1 Pain classification

Distinguishing between different types of pain is critical for proper treatment. A first distinction, based on the duration of the pain, identifies acute and chronic pain. Pain due to injuries and post-operative flares is classified as acute pain. Chronic pain can be wider and last for several months. Pain can also be classified – according to the source of pain generation – as nociceptive, inflammatory and pathological pain.

Nociceptive pain is a physiological protective system, essential to detect and minimize contact with damaging or noxious stimuli. It is mediated by nociceptors activated at the site of injury or tissue damage. Inflammatory pain also has a protective role and it is caused by the activation of the immune system in response to tissue injury or infections. Pathological pain, instead, is not protective. It is due to an abnormal functioning of the nervous system and it is therefore named as maladaptive pain. Two types of pathological pain can be identified: neuropathic and dysfunctional or chronic. Neuropathic pain is defined by IASP as a pain caused by a lesion or disease of the somatosensory nervous system. It can be provoked by an infectious agent, a metabolic disease or a lesion that directly involves central or peripheral nervous system, i.e. spinal cord injury, stroke, diabetes, cancer-induced nerve compression or chemotherapy. Dysfunctional pain is characterized by a hypersensitivity in the absence of nerve injury or inflammation.

Changes in the expression of neuronal ion channels, neurotransmitters, peptides and their receptors are common in all type of pain [42, 43].

1.2.2 Pain pathways and transmission

Pain arises from multiple pathophysiological processes in the nervous system at the peripheral, spinal and supraspinal level starting from the primary afferent (or sensory) neurons. Indeed, if the depolarization driven by a mechanical, thermal or chemical stimuli reaches a critical threshold, an

action potential is propagated from the free ending of nociceptors along the length of the sensory fiber toward the dorsal horn of the spinal cord, where the primary synapse occurs and the signal is modulated – either enhanced or decreased - and then propagated to the thalamus (spinothalamic tract) [44]. From here different areas, as somatosensory cortex, anterior cingulate, prefrontal cortex and amygdala, are activated [45]. The pain information is then processed. The descending inhibitory pathway independently projects to the dorsal horn of the spinal cord where the release of inhibitory neurotransmitters like glycine, γ-amino butyric acid (GABA) and endorphins inhibits pain signals. A graphical representation of the ascending pain pathway is shown in Fig. 3.

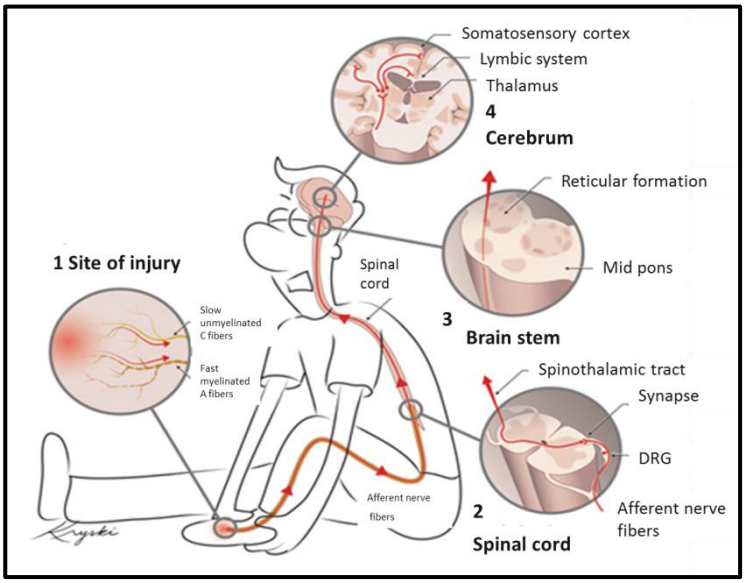

Fig. 3: Ascending pain pathway. The image modified from Krysky Biomedia shows the pain transmission pathway. From the peripheral site of injury (1), the pain is transmitted through afferent nerve fibers to the DRG and the spinal cord (2). The stimuli propagation continues along the brain stem (3) till the cerebrum (4), where the thalamus is located. Here a second synapse occurs and the stimulus is propagated in the somatosensory cortex and in the limbic system.

As mentioned above, the first component of the sensory pathway is the nociceptors. They are all pseudo-unipolar neurons: the cell bodies (somata) of all nociceptors are found in the dorsal root ganglion (DRG) located within the intervertebral foramen (Fig. 4A) and the two branches of their single process – called primary afferent fibers – project into the periphery and to the spinal cord, relaying sensory information coming from the periphery to the CNS [46-48]. The soma of all neurons synthesizes and transports the substances needed for neuronal function to the axon terminals, including receptors, ion channels, as well as molecules essential for synaptic transmission [49]. Opioid receptors and MOP mRNA are also synthesized in the DRG and transported to peripheral terminals of peripheral afferent neurons [50].

Afferent fibers have been classified in four general fiber types – C, Aδ, Aβ, and Aα or proprioceptors. They can be differentiated by soma size, degree of myelination, types of afferent

endings and the laminar targets of their efferent terminals in the spinal cord. Although this classification is reductive – as it disregards the molecular and functional diversity of somatosensory neuron subtypes [51] – it is still largely used.

Sensory neurons giving rise to Aα and Aβ fibers, also called primary afferent neurons, are characterized by a large cell body (>50 µm). The thick myelin around the axon allows for a rapid conduction of muscle contraction stimulus (Aα) and of mechanical stimuli such as touch and vibration (Aβ). Noxious stimuli of mechanical, thermal, chemical origin are transmitted by Aδ- and C-fibers, which are identified as nociceptors. Aδ are small-myelinated fibers issued from medium size cell bodies deputed to transmit noxious or innocuous stimuli (temperature, force and irritants) and to mediate the "first" pain perceived as rapid and sharp. C-fibers are, instead, small unmyelinated fibers comprising afferent and visceroefferent (sympathetic) fibers. Afferent C fibers are issued from small cell bodies (10-25 µm), which are the most abundant type of sensory neurons. Nociceptive C-fibers mediate the so called "second" pain: delayed, diffuse and dull [26, 49, 52] (Fig. 4B).

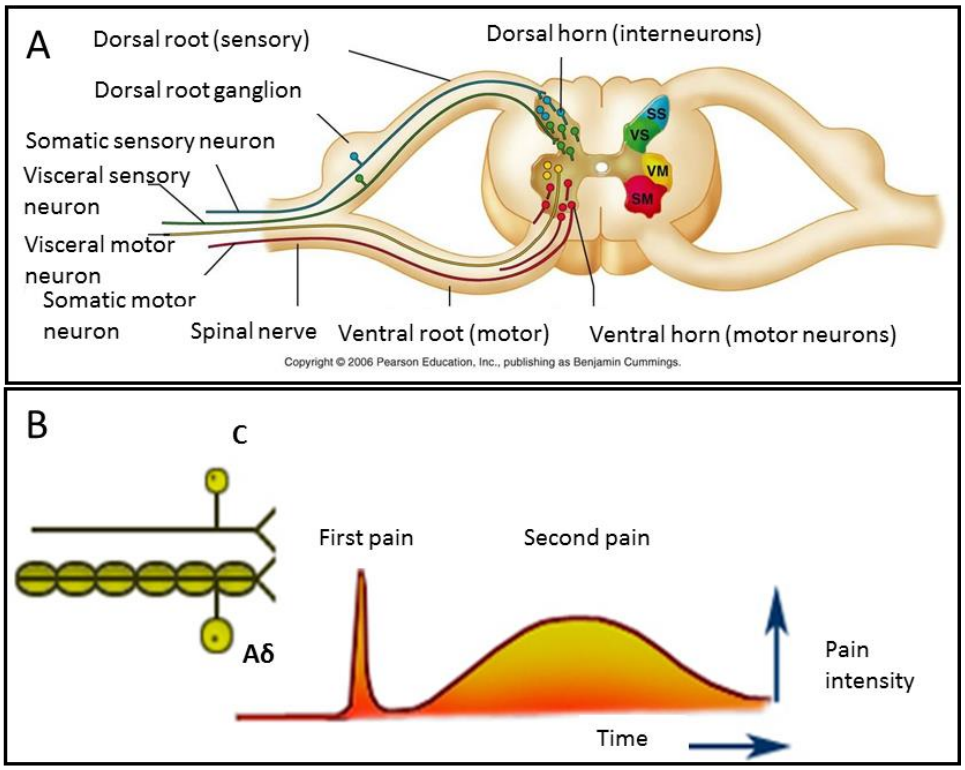

Fig. 4: DRG and pain mediation. (A) Representative image of DRG structure indicating the localization of neuron soma and axon projection into the spinal cord and to the periphery; (B) Aδ- and C-fiber pain mediation (modified from: NIH Pain Consortium).

The DRG neurons that give rise to sensory C-fibers can be divided into two groups: peptidergic neurons release neuropeptides like substance P (SP) and calcitonin gene-related peptide (CGRP). They are responsive to nerve growth factors (NGF) through the expression of trkA (tropomyosin-

receptor-kinase) receptors. In the second group, neurons are non-neuropeptide-releasing (defined as non-peptidergic neurons) but are characterized by isolectin B_4 (IB_4) binding sites [51, 52]. They are responsive to glial cell line-derived neurotrophic factor (GDNF). This classification is commonly accepted but in the last years there is evidence of colocalization between CGRP and IB_4 in the same fiber. Price and Flores findings [53] illustrated a substantial overlap (45%) between peptidergic and non-peptidergic neurons in adult rat DRG. Partial overlap (10-20%) was also observed in the superficial dorsal horn of the spinal cord [54] where both peptidergic and non-peptidergic fiber terminate. It is also important to further note that the expression of CGRP is not restricted to nociceptive C fibers [52, 53, 55], but can be present also in other fiber types [53] like small myelinated nociceptive Aδ fibers [56] and mechanoreceptors (Aα and Aβ fibers) localized in the hair-follicle unit or in the muscle-spindle afferent unit [57].

1.2.3 Pain treatment

The World Health Organization (WHO) classified three grades of pain: mild, mild to moderate and moderate to severe. This results in a step-wise treatment algorithm (ladder for analgesics). Opioids are suggested to treat moderate to severe pain, like intraoperative, postoperative pain and cancer pain. The treatment of chronic non-cancer pain with opioids is only recommended in certain situation for specific diseases like diabetic polyneuropathy [58]. Due to their effectiveness in inducing analgesia in inflammatory pain, opioids are largely used in clinical practice even though they can lead to serious CNS-mediated side effects, as respiratory depression, sedation nausea, addiction and tolerance after systemic. Those side effects can be avoided by spinal administration of opioids [13]. However, a peripheral and local application of opioids would be even more advantageous. Regional anesthesia, the injection of local anesthetics in subcutaneous tissues, is clinically used to treat intra- or post-operative pain. Despite the great efficacy in pain inhibition due to block of sensory fibers by local anesthetics, it has the main disadvantage of blocking also motor fibers, hampering patient´s active movements e.g. active physiotherapy postoperatively. Therefore, specific targeting of sensory nociceptive fibers would be advantageous.

The local application of opioids appears even more relevant if we consider that many syndromes depend, on a different degree, on the peripheral activation of nociceptive neurons [13]. Moreover, the conclusions of recent studies suggests that systemically (intravenously and orally) and centrally injected opioid agonists may act through peripheral OPs [58, 59], which opens new perspectives and indirectly supports the local use of opioids. In contrast, Khalefa and colleagues [60] argued against efficacy of local application of opioid in inflammatory condition and showed a higher antinociceptive effects after systemic administration of fentanyl or morphine.

Other studies showed that peripheral opioid application is particularly efficient in treating pain associated with inflammation or neuropathic pain induced by nerve injury [37, 61]. In neuropathy or inflammation different mechanisms might account for the increased peripheral opioid efficacy: opioid receptor levels along the nerve are upregulated [62] and the transport of OPs from DRG to the nerve is accelerated [63]. Better coupling of receptors to signaling pathways was also discussed by Zöllner and colleagues [34] in the presence of sciatic nerve ligation and inflammation induced by an injection of Freund´s complete adjuvant in the paw. Under these particular conditions, an increase in MOP-specific binding sites in the DRG and the sciatic nerve was observed both for full and partial agonists of MOP. The disruption of the perineurium [64] also facilitates the access of MOP agonists to their receptors [65, 66].

On the contrary, the perineurial application of opioids in non-inflammatory conditions and on uninjured nerves does not reliably induce analgesia [67]. This may be due to two reasons: 1. MOPs may not be present and/or functional in intact afferent fibers if the mechanisms activated by inflammation (i.e. up-regulation of MOP, enhanced efficacy of MOP agonist [34]) are not present, and/or 2. the integrity of perineurium may limit the access of opioids in the nerve.

1.2.4 Opioid receptor agonists and antagonists

OPs agonists represent a large class of natural, semi synthetic and synthetic opioids. They are mostly used for clinical application, namely analgesia, relief of gasping or cough depression [68], but are also employed in research to study pain and pain treatment. Among the opioids, morphine is the best known natural opioid. In 1937 meperidine, the first synthetic opioid, was produced from its central chemical structure. In the following years the synthesis of new compounds increased, leading to a wide range of synthetic OPs agonists and antagonists [69, 70].

Based on their nature opioids are classified as natural, semi synthetic and synthetic opioid. Morphine and thebaine represent natural opioids. Codeine, oxycodone and hydrocodone are classified as semi-synthetic opioids while methadone, tramadol, fentanyl and its derivates – sufentanyl and remifentanil – belong to the synthetic class. Further important synthetic compounds are DAMGO, naloxone and naltrexone. DAMGO is a strong agonist of MOP and used only in research; naloxone and naltrexone are two potent antagonists of MOP and are used in the clinic to contrast serious side effects of opioids as well as in research.

A second classification, based on the opioid analgesic efficacy, is used in the clinic. Tramadol, codeine and hydrocodone are classified as “weak opioids”; morphine, methadone and oxycodone are considered median analgesic properties while fentanyl and derivates are considered the strong opioids [69].

1.3 Sciatic nerve

The sciatic nerve is the longest and thickest nerve both in humans and rodents. Due to both its size and the ease in locating and handling it, the sciatic nerve is the most widely used peripheral nerve for nerve injury and regenerative experimental studies [71]. The sciatic nerve is also relevant for behavioral studies and functional test, since it innervates the posterior paw, more easily tested compared to the frontal paw.

1.3.1 Sciatic nerve structure and perineurial barrier

The sciatic nerve is a mixed nerve containing somatomotor axons projecting from the ventral horn motoneurons to leg muscles, sensory axons with their cell bodies in DRGs (see section 1.2.2) and postganglionic visceroefferent axons arising in the sympathetic ganglia [72, 73]. In the rat, somatomotor and somatosensory fibers originate from motoneurons and DRG neurons of segments L4-L6. The nerve branches distally into two portions which give rise to the common peroneal, the tibial and sural nerve, respectively (Fig. 5).

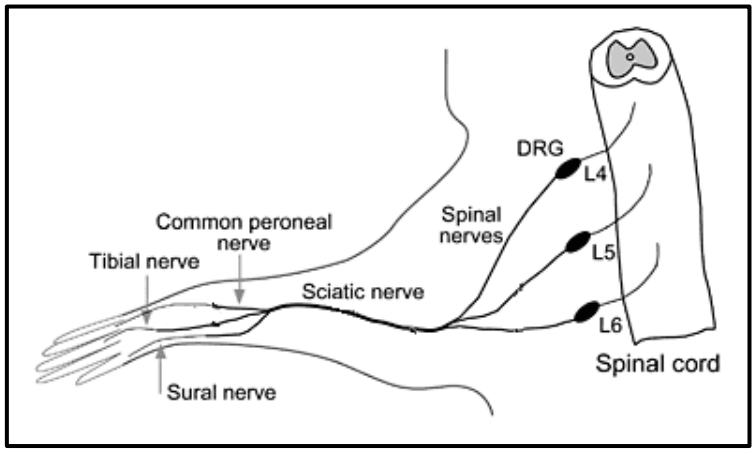

Fig. 5: Sciatic nerve of rat. The three spinal nerves coming from lumbar DRG L4, L5 and L6 first join to form the sciatic nerve, which after 7-10 mm splits again into tibial, sural and common peroneal nerve. Image modified from [74].

1.3.1.1 Fiber type composition

As a mixed peripheral nerve, the sciatic nerve contains all fiber types described above. Each sciatic axon, irrespective of its function, possesses a glial sheath made by Schwann cells, the typical glia of the peripheral nerve, which are essential in maintaining normal axonal function [75]. Two types of Schwann cells can be distinguished: myelinating or non-myelinating. Schwann cells that form myelin are very large cells and ensheath single motor fibers or large sensory fibers (i.e., Aδ) forming several concentric layers of compact myelin. The thickness of this layer is directly related to the dimension of the fibers: the larger the fibers, the more layers of myelin are formed by the Schwann

cell. The non-myelinating Schwann cells ("Remak cells") do not form myelin, but rather ensheath a group of small sensory (unmyelinated) axons (C-fibers), each one usually surrounded and separated from the other axons of the bundle by narrow cytoplasmic extensions of the non-myelinating Schwann cell, creating the Remak bundle [76].

An early study on the sciatic nerve fiber composition in the rat reported approximately 27000 axons, of which 6% were myelinated motor axons, 23% and 48% were myelinated and unmyelinated sensory axons, respectively, and 23% were unmyelinated sympathetic axons [73]. A differential analysis of the presumably nociceptive Aδ myelinated afferent fibers was not carried out.

In the sciatic nerve trunk, Remak bundles were shown to contain a mean of 5-7 unmyelinated axons. Individual Remak bundles in rat sciatic nerve were shown to contain different types of C-axons, including CGRP- and/or IB4-positive sensory, presumably nociceptive, and sympathetic efferent axons [77, 78]. Based on immunoelectron microscopic evidence, the contribution of CGRP-immunoreactive (ir) axons to the total population of unmyelinated fibers was estimated to be near 40% (36,46±9.01%), and there were 2.1 ± 0.5 CGRP-ir axons found per C-fiber bundle [78], indicating that Remak bundles transporting nociceptive information can be quite reliably identified by CGRP-immunolabeling.

1.3.1.2 Nerve sheaths

Each peripheral nerve is ensheathed by three connective tissue sheaths, named epineurium, perineurium and endoneurium. The epineurium forms the external sheath and wraps the entire nerve. It is composed of connective tissue containing elastic fibers protecting the nerve from damages due to strong tractions while having no barrier function. Within the connective tissue, vessels run parallel to nerve fibers and create a capillary net that branches to the inner layer of the nerve fasciculus [79].

The middle layer, which forms the fiber fascicles, is represented by the perineurium. It is thinner than the epineurium in some tissues and is mainly composed of 10-15 concentric layers of flat perineurial cells. They are connected with each other through tight junctions and are enclosed by a collagen- and laminin-containing basal lamina. The extracellular matrix, composed of microfibrillar collagen and fibronectin, is present between the perineurial cell layers, providing the ability to modulate external stretching forces. The inner and thinnest layer, called endoneurium, is composed of connective tissue branching from the perineurium towards the axons. Every single nervous fiber consisting of the axon, its glial sheath formed by Schwann cells, and the Schwann cell basement membrane covering the entire outer surface of the fiber, is wrapped in a net of reticular fibers immersed in a glycoprotein matrix and thin collagen fibrils. All nerve sheath layers become gradually

thinner in the proximodistal course of the nerve and its branches until they disappear at the nerve endings [79-81].

Among the three layers, the perineurium is essential for protecting axons and the associated Schwann cells. It is, indeed, a tight and selective barrier that acts as a metabolically active diffusion barrier, which regulates and maintains the homeostasis of the endoneurium [80-82]. It also acts as an ionic barrier [80] hampering the access of proteins, toxins and pathogen agents to the nerve.

However, the presence of the perineurial barrier is not always advantageous: if on one side the perineurial barrier serves as protection, on the other hand it simultaneously inhibits the delivery of analgesic drugs to the peripheral nerve, preventing local or regional analgesia [66]. This is strongly supported by several experimental studies in which opioids, injected in inflamed and non-inflamed tissue showed a different efficacy. In inflammation opioids are more effective [83]. In contrast, in non-injured tissues, lipophilic opioids like fentanyl have moderate access to opioid receptors, while hydrophilic opioids like DAMGO hardly have an effect [65, 66, 84, 85]. This reduced efficacy of opioids applied in the vicinity to the nerve has been ascribed to tight junctions hampering their access. The opening of the tight junction or the decreased expression of tight junction proteins during inflammation has been correlated with a higher permeability of the perineurium, thus increasing the fraction of opioids reaching receptors and inducing analgesia [86, 87]. It is therefore clear that opening the perineurial barrier is key to extending analgesic opioid effects. A promising strategy is to open the perineurium using a hypertonic solution [86, 88].

1.4 Hypertonic solution

Several studies reported hypertonic solutions, NaCl or mannitol, as a methods to reversibly open barriers to enhance the diffusion of water-soluble drugs (i.e. hydrophilic opioids), peptides and antibodies both into the brain [89] and into peripheral nerves [65, 66]. The enhanced diffusion through the perineurial barrier could target MOP in axons, which are constitutively localized on the axonal membrane of peripheral sensory-nociceptive neurons. Hypertonic solution would not only allow lipophilic drugs as fentanyl, but also with the synthetic hydrophilic agonist [D-Ala2,N-Me-Phe4,Gly5-ol]-enkephalin (DAMGO) to elicit antinociception. This will open new possibilities for regional pain treatment, avoiding the side effects related to the systemically administration of opioid, as well as selectively targeting nociceptive neurons, avoiding motor impairment.

Previous results from our lab [90] demonstrated an HTS-mediated enhancement of opioid analgesia: while treatment with DAMGO alone was ineffective, perisciatic co-injection of HTS enhanced analgesia (Fig. 6A). Further results were reported using fentanyl (Mambretti EM et al, 2015, accepted). Even if this drug is able to cross the perineurial barrier due to its lipophilic nature, a high concentration is needed to obtain analgesic effects. Co-injection of fentanyl with HTS (Fig. 6C)

allowed for a tenfold dose reduction to achieve the same grade of antinociception. Opioid antinociception enhanced by HTS was prevented through treatment with naloxone, a MOP antagonist (Fig. 6B, D, respectively). These finding thus not only suggest an increased permeability of the perineurium, but also a possible role of HTS in increasing MOP activation or availability [90].

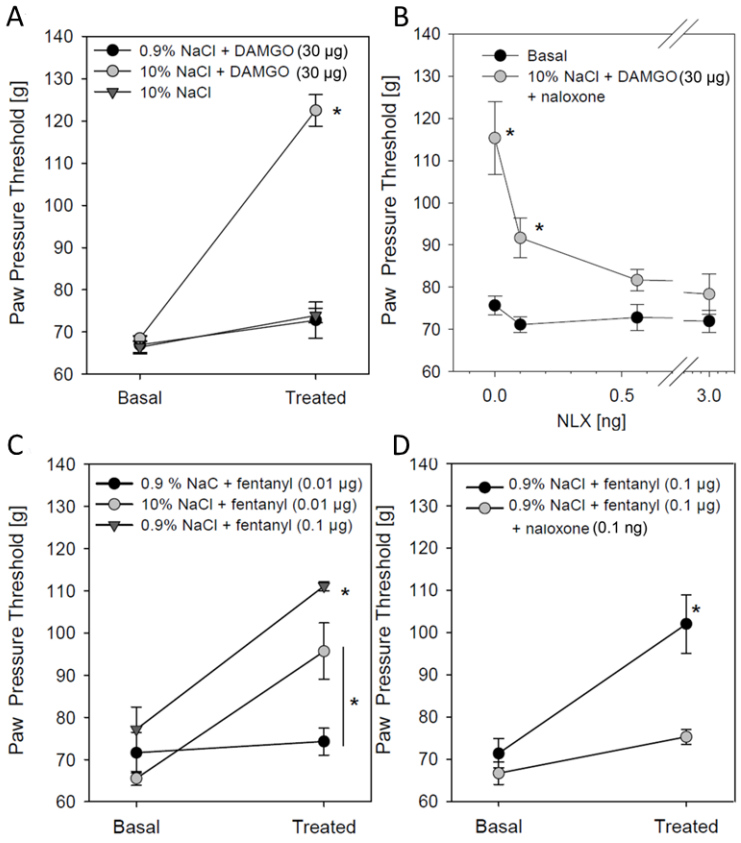

Fig. 6: Co-injection of HTS enhances DAMGO and fentanyl-mediated analgesia. Perisciatic co-injection of HTS and MOP agonists leaded to an increased paw pressure threshold, indicating an enhanced antinocicpetion. The dose dependent inhibitory effect of naloxone supports a specific involvement of MOP. n=6; Time point 10 min (Mambretti EM et al, 2015, accepted).

1.5 Aim of the study

The present work aimed to study the axonal localization of MOP using morphological, biochemical and molecular biological methods, in order to provide further knowledge on the mechanism of opioid action on axonal MOP under different conditions for a possible use in clinical regional anesthesia. Particular attention was directed to specifically localize and quantify MOP in rat and mouse sciatic nerve under basal condition and after the injection of HTS, due to the hypothesized effect of hypertonicity on the availability and/or functionality of axonal MOP.

Indeed, previous studies from our lab have shown that hydrophilic opioids elicit antinociception only if applied together with HTS, indicating that the opening of the barrier is essential for an access of opioids to OPs in the axonal membranes. Injections of the lipophilic opioid fentanyl, which should be

able to pass comparatively freely through the barrier, elicit antinociception even without HTS, indicating the previously disputed presence of functional MOP in nociceptive axons under physiological conditions. The effective fentanyl dose can be significantly lowered by HTS coinjection, suggesting an additional effect of hypertonicity on axonal MOP. Therefore, the main goals of this study were: 1. to develop a protocol suitable for reliably specific and sensitive detection of MOP in the intact sciatic nerve, 2. to apply these methods to study MOP localization on a light and electron microscopic level, 3. to assess the effect of HTS on the availability and functionality of axonal MOPs.

2. MATERIAL and METHODS

2.1 Materials

2.1.1 Animals

Animal protocols were approved by the local animal care committees (Regierung von Unterfranken, Wuerzburg, Germany; protocol number: REG 03/13) and are in accordance with the International Association for the Study of Pain [91].

Animals were kept at 22°C with a light-dark cycle of 12 h. Animals had access to food and water *ad libitum.*

Male Wistar rats (Janvier, France) weighing 200-250 g and male and female homozygous knock-in mice aged 6–12 weeks were used. MOP-mcherry knock-in mice were a kind gift of Dr. Dominique Masotte and Dr. Brigitte L. Kieffer, University of Strasbourg, France. Knock-in mice, expressing the C-terminus of μ-opioid receptor fused to the red protein mcherry, were generated by homologous recombination (HR) [41]. A mcherry cDNA tail was introduced in frame at the C-terminus of the MOP gene (i.e., exon 4). The *Oprm1* stop codon has been replaced by a Gly-Ser-Ile-Ala-Thr-mcherry encoding cDNA followed by a neomycin resistance gene flanked by a FRT site. The whole construct was transfected in embryonic stem (ES) cells of a C57B16/J blastocyst. The knock-in construct and targeting strategy is shown in Fig. 7.

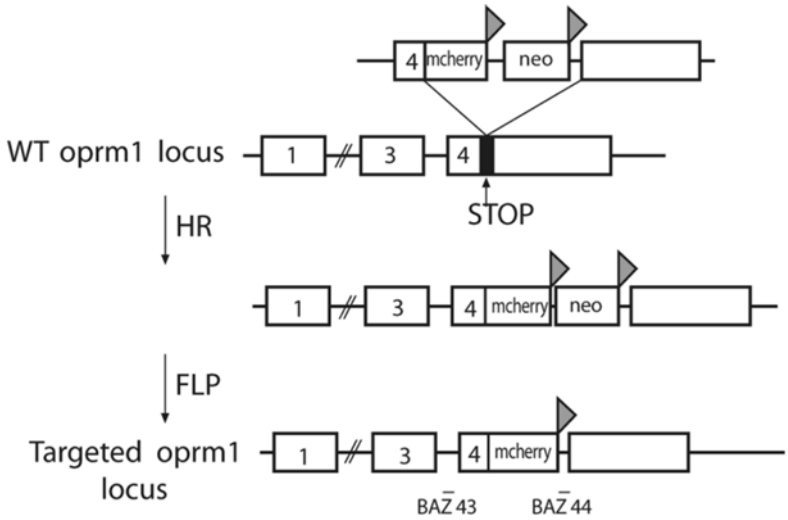

Fig. 7: Scheme of knock-in construct and the targeting strategy. The fusion between the wild type (WT) oprm1 gene and the red fluorescent protein mcherry was obtained by homologous recombination (HR) followed by FLP recombinase treatment (FLP). Positions of the oligonucleotides (BAZ 43, BAZ 44) used for genotyping are indicated.

This C-terminal construct was designed to allow correct native-like MOP expression at sub-cellular level to visualize the MOP protein expressing neuronal population. The genetic background of all

mice was C57/BL6J;129svPas (50:50%). Functional properties of MOP are maintained in MOP-mcherry mice both *in vitro* and *in vivo* [41].

2.1.2 Buffers

	Composition (final concentration)	**Application**
EDTA 0.5 M	EDTA (2H2O) 0.5 M d water	Genotyping
Lysis buffer	Tris Base 0.1 M EDTA 0.5 M SDS 0.2% NaCl 0.2 M d water	Genotyping
TAE, pH 8.5, 50X	Tris Base 2 M Acetic acid glacial 6% EDTA 0.5 M d water	Genotyping
Blocking incubation buffer	TritonX-100 0.5% Normal goat serum (NGS) 5% Phosphate Buffered Saline (PBS) 0.01M or Phosphate buffer (PB) 0.1M	IFL
Incubation buffer	Triton X-100 0.5% NGS 1% PBS 0.01M / PB 0.1M	IFL
Phosphate buffered saline (PBS), pH 7.4, 0.01 M	HNa_2O_4P 7.7 mM H_2NaO_4P 2.7 mM NaCl 0.15 M bd water	IFL/ Immunogold / DAB
Citrate buffer, pH 7.4, 0.2 M	$C_6H_5Na_3O_7$ 0.2M bd water	Immunogold
Phosphate buffer (PB), pH 7.35, 0.2 M	HNa_2O_4P 1.5 M H_2NaO_4P 0.5 mM bd water	Immunogold
Washing incubation buffer, pH 7.4	Gelatin CWFS 40% BSA 0.8% PBS 0.01 M	Immunogold
Blocking buffer	BSA 0.5% TBS 0.1 M	Immunogold / DAB
Incubation buffer	BSA 0. 1% TSB 0.1M	Immunogold / DAB
Tris saline buffer (TSB), pH 7.6, 0.1 M	Tris base 0.1 M NaCl 0.15 M bd water	Immunogold / DAB
RIPA buffer	HEPES 25 mM, EDTA 2 mM NaF 25 mM SDS 1% d water	Protein quantification
RIPA with protease inhibitor cocktail	RIPA buffer Complete Protease inhibitor	Tissue lysis
Blocking incubation buffer	Non-fat milk 5% TBST 1X	WB
Incubation buffer (for secondary Abs)	Non-fat milk 2.5% BSA 2.5% Tris Saline Buffer Tween (TBST) 1X	WB

	Composition (final concentration)	**Application**
Laemmli, 5X	TrisBase 500 mM SDS 0.1 M Glycerol 16% β-mercaptoethanol 1.6% EGTA 3 mM Phenylmethanesulfonyl fluoride (PMSF) 0.01 M Bromophenol blue 5 mM	WB
SDS running buffer, 10X	Tris Base 0.25 M Glycine 2.5 M SDS 35 mM Sterile water	WB
Semi-Dry transfer buffer	Tris Base 25 mM Glycine 0.2 M Methanol 5% Sterile water	WB
Tris saline buffer Tween (TBST), 10X	Tris Base 0.1 M NaCl 1.5 M Tween 20 0.05% Sterile water	WB
Tris, pH 6.8, 0.5 M	Tris Base 0.5 M Sterile water	WB
Tris, pH 8.8, 3 M	Tris Base 3M Sterile water	WB

Table 2: List of buffers. IFL: immunofluorescence; DAB: 3´-3´-Diaminobenzidine reaction; WB: Western blot

2.1.3 Reagent kits

	Code	**Company**	**Application**
ABC kit, Peroxidase Standard	PK4000	Vector	DAB development
Absolute QPCR ROX mix	1138	Applied Biosystems	
BCA Protein assay kit	23225	Thermo Scientific	Protein quantification
cDNA Reverse Transcription Kit	4368814	Applied Biosystems	cDNA transcription
EMBed-812 Embedding Kit (EPON)	14120	Electron Microscope Science	Electron microscopy
Enhanced Chemioluminescent solution (ECL_Lumi Light Kit)	12015218001	Roche	WB band detection
Silver enhancement kit	22708	Polysciences	Immunogold reaction enhancement
GoTaq G2 DNA Polimerase	M7845	Promega	Genotyping

Table 3: List of reagent kits. DAB: 3´-3´- Diaminobenzidine reaction; WB: Western blot

2.1.4 Primers and probes

	Sequence	**Company**	**Application**
BAZ43	5' TGA CGT GAC ATG CAG TTG AGA TTT 3'	Eurofins	Genotyping
BAZ44	5' TCC CAC AAA CCC TGA CAG CAA C 3'	Eurofins	Genotyping
MOR	Rn01430371_m1	Invitrogen	QT PCR
ActB	Rn00667869_m1	Invitrogen	QT PCR

Table 4: List of primers

2.1.5 Antibodies

Antibodies		**Host**	**Dilution**	**Code**	**Company**
Primary	MOP	Rabbit	1:500-1:800	ab10275	Abcam
		Rabbit	1:500-1:800	RA10104	Neuromics
		Rabbit	1:500	ab134054	Abcam (RabMAb)
		Guinea pig	1:50-1:250	ab128013	Abcam
		Guinea pig	1:200-1:500	GP10106	Neuromics
	CGRP	Mouse	1:400-1:600	ab81887	Abcam
		Rabbit	1:400-1:600	24112	Diasorin
	PGP9.5	Chicken	1:500-1:700	ab72910	Abcam
	S100	Mouse	1:250	S2532	Sigma-Aldrich
	DsRed (Mcherry)	Rabbit	1:1000	632496	Clontech
	β-actin	Mouse	1:20000	A3854	Sigma
Secondary	Anti-mouse IgG Cy2	Goat	1:400-1:700	115-547-003	Jackson Immuno Research
	Anti-mouse IgG+IgM Cy3	Goat	1:400-1:700	115-165-068	Jackson Immuno Research
	Anti-rabbit IgG Cy2	Goat	1:400-1:700	111-225-144	Jackson Immuno Research
	Anti-rabbit IgG Cy3	Goat	1:400-1:700	111-165-144	Jackson Immuno Research
	Anti-guinea pig IgG Cy3	Goat	1:250	106-165-003	Dianova
	Anti chicken IgY Alexa Fluor 488	Goat	1:400-1:700	ab150169	Abcam
	Anti rabbit IgG Alexa Fluor 594	Goat	1:2000	A11012	Molecular probes
	Anti rabbit IgG gold US	Goat	1:50	800.011	Aurion
	Anti rabbit IgG biotinylated	Goat	1:500	BA-1000	Vector
	Anti rabbit POD	Sheep	1:3000	12015218001	Roche

Table 5: List of primary and secondary antibodies and relative dilution

2.1.6 Additional reagents and chemicals

	Company, code
Acetic acid glacial	Sigma-Aldrich, #33209
Aclarfoil	Electron Microscopy Sciences, #50426-25
Acrylamide/Bis (30:2)	Carl Roth GmbH, #3029.2
Agarose	Sigma Aldrich, #A9539
Ammonium chloride	Sigma-Aldrich, #A9434
Ammonium nickel sulfate	Sigma-Aldrich, #09885
Ammonium persulphate (APS)	Sigma-Aldrich, #A3678
Beta-Mercaptoethanol	Carl Roth GmbH, #4227.3
Bovine Serum Albumin (BSA)	Sigma-Aldrich , #A9647

	Company, code
Bromophenol blue	Sigma-Aldrich, #114391
Chloroform	Sigma-Aldrich, #32211
Complete ULTRA tablets protease inhibitor	Roche, #05892970001
Coomassie Brilliant blue	Biorad, #161-0400
DAB solution	Fluka, #32748
DAPI	Roche, # 236276
Depex	Serva, #18243.02
D-Glucose	Applichem, #A3666
DMSO	Sigma-Aldrich, #D2650
dNTPs	Sigma-Aldrich, #D7295
Ethanol	Sigma-Aldrich, #32205
Ethylene diamine tetraacetic acid (EDTA)	Serva, #11280
Ethylene glycol tetraacetic acid (EGTA)	Sigma-Aldrich, #E4378
Fluoro-gel	Electron Microscopy Sciences, #17985-11
Gelatin (CWFS 40%)	Aurion, #900.033
Glucose oxidase (GOD)	Sigma-Aldrich, #G6766
Glutardialdehyde	Roth, #4157.2
Glycerol	Serva, #23175
Heparin-Natrium -25000	Ratiopharm, #5394.02.00
HEPES	Applichem, #A1069
Isoflurane	Cp-pharma, #B97D14A
Lead nitrate	Agar scientific, #R1217
Magnesium chloride	Thermo Scientific, #AB-0359
Methanol	Sigma-Aldrich, #32213
Non-fat Dried Milk powder	Applichem, #A0830
Normal goat serum	Sigma-Aldrich, #G6767
Nuclease free water	Ambion, #AM9937
O.C.T Tissue tek compound	Sakura, #4583
Osmium	Electron Microscopy Sciences, #19110
Paraformaldehyde (PFA)	Applichem, #A3813
peqGOLD 100bp DNA-Leiter plus	Peqlab, #25-2020
peqGOLD Protein marker V	Peqlab, #27-2210
Phenylmethanesulfonyl fluoride (PMSF)	FlikaFluka, #78830
Propyilene oxide	Electron Microscopy Sciences, #20401
Proteinase K 37U/mg	Roche, #0311580100137
Sodium chloride	Sigma-Aldrich, #31434
Sodium citrate	Agar scientific, #R1107
Sodium dodecyl sulphate (SDS)	Applichem, #A1112,0500
Sodium fluoride (NaF)	Sigma-Aldrich, #S1504
Sucrose	Sigma, #S0389

	Company, code
SYBR® safe DNA gel stain	Invitrogen, #S33102
T61	MSD, #A206A01
Tetramethylethylendiamine (TEMED)	Sigma-Aldrich, #T9281
Tris hydroxymethyl aminomethane (Tris)	Roth, #5429.3
Triton X-100	Sigma-Aldrich , #T8787
TRIzol®	Invitrogen, #15596-026
Tween20	Sigma-Aldrich, #97949
Uranyl acetate	Serva, #77870.01
Xylol	Roth, #9713.3

Table 6: Additional reagents and chemicals in alphabetical order

2.1.7 Experimental instruments and software

	Company, code	**Application**
Instruments		
7300 System Sequence Detection	Applied Biosystems	RtPCR amplification
Analgesia meter	Ugo Basile, #37215	Behavioural test
Anesthesia Pump		Anesthesia
Biozym MSMIDI	Biozym	Agarose electrophoresis
Centrifuge	Eppendorf, #5418R	
Cryostat	Leica, #CM3050 S	Tissue cryosection preparation
DriBlock DB2A	Techne, #FDB02AD	WB sample denaturation
Eppendorf Thermomixer comfort	Eppendorf AG, #	Tissue lysis RNA isolation
Fastblot	Biometra, #015-200	Gel transfer
Fluorescence microscope	Zeiss, Axioskop 2 mot plus	IFL Image acquisition
Fluorescence microscope	Biorevo, BZ-9000	IFL Image acquisition
FluoroChem FC2 Multi Image II	Alpha-InnoTech	WB acquisition and densitometric analysis
GeneAmp ® PCR System 9600 thermal cycler	Applied Biosystems	Genotyping PCR cDNA transcription
Mini PROTEAN tetra cell	Biorad, # 165-8027	Gel electrophoresis
Monitoring electrode	3M, #2228	Sciatic nerve stimulation
Nikon confocal	Nikon,	IFL Image acquisition
PowerPac Basic Power Supply	Biorad, #164-5050	Gel electrophoresis
Sharp:eye CCD camera controller und TEM-kamera	TRS Tröndle	Immunogold labeling image acquisition
Stimuplex A nerve stimulator	Braun, #4894502	Sciatic nerve stimulation
Stimuplex HSN12	Braun	Sciatic nerve stimulation

	Company, code	**Application**
Sunrise ® Tecan	Tecan	BCA protein quantification assay
Thermoblock	Eppendorf	Tissue incubation
Tissue lyser	Qiagen, #85220	Tissue homogenization
Transmission Electron Microscope	Zeiss, #Leo912AB	Ultrastructural analysis
Vibratome	Leica, #VT1000S	Tissue vibratome section preparation
Software		
FluoroChem FC2 Multi Image II	Alpha-InnoTech	WB acquisition and densitometric analysis
Magellan software	Tecan	BCA protein quantification assay
NIS (Nikon)	Nikon	Image acquisition
EndNoteX5	Thomson Reuters GmbH	Reference management
7300 System Sequence Detection software v1.4.0	Applied Biosystem	PCR amplification
ImageJ 1.47 V	National Institutes of Health, USA	Immunofluorescence quantification
Spot Advanced, version 2.0	Diagnostic Instrument, Inc	Image acquisition
Adobe Photoshop Elements 8.0	Adobe System, Inc.	Images processing
Sigma Plot 11.0	Systat Software GmbH	Statistical analysis and graphics

Table 7: List of instruments and softwares

2.2 Methods

2.2.1 Treatment of rats and mice

Under deep isoflurane anesthesia, the right sciatic nerve was located using a 22-gauge needle connected to a nerve stimulator (Stimuplex Dig RC; Braun) as previously described [90]. A maximum of 300 µl of 10% NaCl in rats and 80 µl in mice were injected. Control nerves were not injected. Sixty min after the injection, animals were anesthetized and sacrificed using an intracardial injection of a solution of T61 (embutramide), cervical dislocation or intracardial perfusion with 4% PFA according to national animal care guidelines.

2.2.2 MOP-mcherry PCR genotyping

Mice genotyping was performed by standard PCR technique using a forward primer recognizing a sequence on the fourth exon of the *Oprm1* gene (BAZ 43) and a reverse primer for the 3' UTR untranslated region (BAZ 44). Introduction of the coding sequence for mcherry increased the size of the amplified fragment by about 800bp enabling identification of wild type *Oprm1* $^{-/-}$ (440 bp), heterozygous *Oprm1* $^{-/mch}$ (440bp and 1270bp) and homozygous *Oprm1* $^{mch/mch}$ (1270 bp) animals by PCR.

Ear punch samples were lysed overnight at 55°C in 500 µl lysis buffer + 100 µg Proteinase K to extract DNA (see table 1 for lysis buffer composition). After lysis the samples were stored at -20°C or immediately used for genotyping PCR. In table 8 PCR reagent volumes and thermal cycling conditions are reported.

Genotyping PCR reaction mix (1 sample, final volume 50µl)		**PCR thermal cycle condition**	
DNA	2 µl	5’ at 94°C	
Taq Polymerase	1 µl	1’ at 94°C	30 cycles
Colorless Buffer 5X	10 µl	1’ at 63°C	
dNTPs 10 mM	2 µl	1’ at 72°c	
BAZ43 10 µM	2.5 µl	10’ at 72°C	
BAZ44 10 µM	2.5 µl	∞ at 4°C	
DMSO	2.5 µl		
$MgCl_2$ 100 mM	1.75 µl		
H_2O	25.75 µl		

Table 8: Genotyping PCR reaction mix and thermal cycle conditions

PCR products (50 µl) were mixed with loading buffer 6X (4 µl); 20 µl of mix were loaded on 1% agarose gel (1 g agarose in 100 ml TAE 1X) containing SYBR® Safe DNA gel stain (10%) and run at 100 V for 90 min. Five µl of peqDNA were loaded as marker. Bands were visualized under UV light and acquired with FluoroChem FC2 Multi Image II (Alpha InnoTech). PCR products from wild type (WT) and homozygous mice display a single band at 440 bp and 1270 bp, respectively; heterozygous mice are characterized by the presence of both bands.

2.2.3 Tissue preparation for immunohistochemistry staining

Rat samples: Under deep isoflurane anesthesia, rats were perfused via the left ventricle. A brief pre-rinse with PBS (0.1 M, pH 7.4) containing heparin (3300 UI diluted in 100 ml PBS, 20 ml/rat) to prevent coagulation was followed by fixation in 4% paraformaldehyde in 0.1 M phosphate buffer (PB, pH 7.4, 300 ml/rat). Perfused tissues were post-fixed overnight at 4 °C in the same fixative. Samples from HTS-treated rat were harvested 60 min after perisciatic injection.

Samples for *electron microscopy* were abundantly washed in 0.01 M PBS to remove PFA and were stored in the cryoprotectant buffer at -20°C. For a better conservation, brains were cut in 40-50 µm slices using a vibratome. Sciatic nerves were conserved in their entirety.

Samples dedicated to *immunofluorescence* were washed in PBS, cryoprotected with 10% and 20% sucrose in PBS overnight at 4°C, embedded in O.C.T., frozen in liquid nitrogen-cooled 2-methylbutane and stored at −80 °C until use. Frozen tissues were sectioned in 10 µm cryosections using a cryostat (CM 3050 S, Leica) set at -20°C. Cryosections were then collected on glass slides

(SuperfrostTM Plus Microscope Slides, code J1800AMNZ, Thermo Scientific). Alternatively, frozen tissues were cut at 30 µm and collected in a multi well in 0.01 M PBS (*free floating sections*). Free floating sections were used immediately after cutting; cryostat sections on glass slides were immediately used or stored at -80°C

Mouse samples: Mouse tissues were perfused and harvested as described above for rat with minor modification, in order to maintain the same conditions described in Erbs et al. [41] In particular, no pre-rinse with heparin was used and PFA was dissolved in 0.1 M PB. For each mouse, 60 ml of fixative were used.

All solutions were freshly prepared and cooled down to RT prior to experiments.

2.2.4 Immunofluorescence

Immunostaining was performed on brain, spinal cord, DRG and sciatic nerve. Cryostat sections from rat tissue were washed in PBS (6x10 min) and blocked for 2h in blocking incubation buffer to prevent unspecific binding. Subsequently, primary antibody incubation was carried out overnight at 4°C in 0.01M PBS+0.5% Triton X-100+1% NGS using the appropriate concentration of one or, for dual labelling, two antibodies from different species (rabbit-anti MOP, monoclonal, 1:250-500; rabbit-anti MOP, polyclonal, 1:500-1:800; guinea pig-anti MOP, polyclonal, 1:50-1:500; mouse-anti-CGRP, 1:400; chicken-anti PGP9.5, 1:500-1:700; anti S100, 1:250). Free floating sections were kept in slight movement. Then, after washing steps in PBS (6x10 min), samples were incubated for 2h at RT with appropriate secondary antibody or combination of antibodies (Cy3-labeled anti-rabbit IgG, 1:400-800; Cy2-labeled anti-mouse IgG, 1:400; Cy3-labeled anti-guinea pig IgG, 1:250), treated for nuclear counterstain with 4',6-diamidino-2-phenylindole (DAPI) and mounted with mounting medium (Fluorogel). Negative controls (omission of one or both primary antibodies) were carried along for each immunolabeling experiment. In dual labeling, cross controls treated with only one of the two primary antibodies but both secondary antibodies were also used.

Immunofluorescence on mouse tissue was carried out as described [41], with overnight incubation at 4°C using rabbit-anti-mcherry antibody (anti-DsRed; 1:1000) alone or in combination with anti-CGRP (see above); free floating sections were kept in slight movement.

2.2.5 DAB reaction

Sciatic nerve cryosection (10 µm) and brain 40 µm free floating vibratome sections were rinsed in 0.1M TBS, pH 7.6 (2x5 min) and incubated 30 min at RT in blocking solution (0.5% BSA in 0.1 M TBS). After washing 2 times for 5 min, sections were incubated overnight at RT with RabMAb 1:250 or DsRed 1:1000 in 0.1% BSA in 0.1 M TBS. The following day samples were rinsed in 0.1 M TBS (3x10 min), incubated 30 min at RT with a biotinylated goat anti-rabbit antibody (1:500) in 0.1% BSA in 0.1

M TBS, rinsed as before and incubated 30 min in ABcomplex (in 5ml 0.1M TBS add 1 drop component A + 1 drop component B, Vector kit). ABcomplex was prepared 30 min before the reaction and kept at 4°C in dark. Before developing the DAB reaction, cryo- or vibratome sections were rinsed briefly in TBS and then in 0.01 M PBS. Cryosections were directly incubated in 200µl of DAB development solution without pre-incubation, while free floating vibratome sections were first pre-incubated 5 min in 20 µl of ammonium nickel sulfate diluted in 1 ml DAB reaction mix (DAB, PBS, NH_4Cl, GOD), then were incubated 15-20 min in the dark after the addition of 20 µl of D-Glucose. Development of reaction was checked under a light microscope. The reaction was blocked by washing sections for 3x10 min in 0.01 M PBS followed by a short wash in distilled water. Vibratome sections were mounted on glass slides. All sections were dried at RT overnight, followed by dehydration in ethanol (3 min in 70% + 3 min in 96% + 2x3 min in 100%) and in xylol and mounted with DEPEX.

DAB development solution		
DAB	333.5 µl	1000 µl
PBS	166.5 µl	
NH_4Cl	496 µl	
GOD	4 µl	
Ammonium nickel sulfate	20µl	
D-Glucose	20 µl	

Table 9: doses of DAB solution

2.2.6 Pre-embedding immunogold

Immunogold labeling was chosen as the best method to detect subcellular localization of MOP. For EM only brain and sciatic nerve samples were used. After perfusion, overnight post-fixation and washing steps as described above, brains were freshly cut in 40µm vibratome sections while sciatic nerves were coronally cut by hand in order to obtain small pieces (2-3mm). All specimens (sections and nerve pieces) were immediately used or stored at -20°C in cryoprotectant medium. For immunoreactions, specimen were rinsed in 0.1 M Tris-saline buffer (TSB, pH 7.6, 2×10 min), incubated 30 min in TSB + 0.5% BSA and briefly rinsed in TSB again. Then, they were incubated for 12-16 h at RT in polyclonal anti-MOP, RabMAb or anti-mcherryMOP antibody diluted in TSB containing 0.1% BSA. For each reaction, control specimens were incubated without primary antibody. After washing in 0,1 M TSB 3x5 min, all specimens were briefly rinsed in 0.01 M PBS and blocked in washing incubation buffer (0.01 M PBS pH 7.4, 0.1% gelatin and 0.8% BSA) for 10 min. The washing incubation buffer was used for the gold-conjugated secondary antibody incubation 2 h at RT. After a short washing step in washing incubation buffer and 0.01 M PBS, sections were incubated 10 min in 2% glutaraldehyde in 0.01 M PBS, washed briefly in 0.2 M citrate buffer, followed by silver

intensification of gold particles using a silver enhancement kit: for each slide enhancer: initiator 1:1 were used. The reaction was developed in a dark chamber for 15-20 min. After double short wash in 0.2 M citrate buffer and 5 min wash in 0.1 M PB, the sections were incubated 1 h at RT in 2% osmium tetroxide in 0.1 M PB, washed in 0.1 M PB (3x10 min), dehydrated first in ethanol (30%x5 min, 50%x 5 min, 70%x 5 min, 96%x5 min, 100% 2x10 min) then in propylen oxide (2x10 min). After overnight incubation in propylene oxide:Epon (1:1), samples were transferred to pure Epon for 2 h and then flat or block embedded. The resin was cured for 48 h at 60°C. Small areas of hippocampus and amygdala were cut from the flat embedded sections and re-embedded onto empty Epon blocks. Ultrathin sections (70 nm) of hippocampus, amygdala and coronal sciatic nerve were cut from the first micrometers below the surface of the specimen, placed onto formvar-coated nickel grids, contrasted with uranyl acetate (2% uranyl acetate in 70% ethanol) and lead citrate (Reynolds 1963) and examined with an electron microscope.

2.2.7 Image acquisition

Observation and image acquisition of immunofluorescence or DAB light microscopy staining was done with the BZ-9000 BIOREVO (Keyence), an Olympus BHS epifluorescence microscope or a Nikon confocal microscope equipped with the appropriate filter systems. 10X, 20X, 40X and 63X objectives were used. The settings of the microscope and the camera were chosen so that signal-to-noise ratio was optimal for the different immunolabelings, and was kept identical for all images taken from the respective tissues.

Reacted specimen were acquired with a transmission electron microscope from Zeiss (LEO912 AB) equipped with a Sharp:eye CCD camera controller und TEM-kamera, (TRS Tröndle, Germany). A range between 5000X and 10000X magnification was used.

2.2.8 Analysis of images and quantification of staining

Immunofluorescence quantification was performed on micrographs of immunolabeled sections taken from sciatic nerve trunks of naïve rats and MOP-mcherry knock-in mice and of rats and MOP-mcherry knock-in mice 60 min after HTS treatment (n=3 in each group). For each rat and mouse nerve, 3 longitudinal cryostat sections with an intersectional distance of at least 40 µm were collected on microscopic slides, and immunolabeled for MOP or MOP-mcherry as described above. Digital images (2 non-overlapping images for each rat and mouse nerve section) were acquired with BZ-9000 BIOREVO (Keyence) using a 40X objective. Immunofluorescence images were converted to grey scale and fluorescence intensity measurements were carried out using Image J 1.46r (National Institutes of Health, USA) in 5 frames of a defined area (Region Of Interest, ROI), which were randomly positioned within the images. Fluorescence intensity/area was averaged for each image,

mean intensity values were calculated for each nerve and group comparisons carried out using Student's t-test.

Assessment of MOP-immunogold labeling specificity: Two different methods were used: the first was adopted at the beginning, to assess the specificity of labeling using polyclonal MOP antibodies on rat sciatic nerve, the second to assess specificity of MOP-mcherry detection in mouse sciatic nerve.

First method: Individual Remak bundles were identified in micrographs of serial ultrathin sections from rat sciatic nerves incubated with and without polyclonal MOP antibody. For each identified Remak bundle, micrographs of 3 to 5 serial sections were analyzed. The area of the entire Remak bundle (non myelinating Schwann cell cytoplasm + unmyelinated axons) was measured. To calculate the Schwann cell cytoplasm area, the area of all unmyelinated axons was subtracted from the entire area. If Schwann cell nucleus was present, the area of the nucleus was measured and subtracted, too.

IGS in unmyelinated axons and Schwann cell cytoplasm were counted and divided by the relative area, in order to obtain the following ratio: n°IGS/area (μm^2). By directly comparing micrographs of serial sections it was ensured that gold dots were not counted twice.

Second method: Individual Remak bundles and the myelinated axons in their vicinity were identified in micrographs of serial ultrathin sections of the following preparations: MOP-mcherry knock-in mouse sciatic nerve reacted with/without mcherry antibody (MOP-mcherry pos/neg); wildtype mouse sciatic nerve reacted with/without mcherry antibody (WT pos/neg). For each identified Remak bundle, micrographs of 3 to 5 serial sections were analyzed. The number of IGS and the Remak bundle area (comprising unmyelinated axons and the surrounding Schwann cell cytoplasm, excluding the Schwann cell nucleus) were determined. By directly comparing micrographs of serial sections it was ensured that gold dots were not counted twice. Dot density was calculated as n°dots /area for each individual Remak bundle. Since most of the myelinated fibers surrounding the Remak bundles were thickly myelinated (presumably MOP-negative motor, Aα and Aβ fibers), overall dot density over myelinated fibers in the analyzed micrographs (including axon, myelin sheath and Schwann cell cytoplasm, excluding Schwann cell nucleus) was determined as intra-sectional background labeling. Thereafter, a labeling enrichment for each Remak bundle was calculated by dividing its individual dot density value by the background density value determined in the same preparation, and a mean labeling enrichment was calculated for all Remak bundles analyzed in each preparation (between 10 and 15).

2.2.9 Western blot

Sample preparation. Rat and mouse tissues were cryopreserved in liquid nitrogen and subsequently homogenized in 200 µl (DRG and sciatic nerve) or 500 µl (brain and spinal cord) of RIPA buffer (25 mM HEPES pH 7.6, 2 mM EDTA, 25 mM NaF, 1% (v/v) SDS) containing protease inhibitors cocktail (1 tablet/10 ml RIPA Complete) using sterilized stainless steel beads (5 mm) by Tissuelyser (4 min at 25 Hz). Samples were then centrifuged at 8600 g for 10 min at 4°C.

Protein quantification. The supernatant was collected and protein concentration was quantified using the bicinchoninic acid (BCA) protein assay kit. Standards controls were prepared according to manufacturer´s protocol: albumin standard dilutions were prepared in the range from 20 to 2000 µg/ml in RIPA buffer (without complete protease inhibitor) and measured in triplicate (25µl/well). Rat and mouse samples were measured in triplicate as well. Brain and spinal cord were diluted 1:10 before quantification due to the high protein content. Two hundred microliter of working solution (reagent A:reagent B, 50:1) was added in each well. After a brief shake, the 96-well plate was incubated 30 min at 37°C. The plate was then cooled down to RT and the absorption at 540nm was measured using an UV/Vis spectrophotometry (Sunrise® Tecan). The concentration of each sample was calculated referring to the absorption values that were interpolated with the values on a linear standard curve.

Protein separation. The amount of protein used for Western blot differed depending on the antibody used for detection: 25 µg of protein from rat samples were used for detection with MOP Neuromics antibody; 50 µg (brain and spinal cord) or 100 µg (DRG and sciatic nerve) of protein were used for detection with RabMAb or mcherry antibody. The calculated amount of protein was added to RIPA (without complete protease inhibitor) and Laemmli buffer, denatured at 95°C for 5 min, briefly spinned, then cooled on ice. Samples were then separated on a 10% sodium dodecyl sulfate polyacrylamide gels (SDS-page, see table 10) at 80 V for 30 min then 110 V for 90 min and subsequently transferred on a nitrocellulose membrane (15 V for 90 min) using a semi-dry transfer buffer and Fastblot. The membrane was blocked in 5% nonfat milk in TBST for 1 h at RT. Primary antibody incubation (rabbit anti-MOP, 1:500; rabbit-anti MOP (RabMAb), 1:250; rabbit-anti mcherry, 1:1000) was carried out overnight at 4°C on a shaking plate. The following day the membrane was washed in TBST (3x10 min) and incubated 2 h at RT with a secondary anti-rabbit antibody (1:3000) conjugated to horseradish peroxidase diluted in 2.5% non-fat milk + 2.5% BSA in TBST. The membrane was kept under slight shake. To remove unspecific binding, the blot was abundantly washed in TBST before ECL detection. β-actin was used as loading control. After ECL detection of the abovementioned antibody bands, the blot was washed in TBST and incubated 2 h at RT in β-actin (1:20000) diluted in 5% non-fat milk + TBST. As the antibody is HRP-conjugated, no secondary antibody incubation was needed. Loading control bands were also detected with ECL.

Negative controls (omission of primary antibody) of RabMAb and mcherry were also carried out.

Acrylamide stacking gel		**Acyrlamide 10% separating gel**	
H_2O	2.85 ml	H_2O	4 ml
Tris 0.5 M, pH6.8	1.25 ml	Tris 3 M, pH8.8	2.5 ml
SDS 20%	50 µl	SDS 20%	100 µl
Acrylamide/Bis 30:2	850 µl	Acrylamide/Bis 30:2	3.33 ml
APS 10%	50 µl	APS 10%	100 µl
TEMED	5 µl	TEMED	5 µl

Table 10: doses for one stacking and one separating acrylamide gel

Band detection. To detect protein band signals, the membrane was incubated 4 min in 1ml of ECL. Chemiluminescent signal was acquired with Imager.

2.2.10 RNA isolation

Sciatic nerves and DRG of control and HTS treated rats were harvested and immediately frozen in liquid nitrogen and stored at -80°C till RNA extraction. Before starting the extraction protocol, all instruments were washed with RNase Zap to remove all RNase that could destroy the RNA. Working on ice, tissue samples were cut in small pieces and collected in a new tube containing 500 µl of TRIzol® and a 5 mm sterilized stainless steel bead. Tissue samples were subsequently homogenized with Tissuelyser for 4 min at 20 Hz and then kept on ice for 6min. After addition of 100 µl of chloroform samples were vortexed for 15 s and then kept at 4°C for 15 min, when two detached phases appeared. After centrifugation at 145000 g for 15 min at 4°C, the upper phase containing the RNA was collected and transferred into a fresh tube containing 250 µl isopropanol (100%). Following complete vortexing, RNA was kept in isopropanol at -20°C overnight (maximal 4 days). On the second day, RNA was centrifuged (15900 g, 5 min, 4°C) and the obtained RNA-enriched supernatant was washed with 75% ethanol. It was subsequently spun down and centrifuged (2300 g, 5 min, 4°C) in order to get a RNA pellet, which was further dried at 37°C for 10 min and resuspended in 100 µl nuclease free water. The final suspension was incubated in Eppendorf Thermomixer® (1400 g, 57°C) for 10 min, and then aliquoted and stored at -80°C before cDNA transcription.

2.2.11 cDNA synthesis and qPCR

cDNA synthesis. cDNA synthesis was performed in 20 µl volumes in 96 well plates. After calculating the extracted RNA concentration, 1 µg purified RNA was brought to 10µl with nuclease free water. 10 µl of components from High-Capacity cDNA Reverse Transcription Kit were then added as described in Table 11. cDNA synthesis was performed according to a well-established program

with the Thermal cycler (25°C for 10 min, 37°C for 120 min, 85°C for 5 min) and was held at 4°C. cDNA products were aliquoted and kept at -80°C before qPCR amplification.

qPCR. Reagents, volumes and thermal cycling conditions for quantitative real time PCR (qPCR) reaction mixture are shown in Table 12. cDNA samples were amplified by qPCR with Taqman gene expression assays for rat MOP and β-actin as a reference gene (see table 3 for relative probes). FAM or VIC refers to specific compatible fluorescein-based 5' end reporter dye. Sequences of FAM/VIC labeled primers were kept confidential from Invitrogen/Life Technologies. Thermal cycling conditions were established according to the manufacturer's instructions: 50 cycles of melting for 15 s at 95°C and 1 min at 60°C for annealing and extension. Two different qPCR-negative controls were conducted: all the reagents were added with either 1) replacement of cDNA by nuclease free water or 2) replacement of enzyme mix "Absolute QPCR ROX Mix" (Thermo Fisher Scientific, Ulm, Germany) with nuclease free water in order to evaluate the contamination from genomic DNA or other sources which would lead to artificial positive amplification in the qPCR reaction. As a result of the relatively uniform expression in injected and non-injected nerve compared to GAPDH and 18S mRNA in preliminary trials (data not shown), β-actin was chosen as an optimal reference gene control.

cDNA synthesis reaction mix (1 sample, final volume 20 µl)	
Reverse Transcription buffer 10X	2 µl
Deoxynucleoside triphosphates (dNTPmix 25X (100 mM)	0.8 µl
Random primer 10X	2 µl
MultiScripeTM Reverse Transcriptase	1 µl
Ribonuclease (RNase) Inhibitor	1 ml
Nuclease-free H2O	Up to 20 µl
RNA template (1 µg)	

Table 11: Pipetting scheme for cDNA synthesis

qPCR mastermix (1 sample, final volume 25 µl)		**qPCR thermal cycle condition**	
Absolute QPCR ROX mix	12.5 µl	15' at 95°C	
Taqman gene expression assay probes (20)	1.25 µl	15'' at 95°C x 50 times	50 cycles
HPLC nuclease free water	6.25 µl	1' at 60°C	
cDNA (1:10 dilution)	5 µl		

Table 12: Pipetting scheme and thermal cycling condition for rtPCR

Data analysis. During qPCR the cDNA of the gene of interest and the reference gene are amplified as happens in a traditional PCR. In every PCR the increase of DNA amount follows a linear pattern before reaching a saturation point. In traditional PCRs, DNA amount is calculated at the end of the run and is thus inaccurate. qPCR, instead, allows to monitor DNA levels in real time, thanks to fluorescent probes (e.g., TaqMan).

According to the ΔΔCt method [92] it is possible to set a threshold intersecting the linear phase of the amplification at a value defined "Ct" (i.e. threshold cycle). Ct values for both the gene of interest and the reference gene of every samples are thus determined to calculate ΔCt values according to the formula:

$$\Delta Ct = Ct\ (gene\ of\ interest) - Ct\ (reference\ gene)$$

Secondly, ΔCt values of controls are subtracted to ΔCt values of treated samples, in order to obtain ΔΔCt values:

$$\Delta\Delta Ct\ values = \Delta Ct\ (treated) - \Delta Ct\ (control)$$

Then ΔCt values of injected and contralateral sciatic nerve were normalized by subtraction of ΔCTt non-injected nerve, thus obtaining the ΔΔCt values. Finally, relative quantitation (RQ) values are calculated as $2^{-\Delta\Delta Ct}$.

In our experiments the reference gene of choice was β-actin.

2.2.12 Statistics

Statistical analyses were performed with SigmaPlot 11.0, Systat Software Inc. Two groups were compared with t-test or by Mann-Whitney rank sum test, if not normally distributed. Data of immunogold quantification are displayed as mean ± SEM (first method) or raw value (median, second method). The 4 groups (MOP-mcherry_pos, MOP-mcherry_neg, WT_pos and WT_neg) were compared with Dunn´s rank sum test, if not normally distributed; *P <0.05 **P<0.01.

3. RESULTS

3.1 MOP-detection using polyclonal MOP antibodies

Specificity and high signal-to-noise ratio of MOP staining is crucial for localization analysis, particularly for immunoelectron microscopic purposes. Therefore, four different polyclonal commercially available MOP antibodies (listed in table 5 in paragraph 2.1.5) were tested in tissues of central and peripheral nervous system. For the central nervous system, the results of labeling in the pyramidal cell layer of hippocampus CA regions and in the intercalated nuclei of amygdala were compared with published data. In the periphery, comparison was carried out for immunoreactions on DRG neurons and sciatic nerve.

3.1.1 MOP-immunolabeling in the brain

All tested antibodies revealed immunoreactivity primarily in fibers and occasional cell bodies in and surrounding the CA pyramidal cell layers of hippocampus (Fig. 8A-D) and particularly strong, mostly diffuse-appearing labelling in the paracapsular intercalated nuclei of amygdala (Ic) with less labelling in the basolateral complex of the amygdala (BLa; Fig. 8E-H). This staining pattern was comparable to previously published data on MOP localization in these brain areas [93, 94]. Antibodies raised in rabbit (produced by Abcam and Neuromics) yielded a strong immunolabeling (Fig. 8B, arrow) and a relative good signal-to-noise ratio. Labeling using guinea pig antibodies showed a strong granular immunofluorescence and the signals appeared, at a first observation with microscope, more specific than rabbit. However, a more careful examination revealed a lower signal-to noise ratio due to a diffuse staining (e.g. in the stratum radiatum of CA1; Fig. 8C, arrow) suggesting additional, possibly unspecific labeling. Presumably unspecific binding using guinea pig antibodies was also more evident in amygdala, in which relative high labelling was seen in the BLa compared to the Ic (Fig. 8G, H, arrows). Signals surrounding the Ics were less intense in samples reacted with the Abcam (C) than with Neuromics (D) guinea pig antibodies. MOP-immunoreactivity using rabbit antibodies was very intense in Ics, with significantly less intense labeling in the adjacent areas (E, F). Negative controls (omission of primary antibody; inserts in the right upper corner of Fig. 8B, D, F, H) showed no staining in hippocampus as well as in amygdala. The comparability of the results with previous reports and the consistent labelling of the same structures using all four antibodies confirmed specificity of MOP detection, with varying levels of additional, presumably unspecific binding. The rabbit polyclonal antibodies provided a higher signal-to-noise ratio than the guinea-pig antibodies.

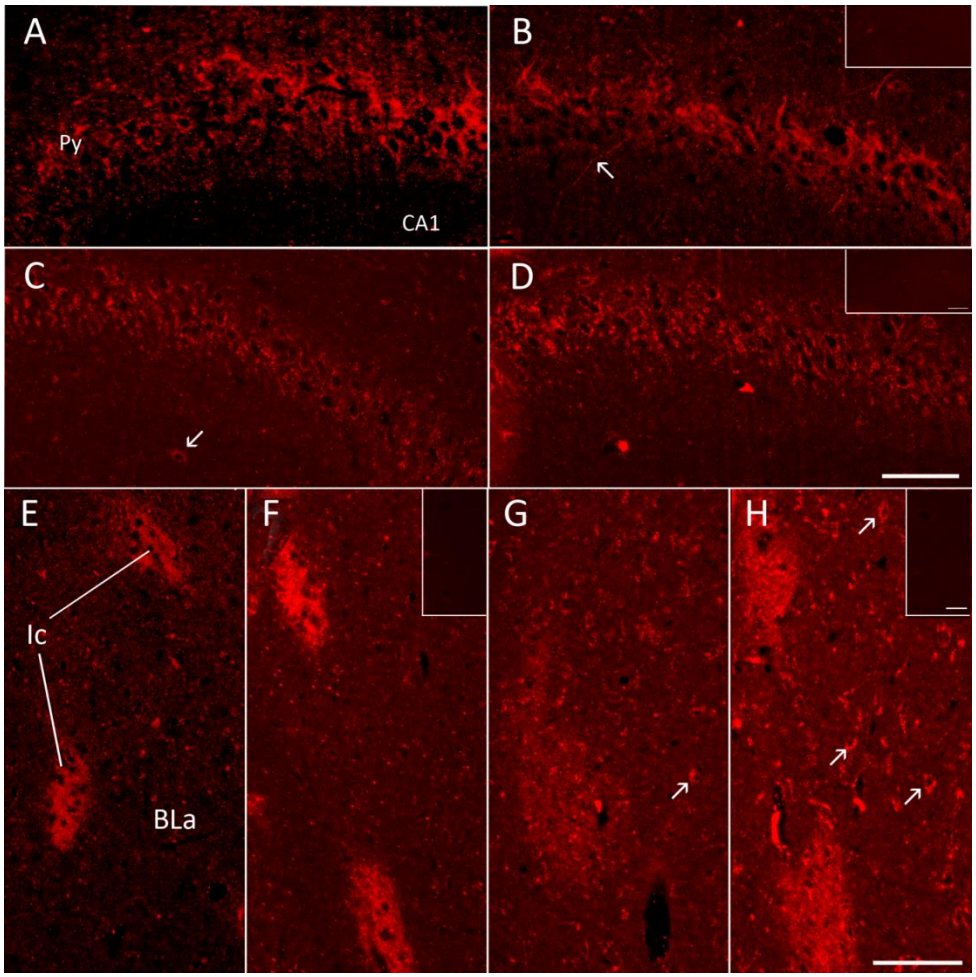

Fig. 8: Detection of MOP using polyclonal antibodies in the pyramidal cell layer of the hippocampus and intercalated nuclei/basolateral complex of the amygdala. Brain cryosections (10 µm) of Wistar rats were incubated overnight with four different MOP primary antibodies raised in rabbit (rbMOR Abcam, A, E; rbMOR Neuromics, B, F) or guinea pig (gpMOR Abcam, C, G; gpMOR Neuromics, D, H) followed by 2 h incubation with a goat-anti rabbit or goat-anti guinea pig Cy3-coniugated secondary antibody. Immunoreactivity of MOP is observed in the pyramidal cell layer (Py) of the hippocampus (A-D). Intense immunoreactivity in paracapsular intercalated nuclei of amygdala (Ic) is detected (E-H). Negative controls (omission of primary antibody) testing for unspecific binding are inserted in the right upper corner in B, D, F and H. Scale bar 100 µm.

3.1.2 MOP-immunolabeling in the peripheral nervous system

To prove the presence of MOP in the axons, all antibodies were further tested in peripheral nervous system, in particular in L4-L6 DRG (Fig. 9) and in the sciatic nerve (Fig. 10). The following results describe the majority of the immunolabeling experiments. However, it is appropriate to remark that the labeling was extremely variable between sections and experiments. DRG immunoreactions with MOP rabbit antibodies exhibited a homogeneous labeling with no remarkable difference in immunofluorescence intensity between small, medium and large neurons (Fig. 9A, B). Thus, the staining pattern did not reflect previous studies immunolabeling MOP, possibly indicating lack of specificity of these antibodies [39]. MOP guinea pig antibody-immunoreactivity was localized in the cytoplasm of small and medium neurons of DRG and revealed again a granular distribution

pattern. Very strong immunofluorescence intensity apparently providing a higher signal-to-noise ratio compared to rabbit antibodies was observed. Small neurons were intensely stained (arrows), suggesting a specific staining, but immunoreactive medium-large neurons, supposed to be MOP negative, were also visible (arrowheads) (Fig. 9C, D). Immunolabeling with omission of primary antibody (inserts in B and D) was negative in all samples.

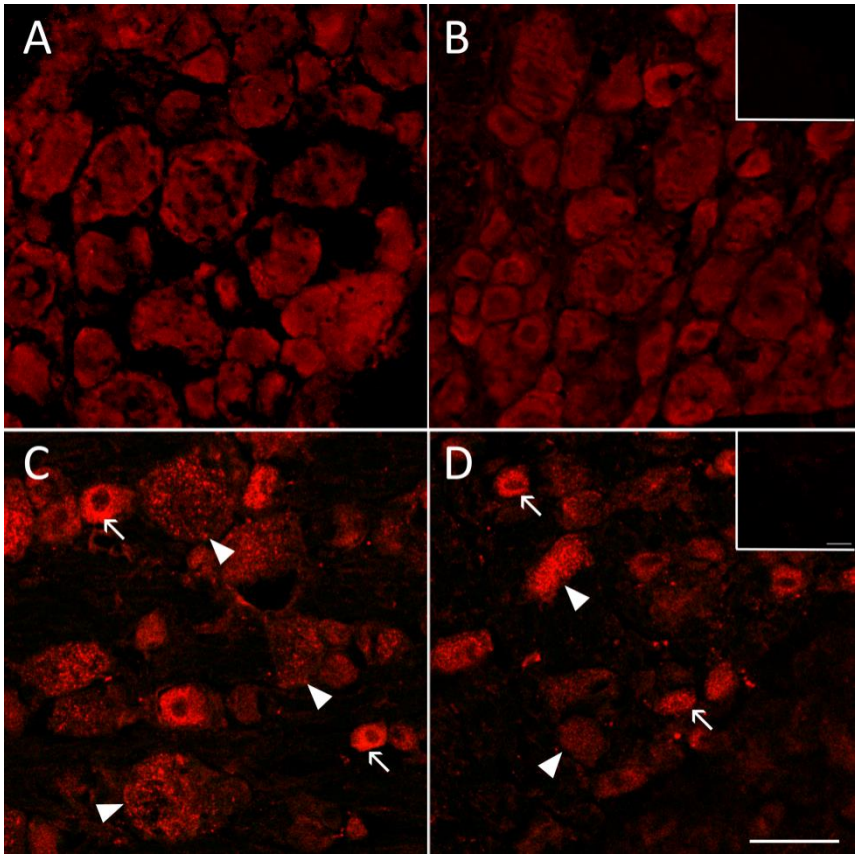

Fig. 9: Guinea pig antibodies yielded stronger staining of small neurons than rabbit antibodies in DRG. Immunoreactivity for MOP in DRG cryosections (10 µm) of Wistar rats. Homogeneous immunoreaction signals after incubation with rabbit antibodies is observed in A and B (Abcam and Neuromics, respectively). Arrows in C and D point to small neurons intensely stained (gpMOR Abcam, C; gpMOR Neuromics, D) while arrowheads indicate staining in medium-large neurons. Granular immunolabeling is detected in C and D. Negative control (omission of primary antibody) is shown in the insert. Scale bar 50 µm.

The next step was to test the specificity of antibodies in the sciatic nerve. To exclude a dependence of the results on immunodetection methods, different immunohistochemical procedures, namely diaminobenzidine (DAB), immunofluorescence and immunogold staining were employed. Results were always comparable. Immunoenzyme labeling with DAB as a chromogen was performed on coronal and longitudinal cryosections of sciatic nerve (Fig. 10A-D) using rabbit (A, C) and guinea pig (B, D) antibodies from Abcam. MOP-Immunoreactivity was detected between presumably myelinated fibers (arrowheads in Fig. 10 A,B) and could be due to specific staining of C-fibers that are organized in Remak bundles and run parallel to myelinated fibers. However, the

staining in presumable Schwann cells (arrows in Fig. 10 A,B) of myelinated axons, as well as near to the node of Ranvier (RN; Fig. 10 C), typical structures of myelinating Schwann cells, suggests the presence of unspecific binding. In the negative control sections some background, maybe due to an excessive development of immunoperoxidase reaction, was observable (Insets in Fig. 10 C, D). The relative labeling intensity compared to background in controls was considerably higher using the rabbit than the guinea pig antibodies.

Immunofluorescence labeling on longitudinal sciatic nerve cryosections using rabbit Abcam and Neuromics antibodies (Fig. 10E, F respectively) yielded signals in fiber or fiber-bundle likes structures (arrowheads in Fig. 10E, F), which could represent axons of sensory and putative nociceptive neurons. However, fluorescence signals were also present in elements resembling Schwann cell cytoplasm (arrows in Fig. 10 E, F), and occasionally fluorescence near to a Ranvier's node was also noticed.

Considering the low labeling intensity in the DAB reaction (Fig. 10B, D), the high background in the brain immunofluorescence (Fig. 8C, D, F, G) and, additionally, lack of detectable immunofluorescence staining above background in sciatic nerve (not shown), it was decided not to use the guinea pig antibodies in further experiments.

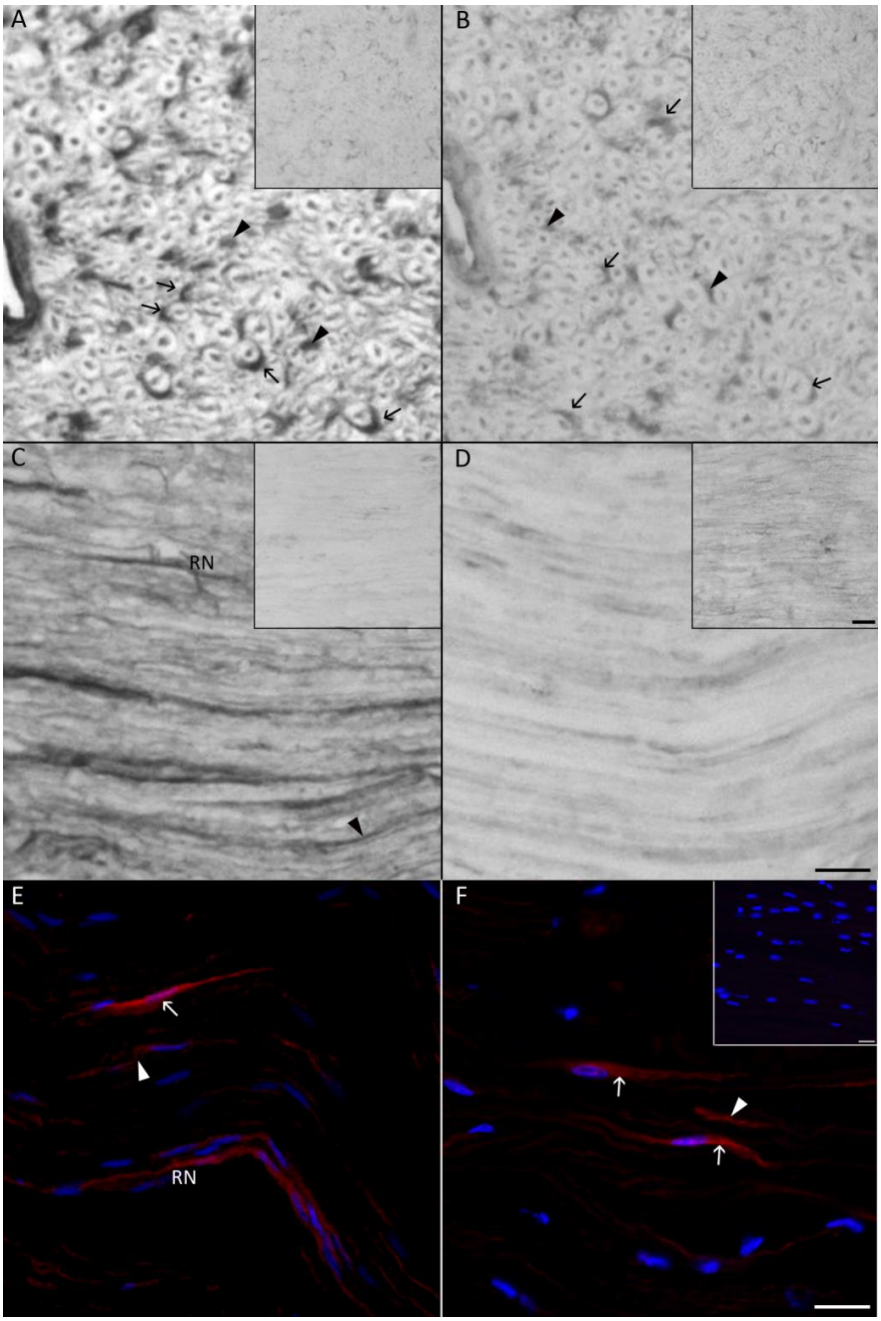

Fig. 10: Detection of Schwann cells in sciatic nerve using MOP antibodies. Immunoreactivity for MOP was seen in coronal (A, B) and longitudinal 10 µm cryosections (C, F) of the sciatic nerve of Wistar rats. For DAB staining (A-D), rabbit (A, C) and guinea pig (B, D) antibodies from Abcam were used. For immunofluorescence (E, F) rabbit antibodies from Abcam and Neuromics, respectively, were used. Arrows point to possible Schwann cells. Arrowheads indicate fiber-like, possibly specific staining. DAPI stains nuclei in immunofluorescence. Negative controls are in the right corner. Scale bar 20 µm.

3.2 Double staining using polyclonal MOP antibodies with CGRP, PGP9.5 and S100-antibodies

In order to obtain additional evidences that could confirm or reject the specificity of rabbit MOP antibodies, sciatic nerve preparations were co-stained with MOP antibodies and CGRP, PGP9.5 or

S100. Rabbit MOP Abcam and Neuromics antibodies showed similar staining along the sciatic nerve. For this reason double staining for MOP and other markers were done using alternatively rabbit MOP antibodies. The following pictures are representative images of double staining on longitudinal and coronal samples of sciatic nerve.

3.2.1 MOP and CGRP

Double staining on longitudinal sciatic nerve fibers revealed a partial co-localization of MOP- (Fig. 11A, Abcam) and CGRP-immunolabeling (B). However, some red fluorescent structures were completely negative for CGRP (arrows in Fig. 11 A, B, D).

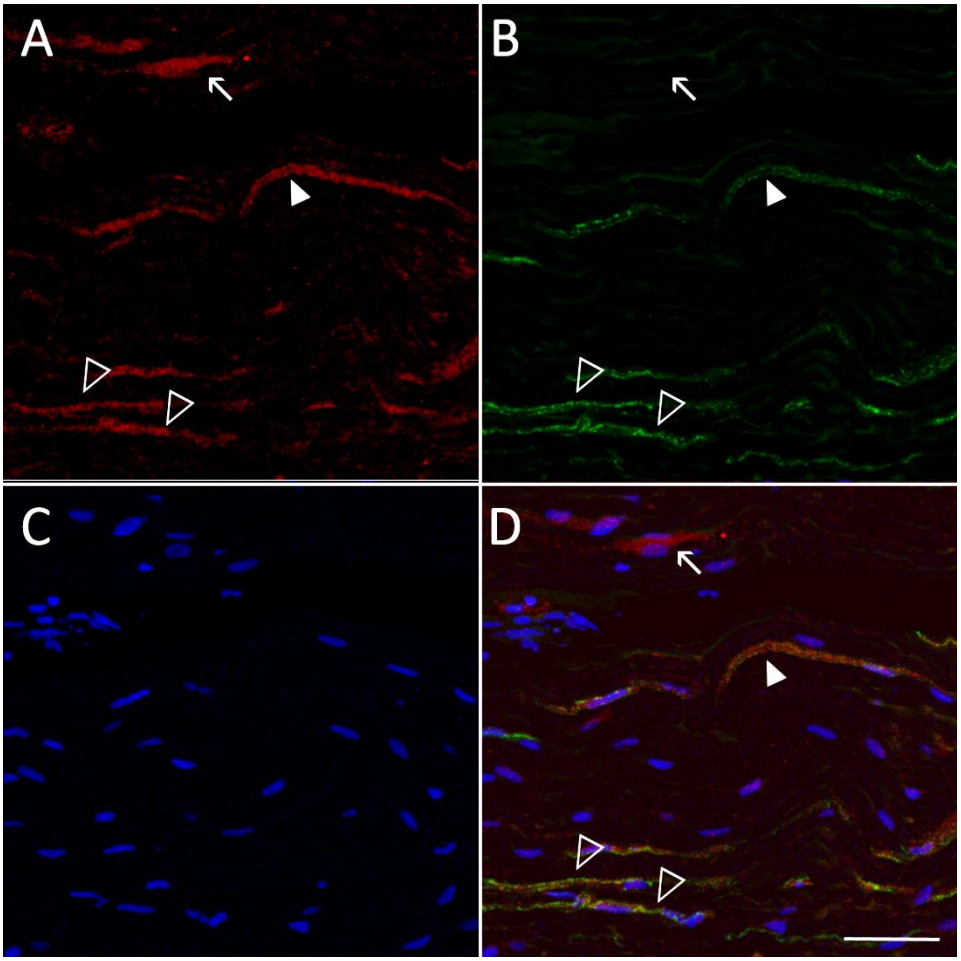

Fig. 11: MOP and CGRP staining on longitudinal sciatic nerve cryosections. Fibers/fiber bundles colocalizing MOP- (A) and CGRP -immunoreactivity (B) are indicated with open arrowheads (Fig A, B, D). Closed arrowheads point to fibers/fiber bundles with high expression of MOP and low amount of CGRP. Fluorescence is also present outside $CGRP^-$ ir fibers or fiber bundles (arrow). Nuclei are stained with DAPI (C, D). rbMOP Abcam and mCGRP were used. Scale bar 50 µm.

The proximity of red fluorescent signals to the nuclei (blue) and the shape of the labeled structures may indicate a Schwann cell, cells that presumably do not express MOP. It was also possible to observe a differential content of MOP in CGRP-ir fibers and fiber bundles, the latter most

probably representing Remak bundles. The closed arrowheads in Fig. 11 point to fibers/fiber bundles with strong MOP- and weak CGRP -immunolabeling intensity. In the fiber bundles indicated by open arrowheads the intensity of staining was similar for MOP and CGRP (Fig. 11A, B, D). CGRP showed a dotted staining that could reflect the localization of the neuropeptide in vesicles.

3.2.2 MOP and PGP9.5

Longitudinal nerve sections were immunoreacted for MOP and the neuronal marker PGP9.5. (green). There was little overlap of MOP-antibody binding in fiber bundles as indicated by red fluorescence, and very light PGP9.5-immunofluorescence (arrow in Fig. 12). In many lightly red-fluorescent structures, which often appeared to run close to and in parallel to PGP9.5-ir fibers, green PRGP9.5-immunofluorescence was not detectable. The negative control (upper corner in Fig. 12D) did not show fluorescence confirming the absence of background and of unspecific binding of secondary antibodies.

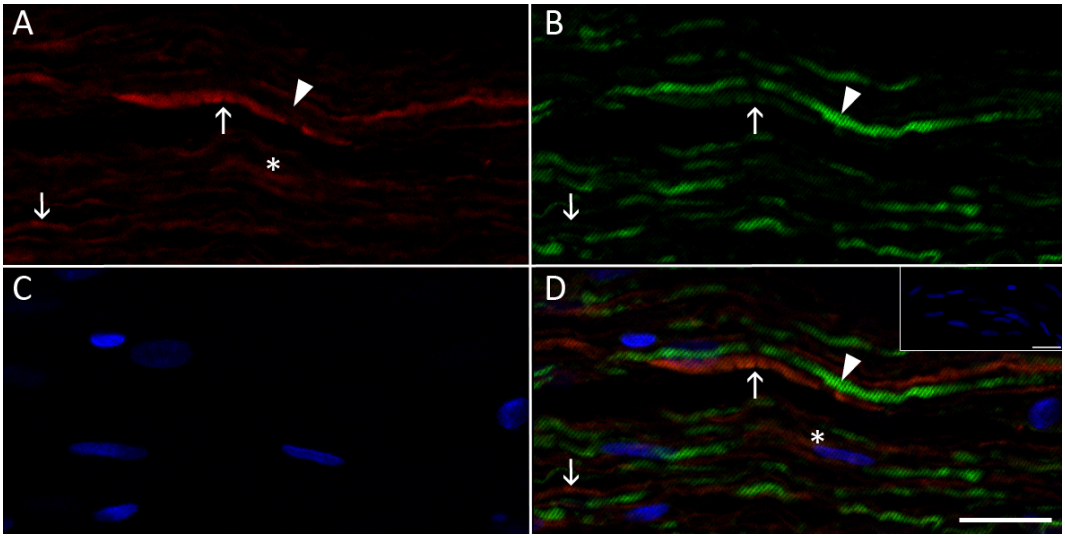

Fig. 12: MOP- and PGP9.5- immunoreactions show little co-localization. Free floating cryosections (30 µm) of longitudinal section of rat sciatic nerve were stained for rbMOP Neuromics (A) and neuronal marker chPGP9.5 (B). Arrows indicate fiber bundle immunoreactive for MOP with light PGP9.5-labeling (in A, B, D); arrowheads point to PGP9.5-ir fibers that are negative for MOP. Asterisk points to presumable MOP-ir Schwann cell. Absence of co-localization between red and green fluorescence is observable in many structures. Nuclei of Schwann cells are stained with DAPI (C, D). Negative control: insert in D. Scale bar 20 µm.

3.2.3 MOP and S100

To further test the specificity of antibodies, double staining with MOP and S100 was carried out. S100 is a marker of the non-compacted cytoplasm of myelinating Schwann cells, localized for instance near the node of Ranvier and in the Cajal bands, longitudinal bands of cytoplasm along the internodal myelin. Coronal sections of sciatic nerve showed low level of MOP staining. However, it

was possible to detect a co-localization of green fluorescence (detecting MOP-antibody binding) and S100 (in red) (Fig. 13A). The co-localization is more evident in the enlarged particular of Fig. 13A, pointed out by arrows in Fig. 13B, C, E.

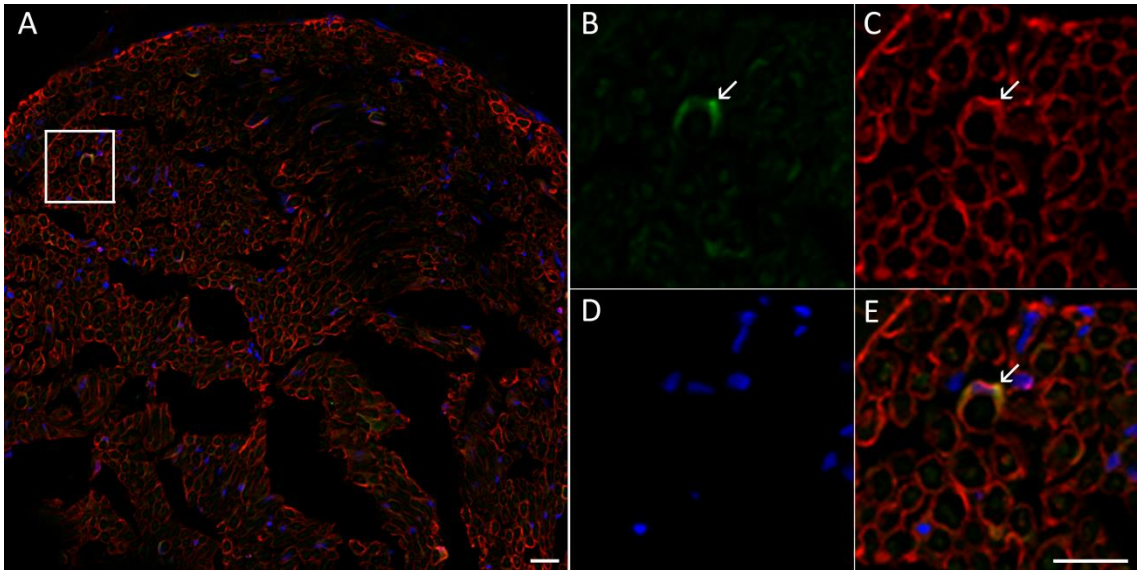

Fig. 13: MOP antibody binding colocalizes with S100. The entire coronal section of the nerve (A) shows immunoreactive fibers for MOR (green) and S100 (red). Selected area of A is enlarged in B-E; arrows point to MOR and S100 co-localization (B, C, E). Nuclei of Schwann cells are stained with DAPI. rbMOP Abcam and mS100 were used. Scale bar 20 µm.

3.3 Pre-embedding immunogold labeling using polyclonal MOP antibodies in rat sciatic nerve

In hippocampus (Fig. 14A, B) and amygdala (Fig. 14C, D), used as positive control tissues, immunogold-silver dots (IGS) were present only in specific structures, mostly dendrites and neurons and usually several IGS could be found in the same structure; in the surrounding areas, IGS were extremely rare. Rabbit MOP Abcam (A, C) showed lower staining intensity compared to rabbit MOP Neuromics (B, D) both in hippocampus and amygdala. IGS were absent or extremely rare in negative control sections (omission of primary antibodies; upper corner in B and D).

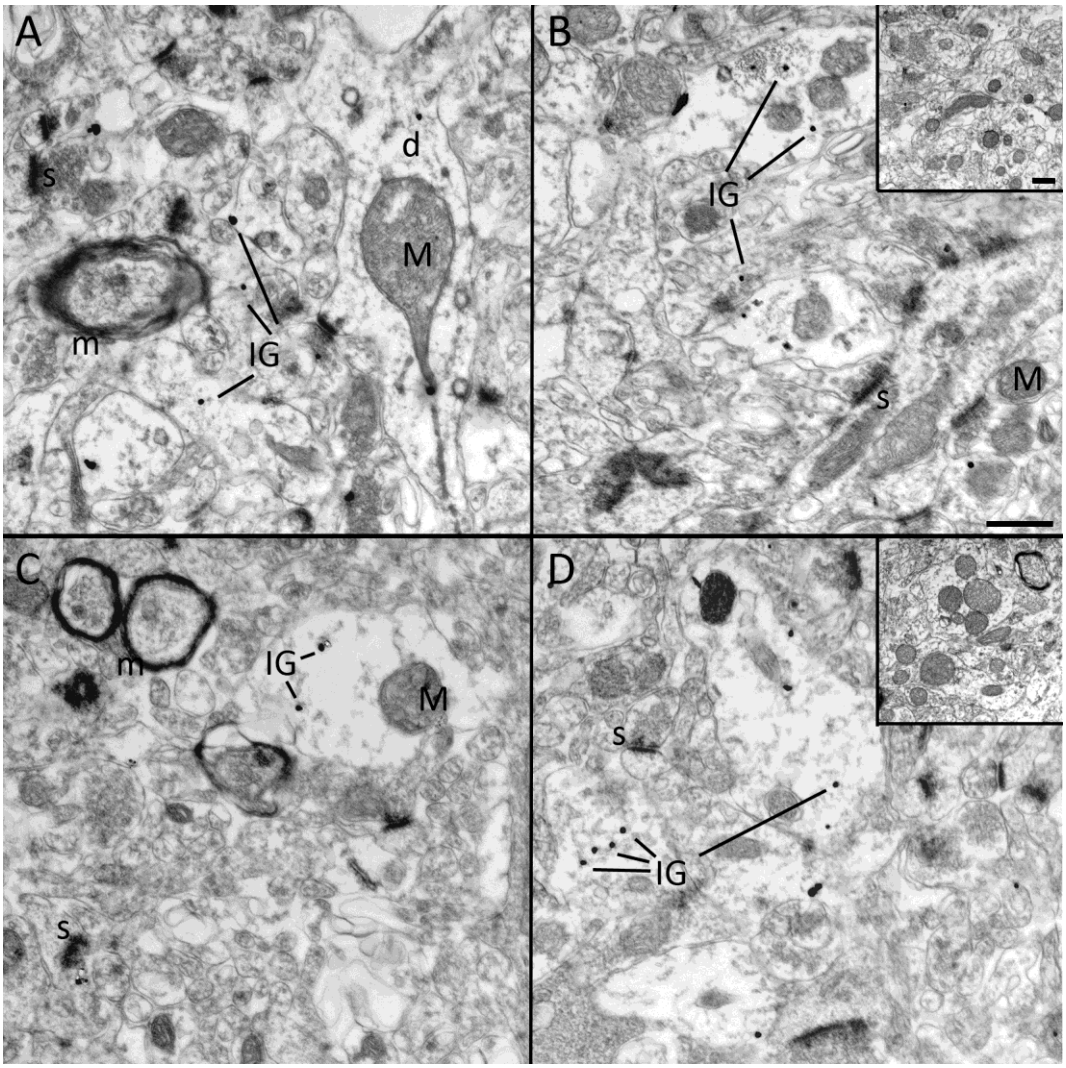

Fig. 14: MOP-pre-embedding immunogold reaction on hippocampus and amygdala indicates labeling specificity. rbMOR Abcam (A, C) and rbMOR Neuromics (B, D) immunogold-silver dots (IGS) are mainly localized in specific elements resembling dendrites (d) of hippocampus (A, B) and amygdala (C, D); often more than one to one structure with little labeling in surrounding structures; no immunogold staining in negative control (in upper corner of B and D). m = myelin; s = synapse; M = mitochondria. Scale bar 500 nm.

Electron microscopy images of coronal section of sciatic nerve stained for rabbit MOP Abcam and Neuromics antibodies (Fig. 15A, B respectively) were characterized by similar staining. In both samples a localization of IGS in unmyelinated axons (ua) of Remak was detectable (closed arrowheads); however, staining in non-myelinating Schwann cell cytoplasm (SC) was visible as well (open arrowheads). Some IGS were also localized on myelinated fibers and in endoneurial tissue between fibers (arrows). Negative controls (omission of primary antibody, upper right corner in B) also contained IGS both on Remak bundles, myelinated fibers and in the endoneurium even if cut at some distance from the surface of the specimen, indicating that secondary antibodies might have diffused into the specimen further than in brain sections, possibly via endoneurial tissue. Consequently, in contrast to labeling in brain sections, it is essential that an in-section internal

control for unspecific labeling due to detection sequence has to be used to assess antibody specificity in sciatic nerve staining.

According to previous studies, a high proportion of unmyelinated fibers in Remak bundles are sensory, presumably nociceptive C-axons, and about 40% of unmyelinated axons contain CRGP [73, 78]. MOP localization has been shown in small and medium sized neurons from which these axons originate, and our fluorescence immunolabeling made presence of specific MOP-reactivity in fiber bundles (possibly Remak-bundles) likely (see section 3.2.1). On the other hand, MOP expression in Schwann cells has not been reported. Therefore, it was attempted to assess MOP-detection specificity using MOP Abcam antibody in immunogold-reacted sciatic nerve sections by comparing the labeling intensity over Remak axons with that over Remak cell cytoplasm. In particular, IGS inside unmyelinated axons (ua) and in the surrounding Schwann cell cytoplasm (SC) were counted in MOP-antibody reacted and in control sections, and the obtained number was divided by the corresponding area (μm^2) (Fig. 16). IGS localized between the fibers or in myelinated axon (m) were not considered. The large variability in IGS counts in unmyelinated axons in some Remak bundles in MOP antibody reacted sections indicates a possible specificity of labeling in some fibers. However, there was no difference in median IGS density noted between unmyelinated axons and non-myelinating Schwann cell cytoplasm. Surprisingly, there was statistically significant difference found in the negative control (omission of primary antibody).

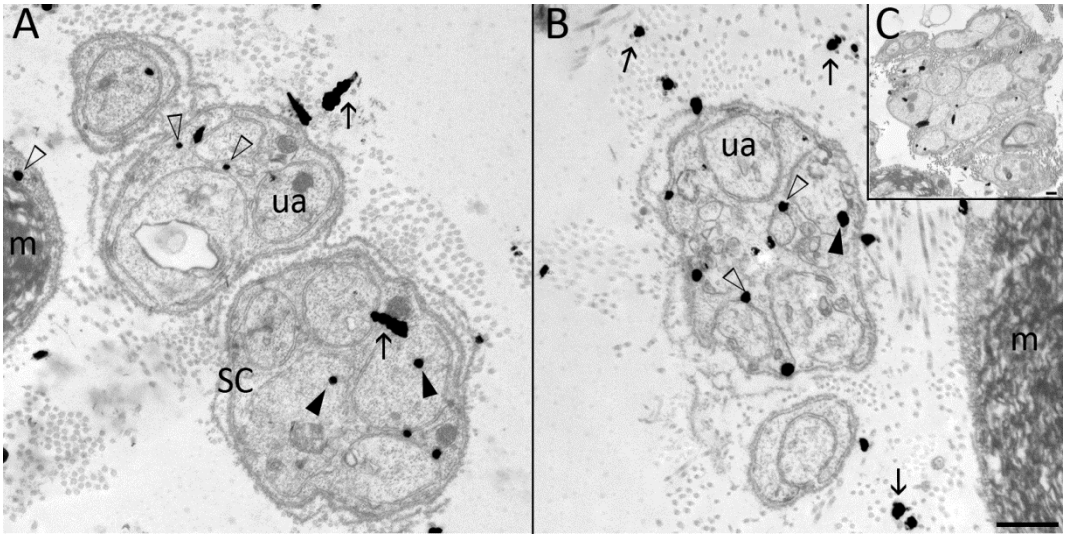

Fig. 15: Immunogold reaction on coronal section of sciatic nerve using polyclonal rabbit MOP antibodies. Closed arrowheads point to immunogold-silver dots localized in unmyelinated axons (a) stained with rbMOP Abcam (A) and rbMOP Neuromics (B); open arrowheads indicate localization of immunogold-silver precipitates in Schwann cell cytoplasm (c); staining in endoneurial tissue is indicated by arrows. Insert in B shows the negative control. ua = unmyelinated axon; SC =Schwann cell cytoplasm; m = myelin. Scale bar 500 nm.

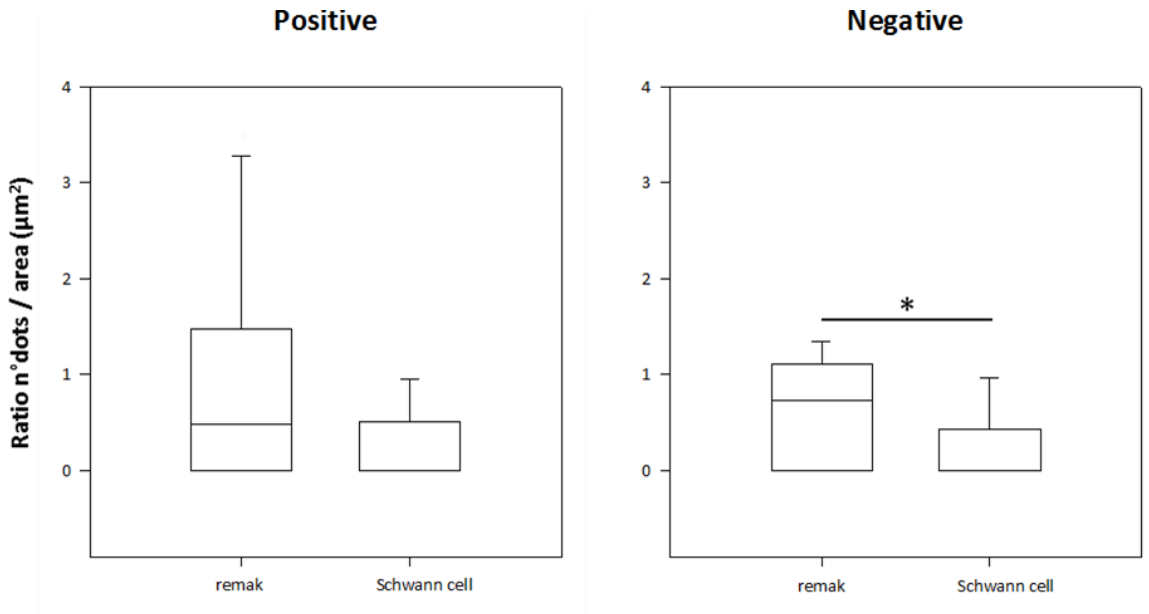

Fig. 16: Quantification of IGS density in unmyelinated axons and Schwann cell cytoplasm (Remak). Data are expressed as a ratio of IGS/area (μm^2). IGS were counted in five different structures identified in three to five serial ultrathin sections of sciatic nerve. Positive: MOP Abcam-reacted, negative: without primary antibody reacted sections. Data are expressed as median. Man-Withney test *P<0.05

3.4 Western blot on neuronal tissues detected possible unspecific signal of MOP antibodies

In addition to immunofluorescence staining, MOP protein was to be quantified in sciatic nerve of treated and untreated rats. The polyclonal rabbit Abcam antibody used for immunohistochemistry appeared not suitable for Western blot analysis , since no bands were detected on blots incubated with this antibody. Instead, rabbit Neuromics detected the presence of MOP in brain, spinal cord, DRG and sciatic nerve. A band of 55 kDa was visible in all samples (Fig. 17). However in all samples more than one band was detected.

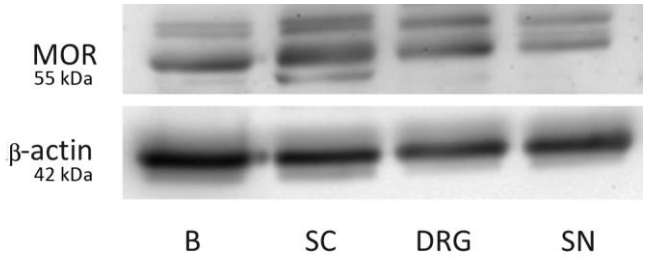

Fig. 17: Western blot using polyclonal MOP antibody. Brain (B), spinal cord (SC), DRG and sciatic nerve (SN) samples were loaded on 10% SDS gel and MOP was detected with rbMOP Neuromics antibody. Presence of several bands is observable. Twenty-five µg of protein was loaded. Representative image of 3 experiments.

3.5 MOP detection using a monoclonal MOP antibody and fusion protein detection in MOP-mcherry knock-in mice

To circumvent difficulties with possible unspecific staining in sciatic nerve we 1. used a new commercial monoclonal rabbit antibody (RabMAb) to detect MOP in rat tissues and 2. employed MOP-mcherry knock-in mice, in which the fluorescent protein mcherry was inserted at the terminal part of intracellular C-tail of MOP. Insertion of mcherry is supposed not to interfere with MOP function and expression [41]. To further improve detection, the fluorescent signal of mcherry was enhanced by immunodetection of the fluorescent protein with a rabbit polyclonal antibody against mcherry (DsRed Living color).

3.5.1 MOP-RabMAB

3.5.1.1 Immunofluorescence labeling on central and peripheral nervous system

Immunoreactions using MOP-RabMAb antibody specifically labeled the intercalated nuclei of amygdala (Ic), the neurons of lamina I and II in the dorsal horn of the spinal cord and small neurons of DRG (arrows) (Fig. 11). Labeling patterns were consistent with previous localization studies and documented superior specificity of the antibody [93, 94]. Negative control (omission of primary antibody; inserts in Fig. 11) revealed no background staining in all tested tissues.

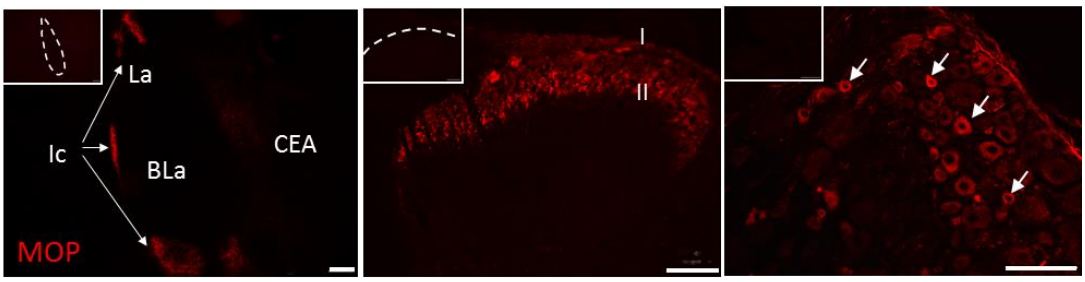

Fig. 18: MOP-immunodetection in neuronal tissue of Wistar rats. Cryosections of amygdala, spinal cord and DRG were incubated with a commercial monoclonal rabbit antibody (RabMAb) for MOP. Immunoreactivity of MOP was seen in the paracapsular intercalated nuclei (Ic) of the amygdala (arrows, left panel), in superficial laminae I/II of spinal dorsal horn (middle panel) and in small/medium DRG neurons (arrow in right panel). Scale bars 100 µm. Negative controls (omission of the primary Ab) are displayed in the upper left corner (nuclei of the amygdala: CEA, central nucleus; La, lateral nucleus; BLa, basolateral nucleus). Scale bar 100 µm.

In contrast to polyclonal antibodies, RabMAb yielded a highly reproducible immunolabeling in the sciatic nerve. Longitudinal sections of sciatic nerve (Fig. 19) showed clearly recognizable but faint MOP-immunoreactivity localized to narrow fibers and fibers bundles. In phase contrast, MOP positive fiber bundles were seen to be localized between myelinated fibers, suggesting MOP localization in axons of Remak bundles. This was also confirmed by dual labeling, which documented the co-localization of MOP and CGRP in fibers and fiber bundles. Moreover, it was possible to appreciate a

differential expression of MOP and CGRP along the fibers. In particular, there were fibers and fiber bundles with high (arrowheads) and low (open arrows) content of MOP, often granular in appearance, as well as fibers that were virtually exclusively CGRP immunoreactive (closed arrows). Close inspection at higher magnification (insets in Fig. 19) documented the differential labeling intensities and indicated that MOP-reactivity was not completely colocalized with CGRP-immunoreactivity within the fibers and fiber bundles.

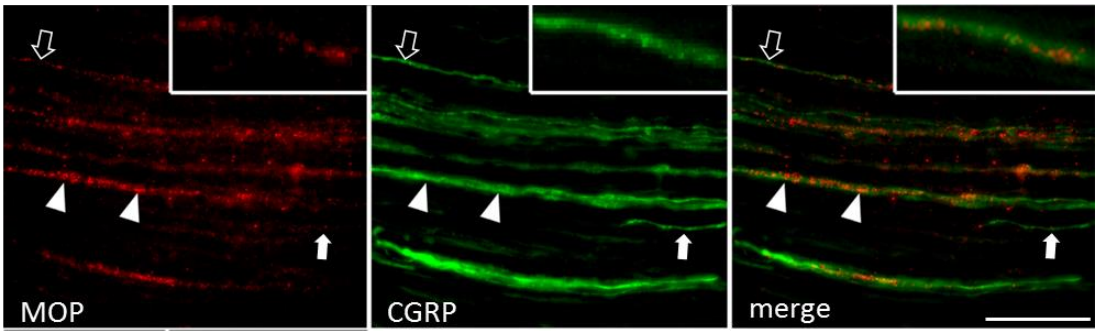

Fig. 19: Specific immunoreactivity of MOP in sciatic nerve of Wistar rats. Longitudinal sciatic nerve sections (10 µm) were stained with RabMAb MOP (red) and the sensory fiber marker CGRP (green). Arrowheads and open arrows point to fibers/fiber bundles with comparatively high and low MOP-ir, respectively. Closed arrows point to fibers containing only CGRP immunoreactivity. Higher magnification is shown in inserts. Scale bar 20 µm.

3.5.1.2 Immunoenzyme labeling

Diaminobenzidine reaction on brain vibratome sections revealed staining in pyramidal cell layer of hippocampus (Py) and in the medial habenula (MH) (Fig. 20A). Intense staining was also visible in the intercalated nuclei of amygdala (Ic) (Fig. 20B). Consistency of results with those of previous localization studies [93, 94] confirmed MOP-RabMAb's immunofluorescence results, again indicating superior specificity of MOP-RabMAb. Absence of background in negative control of hippocampus and amygdala (upper right corner in A and B, respectively) documented quality of detection sequence specificity.

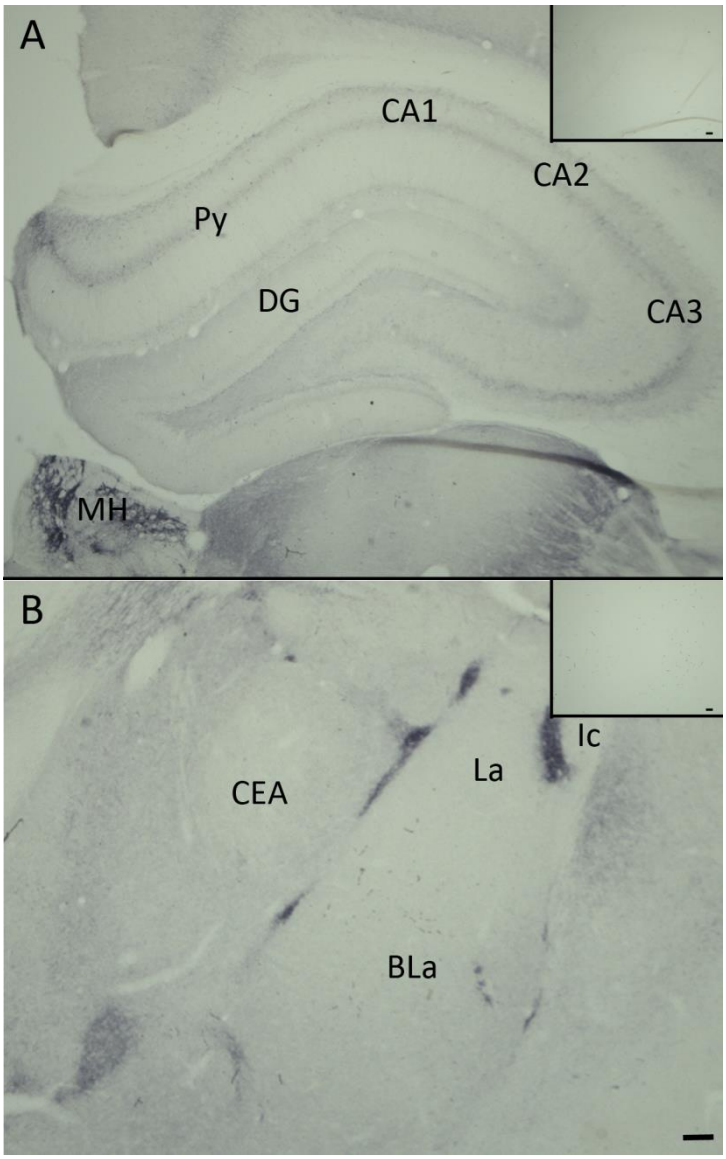

Fig. 20: Detection of MOP in rat brain using RabMAb in diaminobenzidine reaction. Vibratome sections (40 µm) of hippocampus (A) and amygdala (B) were labeled with RabMAb and a goat anti-rabbit biotinylated antibody. MOP-immunoreactivity is visible in pyramidal cell layer of hippocampus (Py) and medial habenula (MH). Strong reaction is also present in the paracapsular intercalated nuclei (Ic) of the amygdala. Negative controls are displayed in the upper right corner. DG=Dentate gyrus; nuclei of the amygdala: CEA = central nucleus; La = lateral nucleus; BLa = basolateral nucleus. Scale bars 100 µm.

3.5.1.3 Immunoelectron microscopic labeling

Ultra-structural analysis on rat amygdala (Fig. 21A, B) and coronal section of sciatic nerve (Fig. 21C, D) provided evidence for specificity of MOP-RabMAb antibody also in immunogold labeling. In the amygdala, IGS present in the section reacted with MOP-RabMAb (A) were specifically clustered in dendrites (d) with almost no labeling in surrounding structures, e.g. myelin (m). Very few IGS and no clustering within specific structures ware observed in the negative control (omission of primary antibody, B). The findings supported, on one side, the specificity of the antibody, and on the other side indicated low background.

In MOP-immunogold-reacted rat sciatic nerve sections, IGS were mostly restricted to unmyelinated axons (ua; Fig. 21C). However, their number was very low, and occasionally IGS were observed in non-myelinating Schwann cell cytoplasm (asterisk), on myelinated axons, and in the endoneurium. As observed in immunogold labeling of sciatic nerve using polyclonal MOP antibodies, negative controls also showed significant numbers of IGS, although close inspection of control reactions showed that the number of IGS outside unmyelinated axons was higher than in MOP-RabMAb-reacted sections. Inserts in C and D clearly show the difference. Therefore, the staining using this antibody appears specific also in the sciatic nerve, but with a low signal-to –noise ratio and high background.

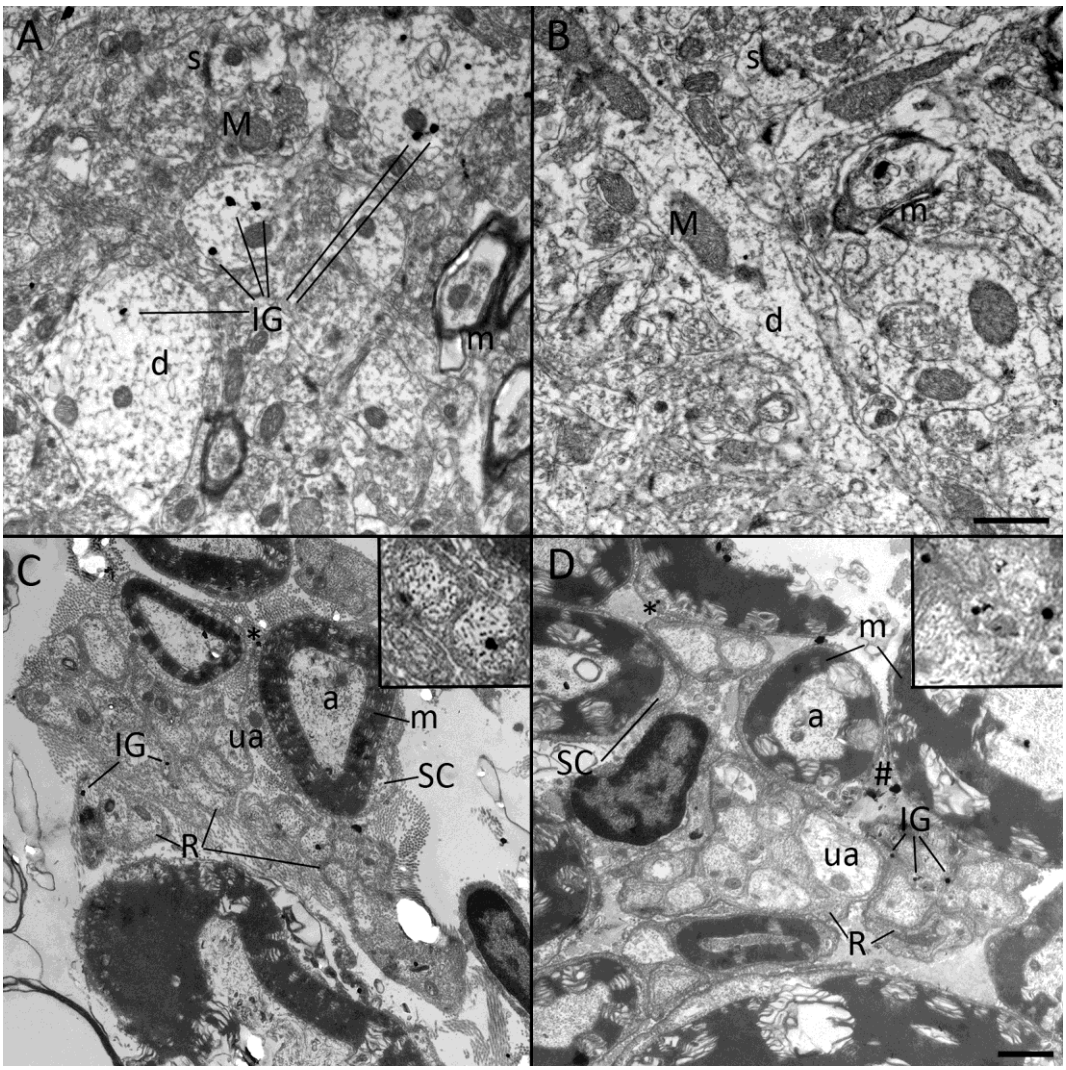

Fig. 21: Ultrastructural immunolocalization of MOP using RabMAb in rat amygdala and sciatic nerve. Image A of amygdala and image C of sciatic nerve show localization of IGS in presumable dendrites (d) and unmyelinated axon (ua) of Remak bundle (R), respectively. Negative controls (omission of primary antibody) show very few IGS in amygdala (B), somewhat more in sciatic nerve (D). Asterisks in C and D indicate unspecific immunoreaction in Schwann cell cytoplasm (SC). Inserts in C and D clearly show different localization of IGS in positive and negative control. Negative controls in B and D. a=myelinated axon; m=myelin sheet; M=mitochondria; s=synapse; #= dirty. Scale bars 1 µm.

3.5.1.4 Protein size verification

MOP-RabMAb detected a signal in Western blot at 70 kDa (as predicted by company datasheet) in brain (B), spinal cord (SC), DRG and sciatic nerve (SN) sample from Wistar rats (Fig. 22). Substantially less MOP protein was observed in the DRG and the sciatic nerve. In addition, in peripheral nervous system tissues other smaller and larger bands were seen, which could be due to posttranslational modification or to different isoforms present in the periphery. No bands were visible in the control blot (omission of primary antibody), confirming the specificity of the primary and the absence of unspecific binding of secondary antibody.

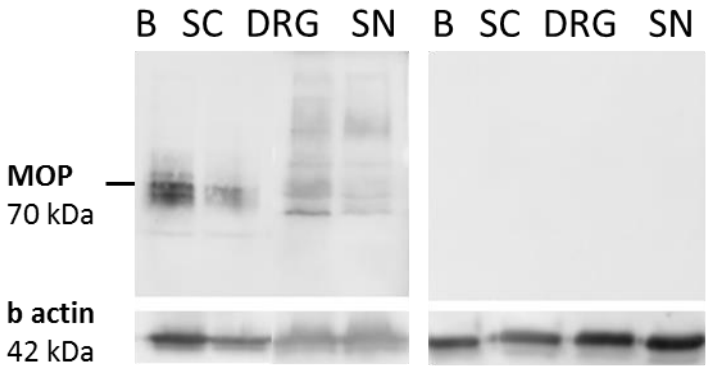

Fig. 22: SDS-page and immunoblot using MOP-RabMAb shows specific band. Tissue lysates from rat brain (B), spinal cord (SC), DRG and sciatic nerve (SN) were separated by electrophoresis. The two blots were incubated with (left) or without (right) MOP-RabMAb. MOP-RabMab detected a band at the predicted size (70 kDa) in brain and spinal cord. -actin (42kDa) was used as loading control. Protein loaded: 5 µg of brain and spinal cord lysate; 10 µg for DRG and sciatic nerve (all representative images, n = 3).

3.5.2 Fusion protein detection in MOP-mcherry knock-in mice

3.5.2.1 Immunofluorescence on central and peripheral nervous tissue

MOP-mcherry-staining (Fig. 23) was localized in intercalated nuclei of amygdala (Ic), in laminae I and II of the dorsal horn of the spinal cord and in small/medium DRG neurons (arrows) of knock-in mice. The negative controls (omission of primary antibody) in the upper left corner of each image revealed no background staining of the detection sequence in all tested tissues.

Moreover, the complete lack of staining in the brain, e.g. the CA2 and CA3 region of the hippocampus (Fig. 24) of wild type mice, in the antibody reacted (A) as well as in negative control sections (B), further supported and strengthened the anti-mcherry detection specificity.

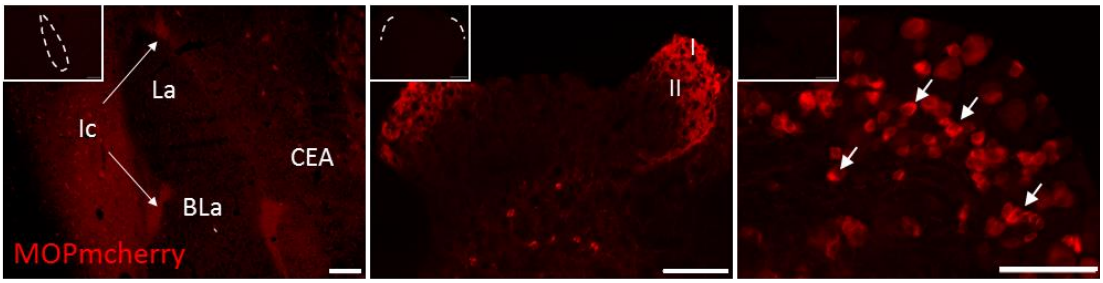

Fig. 23: MOP-mcherry specifically detects MOP in neuronal tissues of knock-in mice. Cryosections of amygdala (left panel), superficial laminae I/II of spinal dorsal horn (middle panel) and small/medium DRG neurons (right panel) of MOP-mcherry+/+ were obtained. Staining was enhanced with mcherry antibody. Negative controls testing for unspecific antibody binding are inserted in the upper left corner. Nuclei of the amygdala: CEA = central nucleus; La = lateral nucleus; BLa = basolateral nucleus; Ic = intercalated nuclei. Scale bar 100 µm.

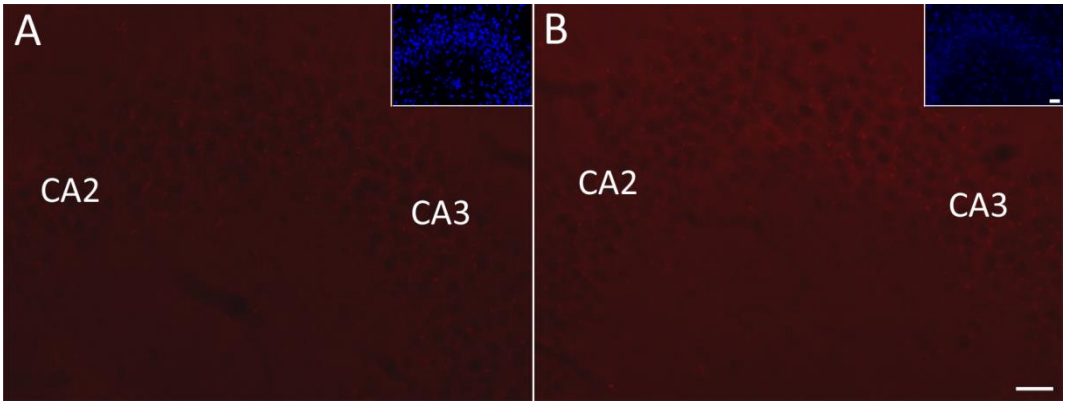

Fig. 24: Absence of MOP-mcherry staining on WT mouse brain. Cryosections of hippocampus were stained with anti-mcherry antibody. Lack of staining in CA2 and CA3 area both in positive (A) and negative (B) control confirm specificity of anti-mcherry antibody. Nuclei (upper right corner in A and B) are stained with DAPI. Scale bar 20 µm.

Specificity of MOP-mcherry immunolabeling was also confirmed in sciatic nerve fibers by studying the co-localization of MOP and CGRP. As for RabMAb stainng in the rat tissue, the results of immunolabeling in different specimen were very consistent. Double labeling of the mouse sciatic nerve (Fig. 25) revealed the presence of differential relative immunofluorescence intensities for MOP and CGRP in fibers and fiber bundles very similar to the labeling patterns shown for MOP detection using RabMAb in rat sciatic nerve. In particular, arrowheads indicate fibers and fiber bundles containing CGRP-reactivity with high content of MOP; open arrows point to fibers with low content of MOP while closed arrows point to fibers that are immunoreactive only to CGRP. MOP-mcherry-immunofluorescence appeared more evenly distributed and less granular than MOP-immunofluorescence in the rat samples. Bleaching of fluorescence by prolonged exposition to UV light, however, revealed granular structure of MOP-mcherry-reactivity also in the mouse sciatic nerve samples.

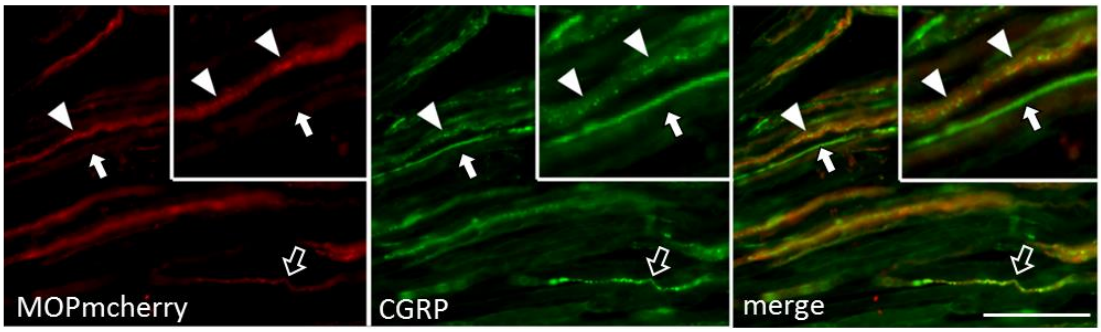

Fig. 25: MOP-mcherry co-localization with CGRP in sciatic nerve of knock-in mice. Longitudinal sections of sciatic nerve (10 µm) were labeled for co-localization of MOP-mcherry (red) with CGRP (green) in putative nociceptive fibers (arrowheads: high MOP-mcherry-ir; open arrow: low MOP-mcherry-ir; closed arrows: CGRP-ir only. Higher magnification is shown in inserts. Scale bar 20 µm.

3.5.2.2 Immunoenzyme labeling

In mcherry knock-in mouse brain, DAB-detection of mcherry-immunoreactions resulted in labeling of the pyramidal cell layer (Py) and scattered cells in hippocampal CA regions. The medial habenula (MH) was intensely stained (Fig. 26A). Specific staining was also visible in the intercalated nuclei of amygdala (Ic) and in the endopiriform area (EP) (Fig. 26B). Negative controls of hippocampus and amygdala (upper right corner in A and B, respectively) showed absence of staining and background. These results were equivalent to previous detections of MOP-mcherry in MOP-mcherry knock-in mice [41] and validated the results of the immunofluorescence staining and the specific detection of fusion protein in MOP-mcherry knock-in mice.

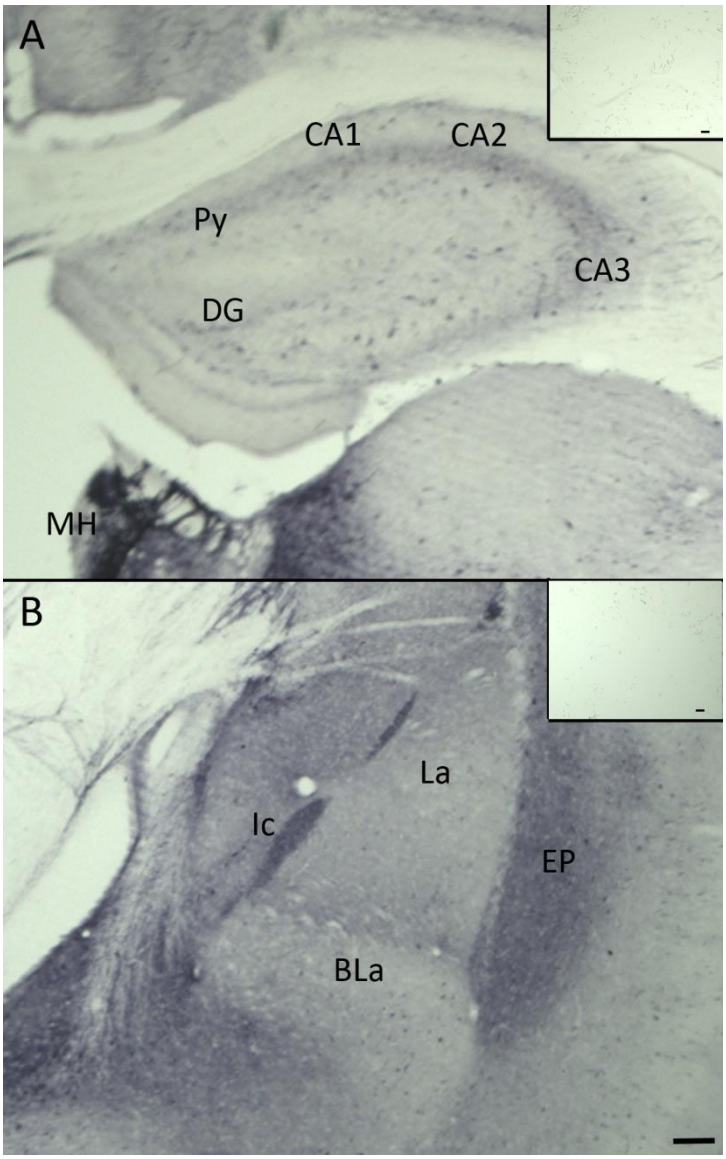

Fig. 26: MOP-mcherry immunoreactivity in diaminobenzidine reaction on MOP-mcherry knock-in mouse brain. Vibratome sections (40 µm) of hippocampus (A) and amygdala (B) were labeled with MOP-mcherry and a goat anti-rabbit biotinylated antibody. Immunoreactivity of MOP is visible hippocampus (Py) and the medial habenula (MH). Strong reaction is also present in the paracapsular intercalated nuclei (Ic) of the amygdala. Endopiriform area (EP) is also stained. Negative controls are displayed in the upper right corner. Nuclei of the amygdala: CEA = central nucleus; La = lateral nucleus; BLa = basolateral nucleus. Scale bars 100 µm.

3.5.2.3 Immunoelectron microscopic labeling

Ultra-structural images of anti-mcherry-immunogold-reacted amygdala sections (Fig. 27A, B) supported the specificity of MOP-mcherry immunoreactivity showing IGS clustered in individual elements, mainly dendrites (d, in A). In sciatic nerve specimen (Fig. 27C, D), IGS were localized on Remak bundles containing tightly clustered axonal profiles surrounded by thin Schwann cell processes. Close inspection documented IGS localization in the cytoplasm as well as near the membrane of unmyelinated axons. IGS were also occasionally seen on presumably non-nociceptive large myelinated axons, Schwann cell cytoplasm, and endoneurial tissue indicating some unspecific

labeling. Negative controls (omission of primary antibody) showed almost complete absence of IG in brain sections. However, in sciatic nerve sections, a few IGS were present on Remak bundles and surrounding tissue.

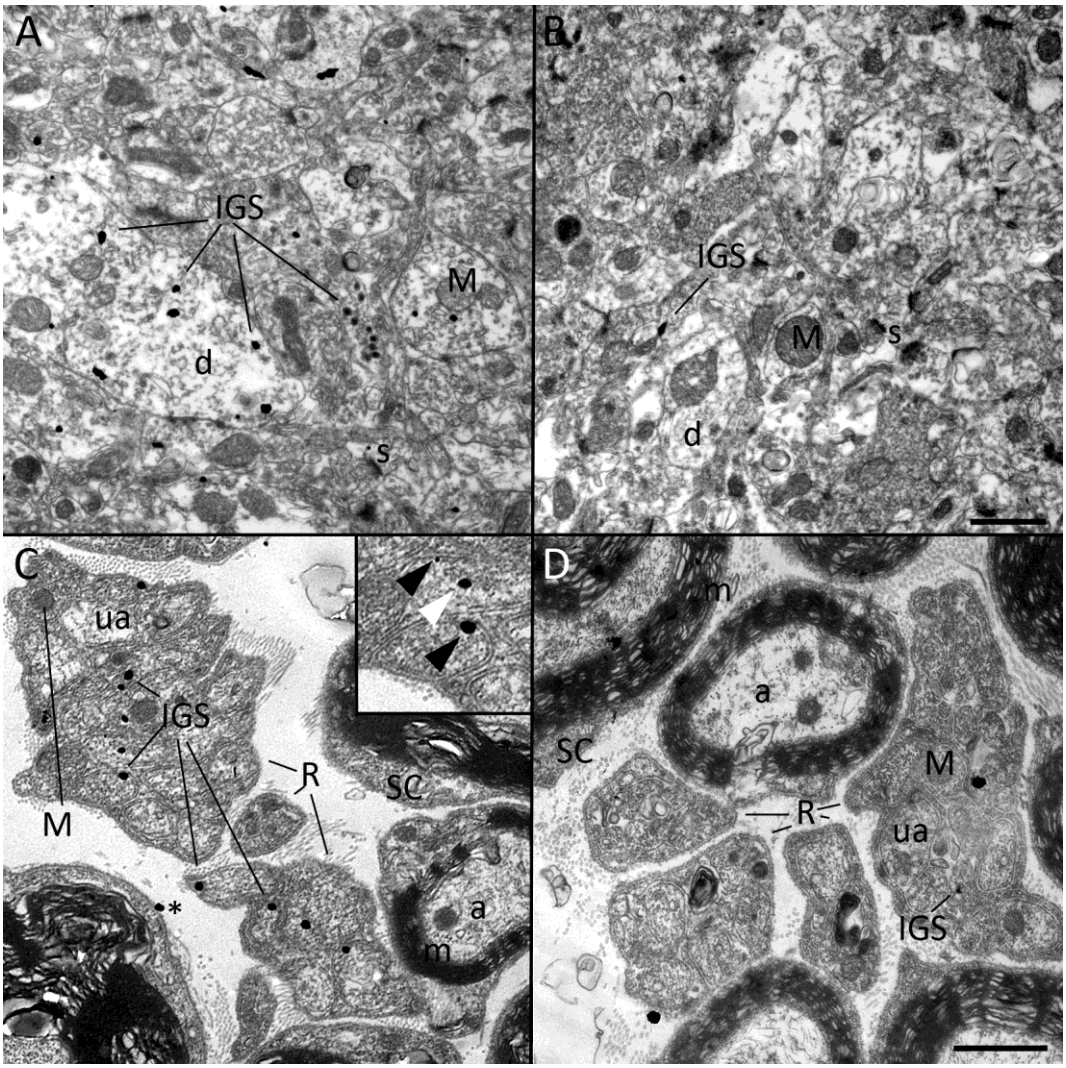

Fig. 27: Ultrastructural immunolocalization of MOP-mcherry in amygdala and sciatic nerve of MOP-mcherry knock-in mouse. Image A of amygdala and image C of sciatic nerve show localization of IGS in dendrites (d) and unmyelinated axon (ua) of Remak bundle (R), respectively. Asterisk in C indicates unspecific immunoreaction in Schwann cell cytoplasm (SC). Insert in C clearly show MOP localization near membrane (black arrowheads) and in the cytoplasm (white arrowhead) of unmyelinated putative nociceptive axon. Negative control in B and D. a=myelinated axon; m=myelin; M=mitochondria; s=synapsis; #= dirty. Scale bars 1 µm.

Wild type mouse samples (Fig. 28) reacted with anti-mcherry antibody and processed for ultrastructural analysis further corroborated the specificity of the antibody. Indeed, amygdala sections showed virtually no IGS both in mcherry-antibody-reacted and in control sections. WT sciatic nerve samples, reacted both with and without mcherry antibody, looked comparable to the negative control of MOP-mcherry knock-in mice.

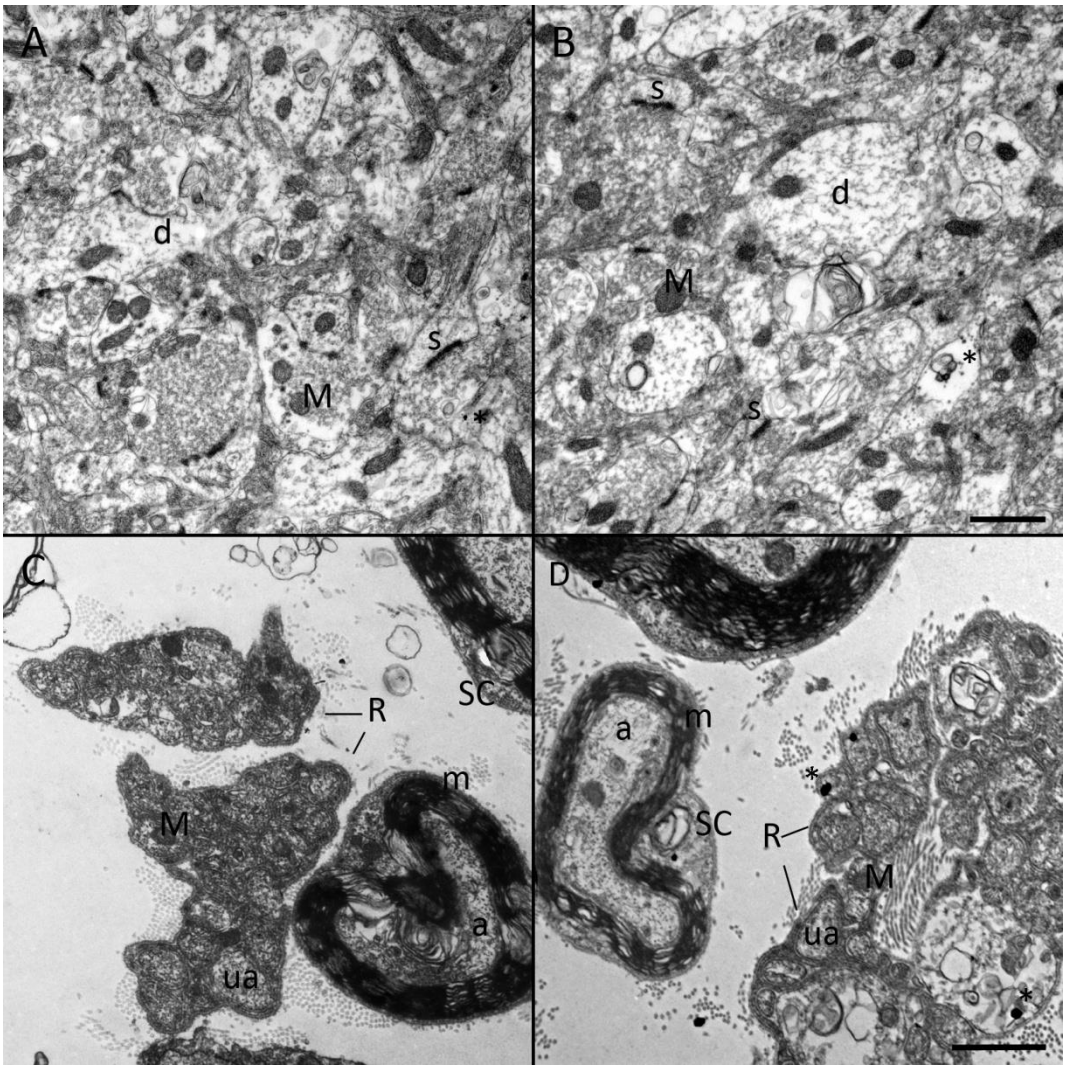

Fig. 28: Immunoreactions using MOP-mcherry antibody on amygdala and sciatic nerve of wild type mice. Amygdala (A),sciatic nerve (C),and the negative controls (B,D) are characterized by the presence of very few IGS (*)in amygdala as well as in sciatic nerve. a=myelinated axon; m=myelin sheet; M=mitochondria; s=synapsis; #= dirty. Scale bars 1 µm.

To validate the specificity of ultrastructural MOP-mcherry localization in sciatic nerve, a comparative quantitative analysis on preparations of mcherry knock-in and wild type mice treated both with and without mcherry antibody was performed. Those preparations are designated, in the following paragraph, as MOP-mcherry-pos, MOP-mcherry-neg, WT-pos, WT-neg. In contrast to the quantifications done on rat sciatic nerve sections (see section 3.3), quantification on mouse sections was done by comparing the enrichment of IGS over entire Remak bundles (containing, presumably, a large proportion of nociceptive unmyelinated axons [73, 78]) relative to that over myelinated fibers (consisting of a vast majority of non-nociceptive axons; internal background control) between the different genotypes and reactions. This different approach was adopted since Schwann cell cytoplasmic extensions between unmyelinated fibers in mouse sciatic nerve were comparatively thin, preventing unequivocally valid recognition of IGS localization in Schwann cell processes versus axons.

Also, the number of IGS both on Remak bundles in surrounding tissue was comparatively low. Results of the quantification, expressed as IGS density over Remak bundles divided by IGS density over myelinated fibers, are shown in Fig. 29.

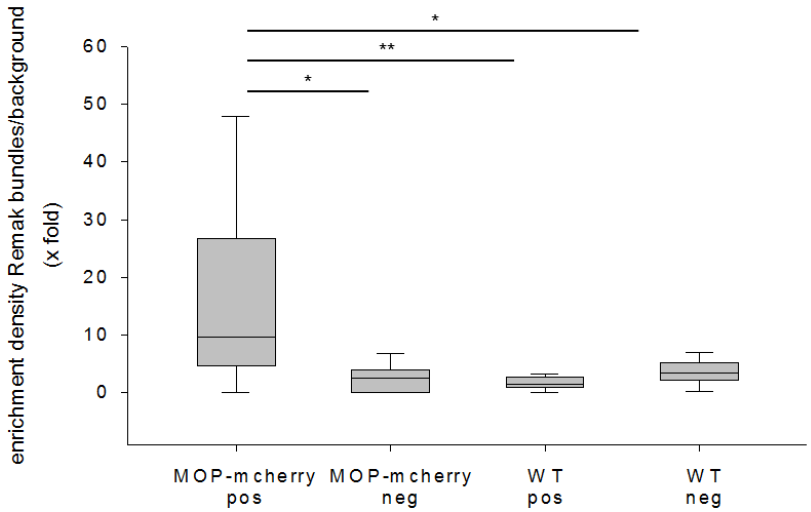

Fig. 29: Significant difference in immunogold quantification on mcherry knock-in and wild type mouse sciatic nerve. Quantification of IGS comparing the four experimental conditions is displayed as median dot density enrichment in Remak bundles over background (x fold) (n = 10-15; oneway ANOVA and Dunn´s test on rank; *P < 0.05, **P < 0.01).

In the MOP-mcherry-pos preparation, the IGS density over Remak bundles was significantly higher than background with median labeling enrichment (IGS density over Remak bundles divided by IGS density over myelinated fibers) of 10.6 fold. To avoid bias due to differential unspecific binding properties of various tissue components, IGS density in Remak bundles over background was also determined in controls (MOP-mcherry-neg, WT-pos, WT-neg). The results indeed indicated a higher IGS density in Remak bundles compared to myelinated fibers also in these preparations (possibly caused by lower unspecific binding affinity of myelin). However, the medians of labeling enrichment in Remak bundles were only between 2.1 and 3.2 fold and were significantly lower than those in MOP mcherry-pos for all controls. This suggests that the localization of IGS in unmyelinated axons (membrane and cytoplasm) in the MOP-mcherry-pos preparation specifically represents the subcellular localization of the fusion protein. Thus, the ultra-structural analysis indicates a membrane localization of MOP in unmyelinated (presumably nociceptive) axons of intact sciatic nerve.

3.5.2.4 Protein size verification

MOP-mcherry detected specific bands in brain, spinal cord, DRG and sciatic nerve samples (Fig. 30). An 80 kDa band was observed in mouse brain and spinal cord. Again, less protein and smaller and larger bands were present in the DRG and the sciatic nerve. The blot incubated with omission of

primary antibody showed no bands, corroborating the specificity both of the primary and the secondary antibody.

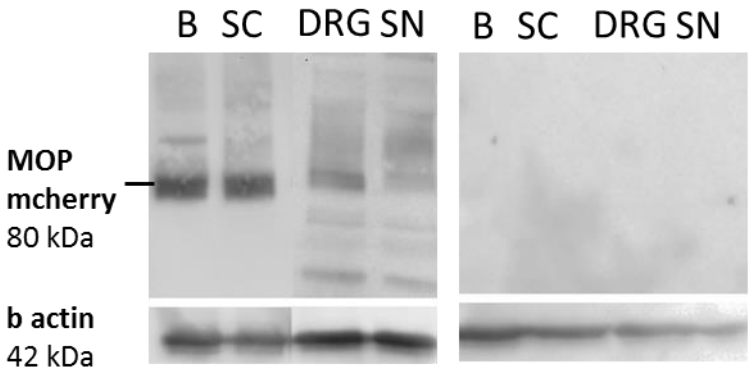

Fig. 30: MOP-mcherry yielded specific detection of MOP in Western blot. Western Blots on tissues from MOP-mcherry mice confirm MOP (80 kDa) localization in brain (B), spinal cord (SC), DRG and sciatic nerve (SN) relative to ß-actin (42 kDa). 50 µg of brain and spinal cord lysate and 100 µg for DRG and sciatic nerve were loaded (all representative images, n = 3).

3.6 No change in MOP mRNA expression 60 min after perisciatic HTS application

To answer the question whether increased antinociception is due to an increased expression or axonal protein level of MOP after HTS perisciatic injection, measurement of MOP mRNA in DRG (site of protein production of sensory neurons) and MOP protein in the nerve 60 min after treatment was performed. β-actin was used as reference gene in the qPCR and as loading control in the western blot. No differences were observed in MOP mRNA expression in DRGs measured by qPCR levels between treated and untreated rats. No differences were present also between untreated and contralateral as well as between contralateral and treated nerve, demonstrating no systemic effect of HTS injection.

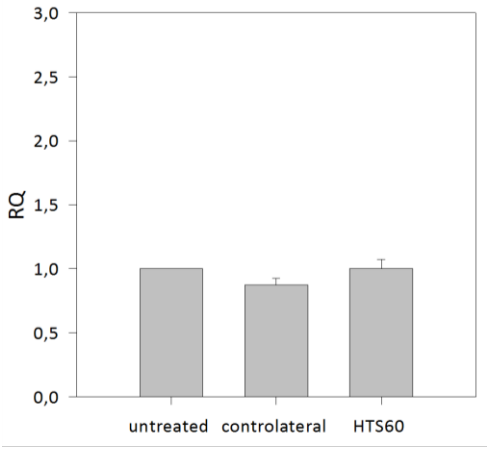

Fig. 31: HTS does not increase MOP mRNA expression in DRG. mRNA levels of MOP, detected with qPCR are not augmented 60 min after perisciatic injection of HTS (HTS60); RQ = relative quantitation; n=6-9; data are represented as mean± SEM; One-way ANOVA; p <0.05.

Similar results were obtained on sciatic nerve MOP mRNA (Fig. 32) measured for axonal protein translation: no differences between untreated and contralateral as well as between contralateral and treated nerves were observed. Compared to DRG, in which the amplification signal appeared at Ct 24, MOP mRNA amplification was detected at Ct 32, a value that is indicating very low expression.

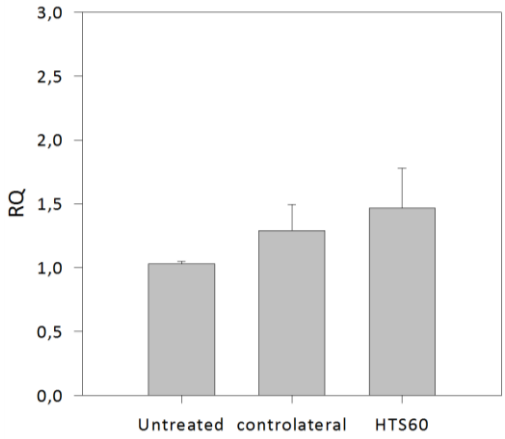

Fig. 32: MOP expression in nerve is not altered by HTS. qPCR on untreated, contralateral and HTS treated sciatic nerve shows no differences; each sample was loaded in triplicate; RQ = relative quantitation; n=6-9; data are represented as mean± SEM; One-way ANOVA; p <0.05.

3.7 No change in MOP immunoreactivity 60 min after perisciatic injection of HTS

Representative images of immunofluorescence qualitatively showed no increase of MOP-immunolabeled fibers/fiber bundles in rat sciatic nerves 60 min after HTS treatment (Fig. 34A) The same was observed in mcherry-immunolabelings in MOP-mcherry knockin mouse sciatic nerve after treatment (Fig. 34B). Quantification of immunofluorescence staining supported the qualitative analysis revealing no significant differences between untreated and HTS-treated nerves.

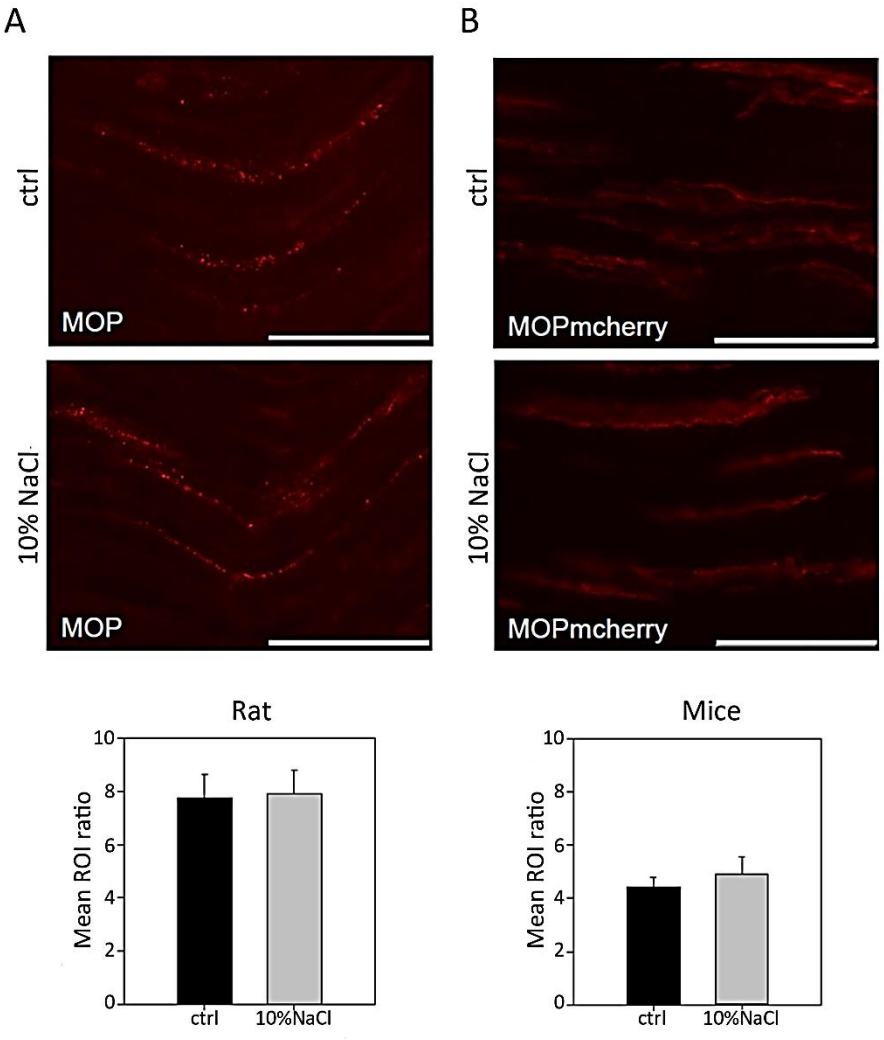

Fig. 34: No increase in axonal MOP immunoreactivity after treatment with HTS. Representative images of MOP- and mcherry-immunoreactions, respectively, of sciatic nerve of rats (A) and MOP-mcherry knock-in mice (B) under control conditions (ctrl) or 60 min after perisciatic injection of 10% NaCl (HTS) were recorded and quantified subsequently (C). MOP expression was calculated as ratio=staining intensity/stained area (ROI) as described in the methods (n=3, scale bars 50 µm; $P > 0.05$ Student's t-test).

To further validate immunofluorescence results, pre-embedding immunogold reactions were carried out for MOP-mcherry detection on HTS treated mcherry knock-in sciatic nerve and compared with the results on untreated nerve . Quantification of IGS in electron microscopy images (Fig. 35) again showed a statistically significant difference between positive and control reaction, confirming the specificity of the MOP-mcherry detection in Remak bundles. The results .validated the immunofluorescence data showing no increase in MOP content after HTS treatment compared to the naïve situation. The results indicate that HTS does not lead to sustained increases in MOP levels in sensory axons.

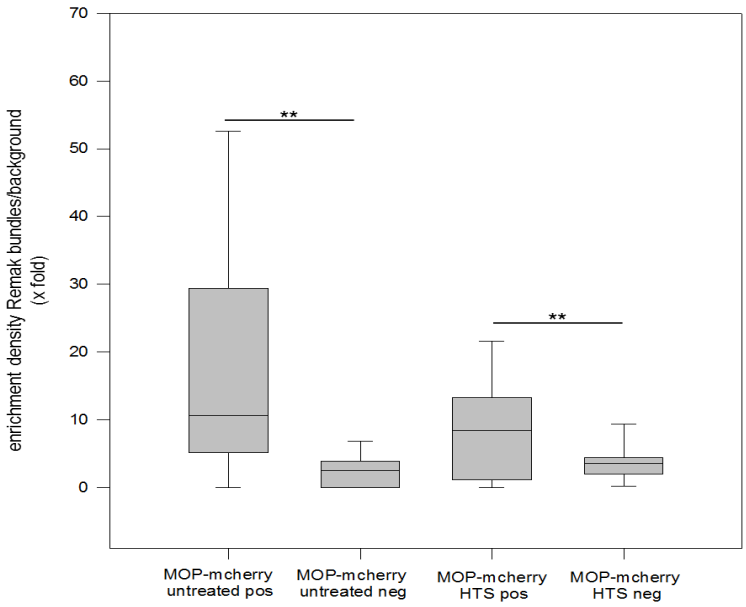

Fig. 35: No increase in enrichment of MOP-mcherry immunolabeling in Remak bundles of HTS treated compared to untreated MOP-mcherry knock-in sciatic nerve. Quantification of IGS comparing the four experimental conditions (untreated pos, untreated neg, HTS pos and HTS neg) is displayed as median dot density enrichment in Remak bundles over background (x fold) (n = 10-15; one way ANOVA and Dunn´s test on rank; *P < 0.05, **P < 0.01).

4. DISCUSSION

The present study documents several polyclonal MOP antibodies, which yield specific labeling of the receptor in the rodent CNS and have been used in previous studies, are less suitable to provide reliable and sensitive MOP detection in the PNS, particularly in the sciatic nerve, and thus cannot be used for quantitative assessment of receptor localization and content at the light- and electron microscopic level. However, a newly available commercial monoclonal rabbit antibody (RabMAb) and immunolabeling analyses of genetically modified mice – in which the fluorescent protein mcherry was inserted in the C-tail of MOP – could be shown to yield specific labeling of MOP in the sciatic nerve. Using these MOP detection techniques, it was possible to confirm the presence of the receptor in intact rat and mouse sciatic nerve sensory fibers and fiber bundles and to document receptor localization in the membrane and cytoplasm of unmyelinated sensory and putative nociceptive axons organized in Remak bundles. Additionally, quantitative analyses in rats and mice showed that the antinociception observed 60 min after perisciatic application of opioids coinjected with a hypertonic saline (HTS, 10% NaCl) is not due to an HTS-induced sustained increase in axonal MOP content.

4.1 Advantages and disadvantages of all the methods employed

To fulfill the aim to study MOP levels and expression under basal conditions as well as after perisciatic HTS injection, both morphological, biochemical, and molecular biological approaches were used. Each of these methods is, indeed, insufficient if applied alone.

Western blot is advantageous, compared to the other techniques, to detect and to compare protein levels of different samples. This is of key importance because protein rather than mRNA eventually carry out the biological function. Thus, data coming from Western blot should be considered more than qPCR data. Nevertheless, it has several main disadvantages: first, specific primary and secondary antibodies are required; second, the quantification of protein level is based on chemiluminescence detection that is highly sensitive and relies on enzymatic reaction that produces light. This enzymatic reaction is dynamic and could change over time making it necessary to optimize reaction times and imaging. Third, western blotting does not distinguish cell types in peripheral tissue, so it is not possible to unequivocally determine the localization of the protein of interest [61]. Furthermore, small differences in protein levels are barely detectable. Finally, separation of the membrane and cytosolic fraction is complicated: it requests a higher amount of protein and a specific fractionation protocol not well-established in nerve tissue. These technical problems are related to the sample nature and its content of specific protein could be only partially circumvented (i.e. by using the entire sciatic nerve).

qPCR provides relative quantification of gene expression and it is particularly advantageous to detect small changes in mRNA levels. However, in order to obtain reliable data, a high quality of RNA is necessary: indeed, the accuracy of gene expression evaluation is influenced by the quality and the quantity of starting RNA [95]. Therefore, the handling of the mRNA is particularly relevant since any problem during the mRNA extraction, purification and storage can affect the reproducibility. In order to preserve the mRNA quality, some precaution during samples harvesting, mRNA isolation and amplification should be used (i.e. immediately freeze the sample in liquid nitrogen, clean the instruments with RNAse inhibitor, use RNAse-free water to dilute the sample and work on ice). Specificity of primers and probes is necessary too, in order to avoid unspecific product amplification [96]. Finally, the mRNA does not necessarily reflect the final protein content, since lack of translation, or modification during or after translation process can occur. qPCR has also some disadvantages regarding the quantification. First of all, most quantitative data are not absolute but relative, since the value of the target gene is 1. normalized to the value of a reference gene (also known as endogenous gene or housekeeping gene) and 2. normalized in relation to a control e.g. untreated sample. This procedure is applied in the ΔCt method. It is one of the most popular means of determining differences in concentrations between samples and is based on normalization with a single reference gene. The difference in Ct values (ΔCt) between the target gene and the reference gene is calculated, and the ΔCts of the different samples (e.g. treated and untreated) are compared directly [96]. For this reason, the appropriateness of the reference gene should be considered and validated for each experiment [92]. Moreover, to ensure the accuracy of the reaction, a non-template control is also requested to check absence of contaminations in the qPCR reagents. Immunohistochemistry is a powerful method for identifying anatomical structure and offers the advantage of enabling the analysis of distribution patterns and subcellular localization of a given protein [97, 98]. Among immunohistochemical techniques, immunofluorescence is a well-established, less-time consuming and relative cheap method. Immunofluorescent labeling is also easily detectable and observable with a fluorescent microscope. However, several aspects could interfere with the quality of the results: the sample fixation, the specificity of the antibody and the fluorescent dye auto-fluorescence. All these aspects could lead to unspecific fluorescence resulting in a low signal-to-noise ratio hampering the detection of the specific signal. Moreover, fluorescent immunoreactivity is highly variable and this variability prevents a complete reliable comparison and immunofluorescence quantification within the same section and also between different sections. Finally, the intensity of fluorescence bleaches during the time with a progressive loss of signal; the process is enhanced by a prolonged exposure to microscope light; it is sometime necessary to detect and investigate the localization of the target of interest. Bleaching is avoided in the 3,3'-Diaminobenzidine-tetrahydrochloride-dihydrate (DAB) reaction: after DAB oxidation by peroxidase

the signal of antigen-antibody binding is detectable as a diffuse brown-black providing stable labeling both in light and electron microscopy. Despite those advantages, the DAB reaction presents four main disadvantages: the possibility to have only a brown-black labeling impedes a double staining used to analyze co-localization. The development of labeling is time-dependent; therefore time optimization is requested in order to obtain a good detectable signal avoiding background. Signals of low expressed protein are difficult to detect. Lastly, the chromogen is toxic; therefore, special precautions should be taken.

The pre-embedding immunogold reaction for electron microscopy is also characterized by disadvantages related to fixation and antibody specificity. However, the combination of immunogold labeling with transmission electron microscopy provides a high-resolution technique for the study of the subcellular distribution and the localization of antigens, e.g. OPs [10], identifying each single antigen:antibody binding as a black dot. However, for unequivocal identification of antigen localization, in particular for analysis of subcellular distribution, e.g. membrane vs. cytoplasmic localization of individual antigen molecules, superior specificity with low interference of unspecific signal is required. Since labeling efficiency may vary with section depth from the surface of the specimen – especially in the sciatic nerve, where unspecific silver precipitates may diffuse into the nerve via endoneurial spaces – and with detection protocol between experiments and specimen, specificity of labeling and signal-to-noise ratio has to be controlled for individual ultrathin sections by analyzing in-section background signal intensity [99, 100].

In the present study, for rat sciatic nerve sections reacted with polyclonal MOP antibodies, enrichment of immunogold-silver precipitates over axons in Remak bundles was analysed, with Remak Schwann cell cytoplasm as in-section control. Surprisingly, analyses showed no axonal enrichment in antibody-treated sections, while significant enrichment was found in controls (omission of primary antibody). Furthermore, since in immunofluorescence experiments using these antibodies specificity could not be ascertained (see below), this approach was abandoned. RabMAb immunoreactions provided qualitative evidence of higher labeling in Remak axons than in surrounding tissue, but there was still considerable unspecific signal detected between axons in the endoneurium and in large myelinated fibers. Nevertheless, since immunofluorescence had provided evidence of detection specificity, the labeling of Remak bundles indicated that the antibody recognized MOP specifically in sensory axons. However, an unequivocal recognition of the specific subcellular localization of MOP molecules using this detection method appeared questionable, since the background labeling was still rather high. Qualitatively, the signal-to-noise ratio of MOP-mcherry-immunolabeling in the sciatic nerve of MOP-mcherry knock-in mouse appeared considerably higher than in RabMAb reactions on rat nerve, with immunogold-silver precipitates more frequently found on Remak bundles than on other components of the nerve. Indeed, quantitative analysis showed

significant enrichment of labeling in Remak bundles over background compared to immunoreactions on wildtype nerve, providing conclusive evidence of MOP detection specificity. Additionally, the fact that background levels were very low in the analyzed sections and IGS density over Remak bundles was more than 10 times higher than background indicated that precipitate localization could be taken to actually represent specific MOP-mcherry antigen detection. Thus, a cytoplasmic and (peri)membraneous localization of the receptor fusion protein in Remak fiber axons could be ascertained using this method.

4.2 Unspecific labeling of rabbit and guinea pig polyclonal MOP-antibodies in peripheral nervous system

Specificity of antibodies against MOP has long been discussed especially for their use in immunohistochemistry [101] and in western blot [102]. Among the four tested antibodies, the polyclonal rabbit antibodies from Abcam (#ab10275) and Neuromics (#RA10104) yielded specific staining in the pyramidal cell layer of the hippocampus and in the intercalated nuclei of the amygdala with high signal-to-noise ratio, but did not deliver a reliable detection of MOP in the DRG and the sciatic nerve.

Those results agree with a recent study of Schmidt and colleagues [103], who described a MOP Abcam antibody tissue-dependent specificity. In immunofluorescence on wild type and MOP knock-out mouse tissues, they observed specific staining in the brain and spinal cord but not in the DRG. Indeed, wild type and MOP knock-out DRG immunoreacted for MOP were characterized by a diffuse and intense background that was comparable to our results. In the sciatic nerve, however, Schmidt noticed a co-localization of MOP and PGP9.5 that we could not reproduce: in our immunofluorescent staining, co-localization was relatively scarce. On the other hand, we did occasionally observe co-localization of MOP-immunoreactivity with CGRP-immunoreactivity in fibers and fiber bundles. However, our results corroborated high unspecific binding levels of polyclonal MOP antibodies in immunohistochemistry. Thus, fluorescence signals were always observed in non-CGRP-ir structures resembling Schwann cells and in double labelings, a strong MOP-immunoreactivity was observed in S100-ir Schwann cells. Finally, the IGS quantification on Remak bundles and Schwann cells showed no statistically significant difference in the positive labeling and an unexpected statistically significant difference in the negative control.

To date, MOP expression in Schwann cells has not been reported. Furthermore, the expression of MOP mRNA in the qPCR experiments of the present study was detectable at Ct 32, normally considered a non-reliable value associated with low expressed mRNA or unspecific annealing. If MOP would be constitutively expressed in Schwann cells, one would expect a Ct between 23 and 27 similar to the DRG. Lack of MOP mRNA detection in sciatic nerve qPCR, performed to measure mRNA in

treated and untreated rats, is thus an additional indirect prove of polyclonal antibody unspecificityIt is also known that MOP-immunoreactivity is very low if at all seen in intact sciatic nerve [60, 103], rendering it extremely difficult to achieve a high signal-to-noise ratio that is required both for good detection and reliable and reproducible data.

Considering all these aspects, one could speculate and ascribe high unspecific staining in sciatic nerve and low signal-to-noise ratio to the low levels of MOP in the peripheral nervous system and/or to the presence of proteins causing antibody binding in glial cells, as Schwann cells, that can compete or interfere with specific antigen:antibody binding leading to a high background. Schwann cells express GPR7 [104], a 7-transmembrane receptor that shares the same amino acid sequence of the immunizing peptide with MOP. However, in GPR7 the sequence is divided in the middle by other amino acids: it is not clear if the two parts are connected in the 3D conformation, leading to reconstruction and detectability of the sequence, or not. Whether polyclonal antibodies might detect GPR7 has to be analysed in further studies. In any case, lack of labeling in Schwann cells using RabMAb antibody (see also 4.3.1) indicates that the binding of the polyclonal antibodies to Schwann cells and other tissue components of the sciatic nerve is not due to the presence of MOP in these compartments: thus, hampering specificity of the receptor detection.

Problems of unspecific binding were also present in Western blot. Using rabbit Neuromics antibody different bands at different molecular weight and also a band at the size of 55 kDa were detected. Similar results were obtained, using the same antibody used in the present study, by Niwa et al [102]: their western blot showed numerous bands and one at the predicted size, of 70 kDa. This difference in expected molecular weight is probably a result of the glycosylated form or of the posttranscriptional modification necessary for a functional receptor. Considering the pure amino acids sequence (398aa in rat and mouse) and considering also all the possible isoforms, the molecular weight should be between 43 and 50 kDa. Unfortunately all those characteristics, linked to the structure of the nerve or to the receptor, are intrinsic and could not be avoided. The only possibility to obtain reliable data is to use more specific antibodies or genetically modified mice.

4.3 Specific labeling of MOP using MOP-RabMAb antibody and mcherry-detection in knock-in mice in peripheral nociceptive axons

Light microscopic immunolabeling patterns, ultra-structural analysis and Western blot showed very similar results using the monoclonal rabbit MOP-antibody on rat tissue and the detection of the fusion protein in MOP-mcherry knock-in mice confirmed the constitutive presence of MOP along sensory, putative nociceptive axons and the similarity of the localization of MOP in rats and in genetically modified mice. Nevertheless, detection of MOP using mcherry was overall better than

using RabMAb antibody since it yielded stronger staining and higher signal-to-noise ratio both in light and electron microscopy.

4.3.1 Specificity of MOP-RabMAb in the sciatic nerve

The MOP-RabMAb antibody specifically detected MOP in the amygdala, the spinal cord, the DRG and the sciatic nerve. However, while the immunofluorescent staining was very sharp and strong in the first three samples, the intensity of the immunoreaction was low in the sciatic nerve, leading to a very low signal-to-noise ratio. This made the identification of MOP in sciatic nerve quite difficult. Nevertheless, it was possible to detect a dotted staining, localized within fibers and fiber bundles also containing the neuropeptide CGRP. The dotted pattern could be explained by localization of MOP in vesicles, responsible for the transport of MOP from the DRG, where the receptor is synthetized, along the axoplasm. It was also interesting to observe a difference in relative immunolabeling intensity for MOP and CGRP between individual axon and axon bundles: this could be an indication of a variable level of MOP in different sensory axon types in naïve rats. MOP reactivity in fiber bundles which was not strictly co-localized with CGRP-reactivity could indicate MOP presence in IB_4-positive C-fibers in the same Remak bundle [77] . It was demonstrated that a partial localization of MOP was also possible in IB_4-positive DRG neurons [105]. Lack of staining in Schwann cells using MOP-RabMAb confirmed the unspecificity of commercial polyclonal antibodies.

Ultra-structural data obtained with electron microscopy also confirmed the specificity of MOP-RabMAb. This was particularly evident in the brain, in which a difference between the positive reaction and negative control (omission of primary antibody) was appreciable. Contrarily, significant unspecific labeling due to the detection sequence was found in the negative control of the rat sciatic nerve, and also in presumably non-MOP-expressing tissue compartments in the antibody-reacted sections (see also above). This led again to a comparatively low signal-to-noise ratio. Nevertheless, IGS in Remak bundles of antibody-reacted sections were almost exclusively localized on the membrane and in the cytoplasm of unmyelinated axons. Few IGS were localized in myelinated fibers, confirming the results of immunofluorescence and specificity of the MOP detection.

The blot incubated with MOP-RabMAb showed, according to the manufacturing datasheet, bands at the right molecular weight (70 kDa) in all samples tested. This molecular weight was also observed by Lupp [101] and Grecksch [106] in a rat brain homogenate. In a recent paper [107] MOP was detected in western blot using an affinity purified polyclonal antibody as a diffuse band between 58 and 84kDa, depending on the brain region and species. After deglycosylation, the band was seen at 43kDa, the expected size considering the amino acid sequence of the receptor. However, in different rodent species, MOP are differentially glycosylated, so different results are possible.

In DRG and sciatic nerve lysate the intensity of the bands were reduced compared to the brain and spinal cord. Moreover, other bands at higher molecular weight were present. This reflects the results already observed using the Neuromics antibody, but since bands were absent in the brain and spinal cord, they are now probably attributable to post-transcriptional modification than to unspecific binding. The negative control showed no bands, confirming the absence of unspecific binding of secondary antibody.

4.3.2 Specific and intense immunoreactivity of MOP-mcherry in the sciatic nerve

MOP-mcherry mice were created by homologous recombination after the insertion of the red fluorescent protein mcherry sequence in the exon 4 at the C-tail of the μ-opioid receptor. Introduction of the coding sequence for mcherry increased the size of the amplified fragment by about 800bp. The sequence insertion and the consequent increased dimension could have caused changes in the receptor conformation, properties and localization. However, several tests confirmed that the genomic modification did not disrupt the transcription of Oprm1 (i.e., MOP murine gene), and changed neither DAMGO ligand affinity nor the opioid's ability to activate the receptor after binding. Localization and internalization studies also proved the complete functionality of MOP-mcherry. Finally, the behavioral test results were comparable between wild type and MOP-mcherry mice [41]. The validity of this model and test's results are further confirmed by a previous study of Scherrer and colleagues [40]. Using the same approach they created a DOP-EGFP construct. The functionality and the expression of the modified receptor were first investigated in HEK transfected cells and later in knock-in mice. In both experiments DOP-EGFP fusion protein showed unchanged binding, signaling and internalization. Western blot, qPCR and distribution results were comparable between the wild type and the knock-in mice.

The red fluorescent mcherry protein, inserted at the MOP C-tail, was visible also without staining. However, to increase the signal, the fluorescence was enhanced with an anti-DsRed antibody. It specifically recognized only the tag, without unspecific binding, as confirmed by the clear and bright immunoreactivity localized in the intercalated nuclei of amygdala, in lamina I and II of spinal cord and DRG of knock-in mice as well as by the lack of staining in the brain of wild type mice reacted with the mcherry antibody. Those results were comparable with results obtained by Erbs and colleagues [41], which investigated mcherry expression in different areas of the brain and in DRG. In addition to brain, in the present study sciatic nerve samples were analysed. In fibers and fibers bundles, mcherry staining was less intense than in other neuronal tissues, but the signal-to-noise ratio was quite high and better than in the rat. Double staining on longitudinal nerve showed a co-localization of MOP-mcherry and CGRP in fibers and fiber bundles, indicating an opioid receptor presence solely in sensory, putative nociceptive fibers. Interestingly, also in mice, a relative MOP

intensity difference between fibers was appreciable: this implicates that different type of fibers contain different levels of MOP both in mice and rats and are maybe differently involved in pain perception and relief. In the context with current literature, CGRP-positive and CGRP-negative (IB_4-positive) nociceptors express MOP. So far, these subtypes cannot be attributed to specialized functions in pain perception [108].

In ultrastructural images, IGS of mcherry were specifically localized in neuronal profiles of the amygdala and in unmyelinated fibers of the sciatic nerve. Some unspecific IGS were visible in both samples, but their amount was scarce in non-MOP-expressing tissue components both in antibody-reacted sections and in the negative controls. Those results are even more reliable since in the immunogold reactions in the amygdala and the sciatic nerve of wild type mice IGS were almost absent.

Specific binding and lack of background led to a very high signal-to-noise ratio that permitted to specifically quantify and localize dots. For this reason the use of mice was preferred to rat samples to perform IGS quantification analysis on electron microscopy images.

The comparative quantification analysis effectively confirmed the specificity of MOP-mcherry detection, showing a higher labeling enrichment (>10 fold) in the positive reaction (mcherry-antibody reaction on MOP-mcherry sciatic nerve) compared to the mcherry-antibody reaction on wildtype sciatic nerve and the respective negative controls (around 2.5 fold).

The high amount of proteins that had to be loaded in western blot to obtain visible bands (50 µg for brain and spinal cord; 100 µg for DRG and sciatic nerve) is an indication of the low quantity of MOP along the nerves, and further support the immunofluorescence results, showing low staining in fibers or fibers bundles. It was however possible to detect a specific strong single band in the brain and the spinal cord at 80 kDa. The increase in the molecular weight from 50 kDa, the expected molecular weight considering the amino acid sequence, to 80 kDa is due to the insertion of mcherry in the C-tail [41]. Presence of multiple bands in DRG and sciatic nerve, already observed in rat, could be due to posttranscriptional modification. The discrepancy in band numbers observed in the brain, spinal cord, DRG and sciatic nerve is maybe due to a different MOP conformation or synthesis in the central and peripheral nervous system [58], or to the presence, in the periphery, of glial cells and connective tissue that interfere with antibody binding [98] and leads to background.

Moreover, the low detection of MOP in western blot hampers the possibility to compare expression of the receptor under different conditions, in particular to compare the expression of MOP in untreated and HTS treated sciatic nerve.

Considering all data from immunofluorescence labeling, pre-embedding immunogold electron microscopic qualitative and quantitative analyses, and Western blots it can be concluded that

RabMAb and mcherry antibodies specifically detect MOP and MOP-mcherry in the rat and mouse sciatic nerve. Secondly, the results conclusively document the constitutive presence of MOP not only at the nerve terminals but also in cytoplasmic and perimembraneous localization in non-myelinated, presumably nociceptive, axons of sciatic nerves. The results support functional studies showing that perisciatic injections of the lipophilic opioid fentanyl induce antinociception in the naïve nerve, indicating the presence of functional MOP in nociceptor membranes along the sciatic nerve trunk (Mambretti et al., 2015, accepted). This opens the possibility to specifically targeting sensory, putative nociceptive axons to induce local analgesia without impairing motor fibers.

4.4 No sustained influence of HTS on MOP levels

Several studies [86, 90, 109, 110] have demonstrated the effect of hypertonic solutions (sucrose or saline) in opening the perineurial barrier, leading to a higher penetration of substances into the nerve. Osmotic gradients have the capability to increase the permeability of epithelial and endothelial cells [110] inducing structural changes and the disruption of the tight junction proteins deputed to regulate the perineurial permeability [86].

This interaction with HTS and perineurium is particularly interesting for substances as hydrophilic opioids: as they normally can´t cross the barrier due to the tight junctions of the perineurium, injection of hypertonic solution could be an alternative to let opioid drugs reach their receptors, expressed on the nociceptive axons membrane and to bind and to activate them inducing antinociception. Previous behavioral results [90] showed an augmented mechanical nociceptive threshold after 10 min HTS injection. The enhancing effect of HTS started after 10 min and lasted for up to 5 h. The effect was specifically and dose-dependently inhibited in presence of naloxone, a MOP antagonist. This excluded a MOP-mediated inhibition of voltage gated-sodium channels, known to be activated by nociceptive stimuli and blocked opioid [90]. HTS also augmented the effect of the lipophilic opioid fentanyl on nociception: considerably lower doses of the drug were required to induce antinociception if it was perisciatically coinjected together with HTS (Mambretti et al., 2015, accepted). Since fentanyl can presumably reach the axons without barrier opening, it was hypothesized that the HTS-induced effect was not only due to an increased perineurial permeability but also to an HTS-mediated enhanced receptor availability/function which could be due to increased synthesis and/or membrane localization of MOP. However, the results obtained by qPCR and with immunofluorescence and immunogold quantification indicated that 60 min after injection of HTS, a time point at which augmented antinociceptive effect is still present, MOP mRNA and protein levels were not increased in DRG and sciatic nerve sensory axons, respectively. Thus, even if an increased MOP expression and/or a transport block with increased membrane insertion should be caused by HTS injections acutely, the treatment does not lead to a sustained MOP level increase in sensory

axons, indicating that 1. HTS does not induce prolonged axonal dysfunction and transport deficits and 2. the sustained HTS-induced increase in antinociception of opioids is likely due to alterations in MOP availability and function in axonal membranes.

Beyond HTS modulation of the perineurium, other mechanisms can be considered to explain this effect. According to Livingstone [111] and Shang [112], sodium ions can allosterically modulate opioid receptors inducing two different answers. On one side they decrease the ligand binding affinity of agonist to the MOP, blocking the recognition site for ligand binding. Moreover, sodium ions – hampering the activation- related conformational changes that normally occur after ligand-receptor binding – give preference to the inactive state of the receptor. This mechanism, however, cannot explain our results, since after HTS injection the analgesia induced by MOP agonist was increased, suggesting an activation of receptor rather than an inactivation.

On the other side, sodium ions can promote agonist-induced activation of MOP while inhibiting the spontaneous Gi/Go-coupled receptor activity, as also reported by Yuan [113]. Sodium ions can facilitate the activation of MOP by inducing the movement of water molecules towards the allosteric site, which influences an action of the orthosteric agonist.

Another possible explanation is a reduced or blocked internalization of MOP. Heuser and Anderson demonstrated that, in fibroblasts, hypertonic solution inhibits LDL (low density lipoprotein) receptor endocytosis by blocking clathrin-coated pit formation [114]. Studies on HEK cells using hypertonic sucrose solution (0.35M) [115] confirmed inhibition of MOP and DOP endocytosis.

Recent studies using HTS solution support those results. In particular, Hoffmann and colleagues demonstrated, in HEK cell transfected with human MOP, that a pre-treatment with 10% NaCl (1.7 M solution) reduced the internalization of the opioid agonist/β-arrestin/MOP complex. (Mambretti E.M. et al, 2015, accepted). The receptor was therefore not internalized and could have been permanently exposed on the axonal membrane. The reduced internalization could, on one side, increase the number of receptors on the membrane that can bind the agonist, activate GPCR and start the pathway involved in antinociception. Secondly, if receptors are not internalized upon agonist binding, the time requested for the turnover is abolished, implying a faster reactivation of the receptor. The reduced internalization of the receptor can be then considered a good explanation for our results. The fact that immunolabeling did not show enhanced membrane localization of MOP after 60 min might be explained by the fact that membrane localization of the receptor is very dilute and thus not detectable with immunolabeling methods. Alternatively, it could be that HTS injections induce an acute and transient axonal transport block with subsequently increased spontaneous insertion of MOP-bearing vesicles into the axonal membrane (see also below), and that binding of coinjected opioids is required to induce membrane retention of the receptors for prolonged time periods. Since coinjections were not carried out in the present study, this effect might have been missed.

In conclusion, it is well accepted that HTS can interfere with opioid receptors and the analgesic properties they mediate. However, there are still quite controversial results on HTS effects and the mechanisms of action are still not completely understood.

One potential weakness of this study is that we looked at only one time interval between the injection and the tissue harvesting. The time (60 min) and the volume of NaCl injected (300 µl) were based on previous pilot and behavioral studies. Since the volume of NaCl injected is diluted within 15 min and Na concentration in the tissue return to normal [86], it is possible that after 60 min a direct effect on the nerve is completely lost, as suggested above. In *in vitro* experiment, HTS effect was observed for 780 seconds (13 min): in this short time HTS, blocking the internalization, leads to MOP localization and expression on the cell surface. However, no increase in the total amount of MOP within the cell was observed. This could be interpreted as further validation of our experiment and confirms the absence of correlation between HTS and MOP increased expression.

4.5 Regulation of axonal transport and membrane-cytoplasm shuttling

Inside the neuron, a highly specialized cell, the axonal transport is directed from the soma to the terminal. To ensure this flow and accommodate the diverse need for function and survival, neurons rely on cellular polarization and sub-cellular compartmentalization [116]. OPs are synthetized in the DRG and further carried to the nerve terminals along intraaxonal microtubules [48]. In particular, nerve ligation experiments clearly demonstrated the presence of anterograde [63, 117] and retrograde [118] transport of OP showing their accumulation at both side of ligature. The directed transport of OP to the periphery is increased during inflammation: under those conditions an upregulation of OP synthesis occurs in the DRG and it is followed by increased axonal transport [48, 62]. A local translation of mRNA in subcellular compartment of the axon could also be possible [119].

To be transported from the DRG to the axon, OPs need to be stored in vesicles. In immunofluorescence and electron microscopy analysis, DOPs were seen to be localized in large dense-core vesicles (LDCV) [120, 121] associated with the Golgi of small-medium neurons. Vesicles are then transported along the axon. Here, LDCV-associated DOPs are recruited to the cell surface by potassium-induced depolarization [121]; the increased concentration of calcium induces the fusion of the LDCV with the membrane and OP release can rapidly modulate the neuronal activity. Even if no localization of MOP in LDCV is described, it is known that newly synthetized receptors are processed in the Golgi and then assembled in vesicles of the constitutive secretory pathway (most often together with proteins required for trafficking and signal transduction [121, 122]) to be transported and inserted spontaneously in the plasma/axonal membrane [123]. This concept supports our immunofluorescence data on sciatic nerve, in which we observed a granular appearance of MOP

staining, both in rat and mouse samples. Punctuate MOP labeling were also observed by Baillie, in nociceptive fibers arising from the trigeminal ganglion [124].

4.6 Potential mechanisms of opioid action on nociceptive axons

Understanding how pain stimuli are encoded and how they could be inhibited is of fundamental importance to the study of pain and pain treatment. Particularly interesting, in the context of this work, is to understand how opioid receptors could reduce mechanical nociceptive threshold in peripheral nerve axons. Some opioids, e.g., buprenorphine, are used in the clinic as local anesthetic since they are able to non-specifically block voltage-gated sodium channel (NaV) [125], known to mediate pain sensation. However, considering previous results of our lab [90], it is unlikely that NaVs are involved in MOP agonist-mediated antinociception, since naloxone, a MOP antagonist, completely reversed the opioid effect. Other mechanism should then be considered. We suggest that the electrical excitability is reduced, e.g. by hyperpolarization via potassium channels, which may filter out the shrinking action potentials that occur during bursts of high-frequency discharge. Two types of potassium channels have been implicated in pain and are expressed in nociceptors: the G protein-coupled inwardly rectifying K^+ channels (GIRKs, e.g. Kir3) and TREK-1, a member of the two-pore domain K^+ (K2P) channel family. GIRKs contribute to the adjustment of the neuronal resting potential and excitability, and are the major type of potassium channel activated by GPCRs. GIRK channels are major effectors of opioid signaling in the CNS as well as the PNS in rats [126]. The TREK-1 K(+) channel is highly expressed in both peptidergic and non-peptidergic small sensory neurons, and extensively co-localized with TRPV1, the capsaicin-activated non selective ion channel [127]. It is also widely distributed in the central nervous system. TREK-1 is a crucial contributor to morphine-induced analgesia in mice. Using electrophysiological techniques it was shown that a functional coupling exists between MOP and the TREK-1 channel [128]. However, other channels can be involved in MOP agonist mediated analgesia. Recently Baillie and colleagues [124] proposed two mechanisms for pain inhibition in trigeminal ganglion, one involving calcium channel (Ca^{++}) and one involving calcium-activated potassium channel (K_{Ca}). MOP activation by peripherally acting MOP agonists causes inhibition of Ca^{++} signaling, mostly attributable to the inhibition of N-typa Ca^{++} channels, that control the release of CGRP. This confirms our *in vitro* results in which KCl-induced CGRP-release was blocked by opioid in desheated sciatic nerve (Mambretti E.M. et al., 2015, accepted). K_{Ca} channel, activated in response to both membrane depolarization and elevated cytosolic Ca^{++}, are involved in presynaptic transmission and neuronal excitability, since they control the action potential duration and firing frequency. If activated, they can suppress the firing inducing an antinociceptive effect that is increased in presence of MOP agonists.

4.7 Conclusion

In conclusion opioid receptors are present and functional in the sciatic nerve, not only at the nerve ending but also along sensory putative nociceptive axon of the sciatic nerve. Therefore the opioid receptor could be a target for local pain treatment. Moreover, the difficulties in targeting them, mostly due to the perineurial barrier, could be overcome by using hypertonic saline. It is now clear that a HTS-mediated increased of antinociception is not related with a sustained increase of the synthesis or intra-axonal levels of MOP; however, it is not clear which mechanism, either allosterically modification or inhibited internalization, is involved, or whether these mechanisms are mutually exclusive or whether they cooperate. Other investigations and more detailed research need to be performed to clarify these questions.

5. REFERENCES

1. Rosenblum, A., et al., *Opioids and the treatment of chronic pain: controversies, current status, and future directions.* Exp Clin Psychopharmacol, 2008. 16(5): p. 405-16.
2. Brownstein, M.J., *A brief history of opiates, opioid peptides and receptors.* PNAS, 1993.
3. Bilfinger, T.V. and V. Kushnerik, *The use of morphine in surgery: an overview.* Adv Neuroimmunol, 1994. 4(2): p. 133-44.
4. Kieffer, B.L. and C.J. Evans, *Opioid receptors: from binding sites to visible molecules in vivo.* Neuropharmacology, 2009. 56 Suppl 1: p. 205-12.
5. Pasternak, G.W., *Opioids and their receptors: Are we there yet?* Neuropharmacology, 2014. 76 Pt B: p. 198-203.
6. Evans, C.J., *Secrets of the opium poppy revealed.* Neuropharmacology, 2004. 47 Suppl 1: p. 293-9.
7. Evans, C.J., et al., *Cloning of a delta opioid receptor by functional expression.* Science, 1992. 258(5090): p. 1952-5.
8. Cox, B.M., et al., *Challenges for opioid receptor nomenclature: IUPHAR Review 9.* Br J Pharmacol, 2015. 172(2): p. 317-23.
9. Mansour, A., et al., *Key residues defining the μ-opioid receptor binding pocket: a site-direct mutagenesis study.* J Neurochem, 1997. 68(1): p. 344-353.
10. Wang, Y., E.J. Van Bockstaele, and L. Liu-Chen, *In vivo trafficking of endogenous opioid receptors.* Life Sciences, 2008. 83: p. 693–699.
11. Lesniak, A. and A.W. Lipkowski, *Opioid peptides in peripheral pain control.* Acta Neurobiol Exp (Wars), 2011. 71(1): p. 129-38.
12. Costantino C.M., et al., *Opioid receptor heteromers in analgesia.* Expert Rev Mol Med 2012. 14.
13. Stein, C., *Opioids, sensory systems and chronic pain.* Eur J Pharmacol, 2013. 716(1-3): p. 179-87.
14. Nguyen, K.D., et al., *Mu-opioid receptor (MOR) expression in the human spiral ganglia.* Brain Res, 2014. 1590: p. 10-19.
15. Wittert, G., P. Hope, and D. Pyle, *Tissue Distribution of Opioid Receptor Gene Expression in the Rat.* Biochem Biophys Res Commun 1996. 218: p. 877–881.
16. Spetea, M., *Opioid receptors and their ligands in the muscoloskeletal system and relevance for pain control.* Curr Pharm Des, 2013. 19(42): p. 7382-90.
17. Agirregoitia, E., et al., *Expression and localization of opioid receptors during the maturation of human oocytes.* Reprod Biomed Online, 2012. 24(5): p. 550-557.
18. Tadevosyan, A., et al., *G protein-coupled receptor signalling in the cardiac nuclear membrane: evidence and possible roles in physiological and pathophysiological function.* J Physiol 2012. 590(6): p. 1313-1330.
19. Feng, Y., et al., *Current Research on Opioid Receptor Function.* Curr Drug Targets. , 2012. 13(2): p. 230–246.
20. Williams, J.T., et al., *Regulation of m-opioid receptors: desensitization, phosphorylation, internalization and tolerance.* Pharmacol Rev 2013. 65: p. 223–254.
21. Pasternak, G.W., *Opiate pharmacology and relief of pain.* J Clin Oncol, 2014. 32(16): p. 1655-61.
22. Dorsam, R.T. and J.S. Gutkind, *G-protein-coupled receptor and cancer.* Nat Rev Cancer, 2007. 7(2): p. 79-94.
23. Stone, L.S. and D.C. Molliver, *In search of analgesia:emerging roles of GPCRs in pain.* Mol Interv, 2009. 9(5): p. 234-251.
24. Raehal, K.M., et al., *Functional selectivity at the μ-opioid receptor: implications for understanding opioid analgesia and tolerance.* Pharmacol Rev 2011. 63(4): p. 1001–1019.
25. Allouche, S., F. Noble, and N. Marie, *Opioid receptor desensitization: mechanisms and its link to tolerance.* frontiers in pharmacology, 2014. 5.

26. Wall, P. and R. Melzack, *Textbook of pain - 6th edition.* Elsevier, 2006.
27. Ritter, S.L. and R.A. Hall, *Fine-tuning of GPCR activity by receptor-interacting protein.* Nat Rev Mol Cell Biol, 2009. 10(12): p. 819-830.
28. Moyse, E., et al., *Electron microscopic distribution of Mu opioid receptors on noradrenergic neurons of the locus coeruleus.* Eur J Neurosci, 1997. 9(1): p. 129-139.
29. Aicher, S.A., et al., *Dual ultrastructural localization of μ-opiate receptors and substance P in the dorsal horn.* Synapse, 2000. 36(1): p. 12-20.
30. Zahng, J., J.F. Muller, and A.J. Mcdonald, *Mu opioid receptor localization in the basolateral amygdala: an ultrastructural analysis.* Neuroscience, 2015. 303: p. 352-363.
31. Beckerman, M.A. and M.J. Glass, *Ultrastructural relationship between the AMPS-GluR2 receptor subunit and the mu-opioid receptor in the mouse central nucleus of amygdala.* Exp Neurol, 2011. 227(1): p. 149-158.
32. Coggeshall, R.E., S. Zhou, and S.M. Carlton, *Opioid receptors on peripheral sensory axons.* Brain Res, 1997. 764(1-2): p. 126-32.
33. Sanderson Nydahl, K., et al., *Co-localization of endomorphine-2 and substance P in primary afferent nociceptors and effects on injury: a light and electron microscopic study in the rat.* Eur J Neurosci, 2004. 19(7): p. 1789-1799.
34. Zollner, C., et al., *Painful inflammation-induced increase in mu-opioid receptor binding and G-protein coupling in primary afferent neurons.* Mol Pharmacol, 2003. 64(2): p. 202-10.
35. Arvidsson, U., et al., *Distribution and targeting of μ-opioid receptor (MOR1) in brain and spinal cord.* J Neurosci, 1995. 15(5): p. 3328-3341.
36. Mousa, S.A., et al., *Nerve growth factor governs the enhanced ability of opioids to suppress inflammatory pain.* Brain, 2007. 130(Pt 2): p. 502-13.
37. Truong, W., et al., *Mu opioid receptors and analgesia at the site of a peripheral nerve injury.* Ann Neurol, 2003. 53(3): p. 366-75.
38. Michel, M.C., T. Wieland, and G. Tsujimoto, *How reliable are G-protein-coupled receptor antibodies?* Naunyn Schmiedebergs Arch Pharmacol, 2009. 379(4): p. 385-388.
39. Schmidt, Y., C. Gaveriaux-Ruff, and H. Machelska, *mu-Opioid receptor antibody reveals tissue-dependent specific staining and increased neuronal mu-receptor immunoreactivity at the injured nerve trunk in mice*, in *PLoS One*2013. p. e79099.
40. Scherrer, G., et al., *Knockin mice expressing fluorescent delta-opioid receptors uncover G protein-coupled receptor dynamics in vivo.* Proc Natl Acad Sci U S A, 2006. 103(25): p. 9691-9696.
41. Erbs, E., et al., *A mu-delta opioid receptor brain atlas reveals neuronal co-occurrence in subcortical networks.* Brain Struct Funct, 2014.
42. Machelska, H., P.A. Heppenstall, and C. Stein, *Breaking the pain barrier.* Nat Med, 2003. 9(11): p. 1353-4.
43. Woolf, C.J., *What is this thing called pain?* J Clin Invest, 2010. 120(11): p. 3742-3744.
44. Kitahata, L.M., *Pain pathways and transmission.* Yale J Biol Med, 1993. 66(5): p. 437-442.
45. Carr, F.B. and V. Zachariou, *Nociception and pain: lessons from optogenetics.* Fron Behav Neurosci, 2014. 8(69).
46. Ambrosi, G., *Anatomia dell'uomo.* edi-ermes, 2006: p. 373.
47. Siegel, A. and H.N. Sapru, *Essential neuroscience - second edition.* the Point - Lippincott Williams and Wilkins, 2011: p. 141.
48. Stein, C. and L.J. Lang, *Peripheral mechanisms of opioid analgesia.* Curr Opin Pharmacol, 2009. 9(1): p. 3-8.
49. Bourne, S., A.G. Machado, and S.J. Nagel, *Basic Anatomy and Physiology of Pain Pathways.* lNeurosurg Clin N Am, 2014. 25(4): p. 629-638.
50. Zhou, L., et al., *Contribution of opioid receptors on primary afferent versus sympathetic neruons to peripheral opioid analgesia.* J Pharmacol Exp Ther, 1998. 286(2): p. 1000-1006.
51. LePichon, C.E. and A.T. Chesler, *The functional and anatomical dissection of somatosensory subpopulations using mouse genetics.* Front Neuroanat, 2014. 8.

52. Obara, I. and S.P. Hunt, *Axonal Protein Synthesis and the Regulation of Primary Afferent Function.* Dev Neurobiol, 2013. 74(3): p. 269-278.
53. Price, T.J. and C.M. Flores, *Critical evaluation of the colocalization between calcitonin generelated peptide, substance P, transient receptor potential vanilloid subfamily type 1 immunoreactivities and isolectin B4 binding in primary afferent neurons of the rat and mouse.* J Pain 2007. 8(3): p. 263-272.
54. Lorenzo, L., et al., *Postnatal changes in the redex lamination and markers of nociceptive afferents in the superficial dorsal horn of the rat.* J Comp Neurol, 2008. 508(4): p. 592-604.
55. McCoy, E.S., et al., *Peptidergic CGRPα primary sensory neurons encode heat and itch and tonically suppress sensitivity to cold.* Neuron., 2013. 78(1): p. 138-151.
56. Bae, J., et al., *Quantitative analysis of afferents expressing substance P, calcitonin gene-related peptide, isolectin B4, neurofilament 200, and Peripherin in the sensory root of the rat trigeminal ganglion.* J Comp Neurol, 2015. 523(1): p. 126-138.
57. Lawson, S.N., B. Crepps, and E.R. Perl, *Cacitonin gene-related peptide immunoreactivity and afferent receptive properties of dorsal root ganglion neurones in guinea-pigs.* J Physiol, 2002. 540: p. 989-1002.
58. Stein, C., M. Schafer, and H. Machelska, *Attacking pain at its source: new perspectives on opioids.* Nat Med, 2003. 9(8): p. 1003-8.
59. Jagla, C. and C. Stein, *Peripheral opioid receptor blockade increases postoperative morphine demands—A randomized, double-blind, placebo-controlled trial.* Pain Med, 2014. 155(10): p. 2056-2062.
60. Khalefa, B.I., et al., *Relative contributions of peripheral versus supraspinal or spinal opioid receptors to the antinociception of systemic opioids.* European Jourral of Pain, 2012. 16(5): p. 690-705.
61. Labuz, D. and H. Machelska, *Stronger antinociceptive efficacy of opioids at the injured nerve trunk than at its peripheral terminals in neuropathic pain.* J Pharmacol Exp Ther, 2013. 346(3): p. 535-44.
62. Puehler, W., et al., *Rapid upregulation of μ opioid recepto mRNA in dorsal root ganglia in response to peripheral inflammation depends on neuronal conduction.* Neuroscience, 2004. 129: p. 473-479.
63. Hassan, A.H., et al., *Inflammation of the rat paw enhances axonal transport of opioid receptors in the sciatic nerve and increases their density in the inflamed tissue.* Neuroscience, 1993. 55(1): p. 185-95.
64. Abram, S.E., et al., *Permeability of injured and intact peripheral nerves and dorsal root ganglia.* Anesthesiology, 2006. 105(1): p. 146-153.
65. Antonijevic, I., et al., *Perineurial defect and peripheral opioid analgesia in inflammation.* J Neurosci, 1995. 15(1 Pt 1): p. 165-72.
66. Rittner, H.L., et al., *Antinociception by neutrophil-derived opioid peptides in noninflamed tissue--role of hypertonicity and the perineurium.* Brain Behav Immun, 2009. 23(4): p. 548-57.
67. Picard, P.R., et al., *Analgesic efficacy of peripheral opioids (all except intra-articular): a qualitative systematic review of randomised controlled trials.* Pain, 1997. 72(3): p. 309-18.
68. Hug, C.C.J., *Opioids: clinical use as anesthetic agents.* J Pai Symptom Manage, 1992. 7(6): p. 350-355.
69. Barash, P.G., et al., *Handbook of clinical anesthesia* Lippincott Williams and Wilkins, 2013. 7th edition.
70. Netter, F.H., *The Netter collection of medical illustration.* Saunders, 2013. 7, second edition.
71. Swett, J.E., et al., *Sensory Neurons of the Rat Sciatic Nerve.* Exp Neurolog, 1991. 114(1): p. 82-103.
72. Chad, D., et al., *Sympathetic postganglionic unmyelinated axons in the rat peripheral nervous system.* Neurology, 1983. 33(7): p. 841-847.
73. Schmalbruch, H., *Fiber composition of the rat sciatic nerve.* Anat Rec, 1986. 215(1): p. 71-81.

74. Ueda, H. and M.H. Rashid, *Molecular mechanisms of neuropathic pain.* Drug News Perspect, 2003. 16(9): p. 605-613.
75. Armati, P.J. and E.K. Mathey, *An update on Schwann cell biology - Immunomodulation, neural regulation and other surprises.* J Neurol Sci, 2013. 333(1-2): p. 68-72.
76. Griffin, J.W. and W.J. Thompson, *Biology and pathology of nonmyelinating Schwann cells* Glia, 2008. 56(14): p. 1518-1531.
77. Murinson, B.B., et al., *C-fiber (Remak) bundles contain both isolectin B4-binding and calcitonin-gene-related peptide-positive axons.* J Comp Neurol, 2005. 484(4): p. 392-402.
78. Loesch, A., et al., *Sciatic nerve of diabetic rat treated with epoetin delta: effects on C-fibers and blood vessels including pericytes.* Angiology, 2010. 61(7): p. 651-668.
79. Peltonen, S., M. Alanne, and J. Peltonen, *Barriers of the peripheral nerve.* Tissue Barriers, 2013. 1(3).
80. Shanthaveerappa, T.R. and G.H. Bourne, *The 'perineural epithelium', a metabolically active,continuous, protoplasmic cell barrier surrounding peripheral nerve fasciculi.* J Anat., 1962. 96: p. 527-537.
81. Mizisin, A.P. and A. Weerasuriya, *Homeostatic regulation of the endoneurial microenvironment during development, aging and in response to trauma, disease and toxic insult.* Acta Neuropathol, 2011. 121: p. 291–312.
82. Ask, P., et al., *Peripheral nerve as an osmometer: role of the perineurium in frog sciatic nerve.* Am. J. Physiol., 1983. 244(13): p. C75-C81.
83. Stein, C. and C. Zollner, *Opioids and sensory nerves.* Handb Exp Pharmacol, 2009(194): p. 495-518.
84. Likar, R., et al., *Efficacy of Peripheral Morphine Analgesia in Inflamed, Non-Inflamed and Perineural Tissue of Dental Surgery Patients.* J Pain Symptom Manage, 2001. 21(4): p. 330-337.
85. Wenk, H.N., J.-D. Brederson, and C.N. Honda, *Morphine Directly Inhibits Nociceptors in Inflamed Skin.* J Neurophysiol 2006. 95(4): p. 2083-2097.
86. Rittner, H.L., et al., *Modulation of tight junction proteins in the perineurium to facilitate peripheral opioid analgesia.* Anesthesiology, 2012. 116(6): p. 1323-34.
87. Zwanziger, D., et al., *A peptidomimetic tight junction modulator to improve regional analgesia.* Mol Pharm, 2012. 9(6): p. 1785-94.
88. Hackel, D., et al., *Modulation of tight junction proteins in the perineurium for regional pain control.* Ann N Y Acad Sci, 2012. 1257: p. 199-206.
89. Rapoport, S.I., *Osmotic opening of the blood-brain barrier.* Ciba Found Symp, 1978(56): p. 237-55.
90. Hackel, D., et al., *Transient opening of the perineurial barrier for analgesic drug delivery.* Proc Natl Acad Sci U S A, 2012. 109(29): p. E2018-27.
91. Zimmermann, M., *Ethical guidelines for investigations of experimental pain in conscious animals.* Pain, 1983. 16(2): p. 109-10.
92. Livak, K.J. and T. Schmittgen, *Analysis of relative gene expression data using Real-Time Quantitative PCR and the* $2^{-DeltaDeltaC}T$ *Method.* Methods, 2001. 25(4): p. 402-408.
93. Mansour, A., et al., *Immunohistochemical localization of the cloned mu opioid receptor in the rat CNS.* J Chem Neuroanat, 1995. 8(4): p. 283-305.
94. Pinard, C.R., Mascagni F. and McDonald A.J., *Medial prefrontal cortical innervation of the intercalated nuclear region of the amygdala.* Neuroscience, 2012: p. 112-124.
95. Fleige, S. and M.W. Pfaffi, *RNA integrity and the effect on the real-time qRT-PCR performance.* Mol Aspects Med, 2006. 27(2-3): p. 126-139.
96. Bustin, S.A., et al., *The MIQE Guidelines:Minimum Information for Publication of Quantitative Real-Time PCR Experiments.* Clin Chem, 2009. 55(4): p. 611-622.
97. Schmidt, Y. and H. Machelska, *Immunohistochemical analysis of opioid receptors in peripheral tissues.* Methods Mol Med, 2015. 1230: p. 15-165.

98. Schacht, V. and J.S. Kern, *Basics of immunohistochemistry.* Journal of investigative dermatology, 2015. 135.
99. Rothe, F., M. Brosz, and J. Storm-Mathiens, *Quantitative ultrastructural localization of glutamate dehydrogenase in the rat cerebellum cortex.* Neuroscience, 1995. 64(4).
100. Mayhew, T.M., *Quantifying immunogold localization patterns on electron microscopic this section of placenta: recent developments.* Placenta, 2009. 30(7): p. 565-570.
101. Lupp, A., et al., *UMB-3, a novel rabbit monoclonal antibody, for assessing mu-opioid receptor expression in mouse, rat and human formalin-fixed and paraffin-embedded tissues.* Regul Pept, 2011. 167(1): p. 9-13.
102. Niwa, H., D.J. Rowbotham, and D.G. Lambert, *Evaluation of primary opioid receptor antibodies for use in western blotting.* Br J Anaesth, 2012. 108(3): p. 530-532.
103. Schmidt, Y., C. Gaveriaux-Ruff, and H. Machelska, *mu-Opioid receptor antibody reveals tissue-dependent specific staining and increased neuronal mu-receptor immunoreactivity at the injured nerve trunk in mice.* PloS one, 2013. 8(11): p. e79099.
104. Zaratin, P.F., et al., *Schwann cell overexpression of the GPR7 receptor in inflammatory and painful neuropathies.* Mol. Cell. Neurosci. , 2005. 28: p. 55-63.
105. Wu, Z.Z. and H.L. Pan, *High voltage-activated Ca(2+) channel currents in isolectin B(4)-positive and -negative small dorsal root ganglion neurons of rats.* Neurosci Lett, 2004. 368(1): p. 96-101.
106. Grecksch, G., et al., *Analgesic tolerance to high-efficacy agonists but not to morphine is diminisched in phosphorylation-deficient S375A μ-opioid receptor knock-in mice.* J Neurosci, 2011. 31(39): p. 13890-13896.
107. Huang, P., C. Chen, and L. Liu-Chen, *Detection of mu opioid rceptor (MOPR) and its glycosylation in rat and mouse brains by western blot with anti-μC, an affinity-purified polyclonal anti-MOPR antibody.* Methods Mol Biol, 2015. 1230: p. 141-154.
108. Wang, H., et al., *Coexpression of δ- and μ-opioid receptors in nociceptive sensory neurons.* PNAS, 2010. 107(")): p. 13117-13122.
109. Antonijevic, I., et al., *Perineurial defect and peripheral opioid analgesia in inflammation.* J Neurosci, 1995. 15: p. 165-72.
110. Weerasuriya, A., S.I. Rapoport, and R.E. Taylor, *Modification of permeability of frog perineurium to [14C]-sucrose by stretch and hypertonicity.* Brain Res, 1979. 173(3): p. 503-12.
111. Livingstone, K.E. and J.R. Traynor, *Disruption of the Na+ ion binding site as a mechanism for positive allosteric modulation of the mu-opioid receptor.* Proc Natl Acad Sci U S A, 2014. 111(51): p. 18369-18374.
112. Shang, Y., et al., *Mechanistic Insights into the Allosteric Modulation of Opioid Receptors by Sodium Ions.* Biochemistry, 2014. 53(31).
113. Yuan, S., H. Vogel, and S. Filipek, *The Role of Water and Sodium Ions in the Activation of the m-Opioid Receptor.* Angew. Chem. Int. Ed. , 2013. 52: p. 10112 –10115.
114. Heuser, J.E. and R.G.W. Anderson, *Hypertonic Media Inhibit Receptor-mediated Endocytosis by Blocking Clathrin-coated Pit Formation.* J Cell Biol, 1989. 108(2): p. 389-400.
115. Keith, D.E., et al., *Morphine Activates Opioid Receptors without Causing Their Rapid Internalization.* J Biol Chem, 1996. 271(August 9): p. 19021–19024.
116. Wei, L.N., *The RNA superhighway: axonal RNA trafficking of kappa opioid receptor mRNA for neurite growth.* Integr Biol (Camb), 2011. 3(1): p. 10-6.
117. Zarbin, M.A., J.K. Wamsley, and M.J. Kuhar, *Anterograde transport of opioid receptors in rat vagus nerves and dorsal roots of spinal nerves: pharmacology and sensitivity to sodium and guanine nucleotides.* Exp Brain Res, 1990. 81(2): p. 267-78.
118. Laduron, P.M. and P.F. Janssen, *Retrograde axonal transport of receptor-bound opiate in the vagus and delayed accumulation in the nodose ganglion.* Brain Res, 1985. 333(2): p. 389-92.
119. Bi, J., et al., *Axonal mRNA transport and localized translational regulation of kappa-opioid receptor in primary neurons of dorsal root ganglia.* Proc Natl Acad Sci U S A, 2006. 103(52): p. 19919-24.

120. Zhang, X., et al., *Localization and regulation of the delta-opioid receptor in dorsal root ganglia and spinal cord of the rat and monkey: evidence for association with the membrane of large dense-core vesicles.* Neuroscience, 1998. 82(4): p. 1225-42.
121. Zhao, B., et al., *Transport of receptors, receptor signaling complexes and ion channels via neuropeptide-secretory vesicles.* Cell Res, 2011. 21(5): p. 741-53.
122. Luo, W., Y. Wang, and G. Reiser, *Proteinase-activated receptors, nucleotide P2Y receptors, and μ-opiid receptor-1B under the control of the type I transmembrane protein p23 and p24A in post-Golgi trafficking.* J Neurochem, 2011. 117(1): p. 71-81.
123. Zhang, X., L. Bao, and S. Li, *Opioid receptor traffiking and interactionin nociceptors.* Br J Pharmacol, 2014. 172(2): p. 364-374.
124. Baillie, L.D., H. Schmidhammer, and S.J. Mulligan, *Peripheral m-opioid receptor mediated inhibition of calcium signaling and action potential-evoked calcium fluorescent transients in primary afferent CGRP nociceptive terminals.* Neuropharmacology, 2015. 93: p. 267-273.
125. Leffler, A., et al., *Local anesthetic-like inhibition of voltage-gated Na(+) channels by the partial mu-opioid receptor agonist buprenorphine.* Anesthesiology, 2012. 116(6): p. 1335-46.
126. Nockemann, D., et al., *The K(+) channel GIRK2 is both necessary and sufficient for peripheral opioid-mediated analgesia.* EMBO Mol Med, 2013. 5(8): p. 1263-77.
127. Alloui, A., et al., *TREK-1, a K+ channel involved in polymodal pain perception.* EMBO J, 2006. 25(11): p. 2368-76.
128. Devilliers, M., et al., *Activation of TREK-1 by morphine results in analgesia without adverse side effects.* Nat Commun, 2013. 4: p. 2941.

PUBLICATIONS

2015 **Egle M. Mambretti**, Katrin Kistner, Stefanie Mayer, Dominique Massotte, Brigitte L. Kieffer, Carsten Hoffmann, Peter W. Reeh, Alexander Brack, Esther Asan, Heike L. Rittner. Functional and structural characterization of axonal opioid receptors as targets for analgesia. Molecular Pain (accepted)